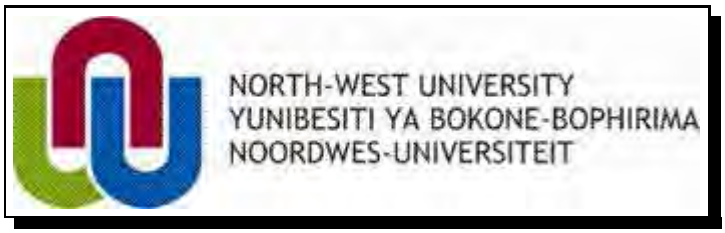

Nitric Oxide Reduction by Chars Derived from High Ash Inertinite-Rich Discard Coals

Zebron Phiri

B.Sc Honours (Applied Chemistry)

(National University of Science & Technology - Bulawayo)

Dissertation submitted in partial fulfilment of the requirements for the degree Master of Science (Engineering Science) in the School of Chemical and Minerals Engineering at North-West University, Potchefstroom Campus.

Supervisor	:	Professor R.C. Everson
Co-Supervisor	:	Professor H.W.J.P. Neomagus
Assistant Supervisor	:	Doctor R. Kaitano

May 2010

Potchefstroom

“A man should look for what is, and not for what he thinks should be.”

- Albert Einstein -

DECLARATION

I, Zebron Phiri do hereby declare that the dissertation with the title: NITRIC OXIDE REDUCTION BY CHARS DERIVED FROM HIGH ASH INERTINITE-RICH DISCARD COALS submitted in partial fulfilment of the requirements for the degree Master of Science (Engineering Science) is my work and has not been submitted at any other university either in part or as a whole.

Signed at Potchefstroom on the.....day of .....2010.

.....

Z. Phiri

ACKNOWLEDGEMENTS

I would like to extend my sincere gratitude to the following individuals and organisations for the immeasurable contributions, support and assistance towards the outcome of this research project:

- God, the Heavenly Father.
- My mother, Mrs. Ngonidzashe Phiri, for instilling the importance of education unto me at a tender age.
- Professor R.C. Everson, Professor H.W.J.P. Neomagus and Doctor Rufaro Kaitano their expert guidance, wealth of experience, critical evaluation and enthusiastic motivation throughout the course of this study.
- The entire Coal Research group for its contributions and critical analysis of my work during the weekly presentations.
- Mr. Jan Kroeze and Mr. Adrian Brock, for the excellent maintenance of equipment ensuring both smooth and safe operation of the experimental apparatus.
- Mrs Vivien Du Cann and Dr. Sabine Verryn, for their immense contribution on characterisation work and the subsequent interpretation.
- All the personnel in the School of Chemical and Minerals Engineering for their professional support and constant willingness to help.
- The financial assistance of the South African National Energy Research Institute (SANERI) towards this research is greatly appreciated.
- My fiancée, Ms. Bongiwe Nhlapo for her understanding, patience and love that gave me strength to see the light at the end of the tunnel.
- My son and the entire family, for the unconditional love, continuous inspiration, and giving me the willpower to envision a brighter day.
- My friend, Busani Ngwenya, for the plethora of favours, advice and encouragement.
- The moral support from all my friends cannot go unmentioned; *Sho Majimbos!*

ABSTRACT

An investigation was performed to determine the kinetics of nitric oxide (NO) reduction by six different chars derived from inertinite-rich low grade coals. The experimentation involving the reduction of NO was confined to conditions used in fluidised bed combustion with aspirations to provide information for the fluidised bed technology using high ash and inertinite rich South African coals.

A detailed characterisation of six different chars was executed with respect to physical structural, chemical, mineralogical and petrographic properties. The coal samples had ash content ranging from 37% to 48.7% (% by mass, dry basis) and the respective chars had 49% to 63.7% ash (dry basis). The organic constituents of the parent coals were inertinite-rich, with inertinite content ranging from 25% to 66% (% volume, mmb). The charring process, conducted at 900°C for 60 minutes, significantly shifted the total reflectance scans of the parent coals (1.09-1.46% Rsc) to higher values in the corresponding chars (4.84-5.45% Rsc). The chars were characterised by carbon forms which marked the macerals transformation during char formation. These char carbon forms constituted of dense chars, isotropic coke, char networks and partially reacted macerals.

The reactivity experiments were carried out using 1 mm char particles in a thermogravimetric analyser (TGA) under isothermal conditions at temperatures in the range of 750 to 900°C at atmospheric pressure using varying dilute mixtures (1.25-5.0%) of nitric oxide (NO) in nitrogen (N_2). The effects of temperature and gas composition on reactivity were established to conform to published trends. The kinetic parameters were determined by using the random pore model (RPM), the model was based on the random pore model without pore diffusion (chemical reaction controlled). Validation of the model against experimental results displayed a good correlation for all the six chars. Due to the complex nature of the model which consists of numerous unknown parameters, a step-wise regression was applied with success. Correlation of reactivity with coal attributes was undertaken but only the modified reactive maceral index (RMI*) gave a meaningful relation.

Table of Contents

List of Figures

List of Tables

Nomenclature

		Units
C	concentration of reacting gas	moles·m^{-3}
E	activation energy	kJ·mole^{-1}
$f(X)$	structure factor	m^{-1}
k	reaction rate constant	s^{-1}
L$_\circ$	total pore length per unit volume	m·m^{-3}
m$_{ash}$	mass of ash	g
m$_\circ$	initial mass of char	g
m$_t$	mass of char at time t	g
n	order of reaction	-
Rr	vitrinite reflectance, %	-
Rsc	total (full) maceral reflectance, %	-
r$_s$	reaction rate	mole·s^{-1}
S$_{D-R}$	Dubinin-Radushkevich micropore surface area	m^2·g^{-1}
S$_\circ$	initial surface area	m^2
T	temperature	K
t	time	s
t_f	time factor, $t_f = \frac{r_s S_\circ}{1-\varepsilon_\circ}$	s^{-1}
$t_{0.9}$	time for fractional carbon conversion of 90%	s
X	fractional conversion of carbon	-

Greek symbols

ε	porosity	-
$\varepsilon_\circ$	initial porosity	-
τ	dimensionless time, $\tau = \frac{r_s S_\circ t}{1-\varepsilon_\circ}$	-
σ	standard deviation of reflectance measurements	
ψ	structural parameter, $\psi = \frac{4\pi L_\circ (1-\varepsilon_\circ)}{S_\circ^2}$	-

Acronyms/Abbreviations

Afrox	African Oxygen
ASTM	American Society for Testing and Materials
BET	Brunauer, Emmett and Teller Isotherm
BFBC	bubbling fluidised bed combustion
CCT	clean coal technology
CFBC	circulating fluidised bed combustion
daf	dry and ash free
db	dry basis
DME	Department of Minerals and Energy (South Africa)
DTF	drope-tube furnace
D-R	Dubinin-Radushkevich
EC	European Community
EPA	Environment Protection Agency (United States)
Eskom	South African Electricity Supply Commission
FBC	fluidised bed combustor
IEA	International Energy Agency
IEO	International Energy Outlook
IGCC	intergrated gasification combined cycle
ISO	International Standards Organisation
LCPD	large combustion plant directive
MI	Maceral index
mmb	mineral matter basis
RMI	reactive maceral index
RMI*	modified reactive maceral index
RPM	Random Pore Model
SA	South Africa
SABS	South African Bureau of Standards
SANERI	South African National Energy Research Institute
TG	thermogravimetric
TGA	thermogravimetric analyser
WCI	World Coal Institute
XRD	X-ray diffraction analysis

Publication Resulting from this Investigation

- Zebron Phiri, Raymond C. Everson, Hein W.J.P. Neomagus, Rufaro Kaitano. (2009).
  Nitric Oxide Reduction With Chars Derived From High Ash Inertinite-Rich Coals.
  Submitted for publication to *Fuel Processing Technology*.
  Oral presentation of paper at the International Conference on Coal Science & Technology (ICCS&T), 26-29 October 2009, Cape Town, South Africa.

CHAPTER 1

General Introduction

1.1 General

This chapter is divided into four sections which give an overview of the research study undertaken consisting of: background, motivation, objectives and scope of the study furnished at the end of the chapter.

1.2 Background

Coal is broadly used for electricity generation and steel production (Mohr and Evans, 2009) and it plays an important role in energy systems that are bound to support sustainable development for the foreseeable future. This is due to coal's unique combination of advantages, which include its diversity and availability (it is the most abundant and geographically well spread fossil fuel), its is affordability and the fact that it is chemically stable and hence safe to transport and store (Mochida and Sakanishi, 2000; WCI, 2007). Coal's abundancy makes it vital in achieving a diverse and balanced energy mix, and hence it plays a pivotal role in meeting the energy needs of both developed and developing countries.
Even though coal has remained the main source for power generation, it has

been largely discredited for causing pollution (Harding *et al.*, 1996; Köpsel and Halang, 1997).

Coal provides 26.5% of the world's primary energy requirements and also generates 41.5% of the world's electricity (WCI, 2010). In 2007, South Africa generated 94% of its electricity from coal combustion (WCI, 2010) and 68% of its primary energy needs in 2004 came from coal (DME, 2006), making it one of the countries in the world that are heavily dependent on coal. For the past 10 years world primary energy needs have risen by over 20% and this upward trend is projected to continue (WCI, 2007). Energy needs will continue to be met largely by fossil fuels, accounting for approximately 80% of energy needs in 2030. Over 25% of this global energy demand will be met by coal.

Coal remains South Africa's prime energy source. The South African electricity supply commission (Eskom) combusts 87.4 million tonnes of coal annually for electricity generation while Sasol gasifies and processes almost 48.8 million tonnes of low grade coals into high quality synthetic-fuels, including transport fuels, using the Fischer-Tropsch process (DME, 2003). South Africa (SA) is an energy intensive country, generating 45% of the total electricity in Africa (Eskom, 2007).

Coal combustion produces an indisputable amount of pollutants, encompassing particulate matter, carbon dioxide (CO_2) a potent greenhouse gas, sulphur dioxide (SO_2) which causes acid rain, and nitrogen oxides of which NO and NO_2 are also responsible for the production of acid rain and photochemical smog (Glarborg *et al.*, 2003), while nitrous oxide (N_2O) contributes significantly towards global warming and depletion of the ozone layer (Hayhurst and Lawrence, 1992; Mann *et al.*, 1992; Wojtowicz *et al.*, 1993; Thomas, 1997; Chen *et al.*, 2001).

Renewable energy technologies currently have inherent limitations, which include the fact that they are mostly intermittent and storage is a problem. The South African government is pushing for biofuels as part of its growth strategy and to increase the use of renewable sources. Biofuels are controversial internationally because they push up food prices and increase deforestation. Depending on the crop source, the energy equation can be negative, as more energy is used to produce the fuel than it actually contains. South Africa has a high solar radiation intensity therefore the potential of developing solar energy is high. However harnessing solar power is difficult and expensive, rendering it economically non viable.

The potential of using wind power varies from region to region, with coastal areas showing the greatest potential. Since wind power is dependent on the vagaries of nature, it cannot be considered as a reliable form of energy. The country's river flows are not steady and strong enough to make large scale hydro-electric generation possible. South Africa is home to the only nuclear power station on the continent, the Koeberg power station in the Western Cape Province, it produces 1800MW which is about 6% of national electricity needs. Fear of catastrophic accidents, international politics and the dilemma of disposal of dangerous waste products are always associated with nuclear power technology.

Despite the environmental concerns associated with coal usage, it has continued to be an attractive energy option for power generation. Clean coal technologies (CCTs) have been developed to reduce the emissions associated with coal combustion. CCTs will continue to play an important role in the coming decades to minimise the environmental impact of the substantial coal usage that is forecast. These technologies were developed to remove or prevent the formation of CO_2, SO_2, oxides of nitrogen and particulates when coal is burned to generate electricity. Fluidised bed combustion (FBC) and integrated gasification combined cycle (IGCC) have emerged as technologies capable of reducing these pollutants to acceptable levels.

The major advantages of FBC are fuel flexibility, ability to handle low grade solid fuels, and low emissions of SO_2 and NO (Johnsson, 1994; Tomita, 2001; Armesto *et al.*, 2003; Basu, 2006; Gungor, 2009). The aim is to achieve high thermal efficiency, reduced emissions and improved economics. Thus, FBC operated at 750-900°C has achieved low levels of NO emissions. In addition to good environmental performance another attractive feature of FBC is that it is versatile and particularly suited to poor quality coals like those widely used in South Africa.

1.2.1 Environmental legislation

As legislation and environmental regulations become progressively more stringent, governments and non governmental organisations are putting immense pressure on power generation companies and boiler manufacturers to come up with ways of minimising emissions drastically, such that compliance with the statutes on pollutant limits and standards is achieved.

The overriding expectation from legislation on electricity generation from coal combustion is to meet the needs of the present generation without compromising the ability of future generations to meet their own needs. In the European Community (EC) the Large Combustion Plant Directive (LCPD) came into effect on 1 January 2008. It calls for an exigent reduction of pollutants from plants with a capacity of 50MW$_{(\mathrm{th})}$ or more within member countries (European Commission, 2001). By the end of November 2007, 174 nations (Parties) had signed the Kyoto Protocol whose primary aim is to reduce greenhouse gas emissions and other pollutants to levels specified to each Party in the treaty, once the Protocol comes into force.

1.2.2 Hazards associated with nitric oxide

Nitrogen oxides and their derivatives cause a wide variety of health problems and environmental impacts due to their wide range of hazardous characteristics (EPA, 1998). Some of the dangers caused by the oxides of nitrogen as outlined by the United States EPA (1998) include the following:

- Water quality deterioration; acid rain poses an environmental danger to the aquatic life and also reduces the life-span of erected structures like buildings and bridges.
- Visibility impairment; NO is a major precursor to the formation of ground-level ozone also referred to as photochemical smog.
- Serious lung damage, shortness of breath and chest pains if inhaled in significant concentrations.
- Contributes to heart problems and also damages the central nervous system.
- Contributes to low birth rates and causes a marked decrease in resistance to infection.

1.3 Motivation

World energy requirements escalate at a rate greater than population growth. In the International Energy Outlook of 2009 (IEO, 2009), world coal con-

sumption is projected to increase by 1.7% annually on average from 2006 to 2030, accounting for 28% of total world energy consumption in 2030. Utilisable coal reserves around the world are sufficient enough to provide energy for approximately the next 147 years at current production levels and projected energy demand growth (WCI, 2007). South Africa has the fifth largest coal reserves in the world and coal continues to remain its prime energy source.

This importance of fossil fuels in meeting energy requirements is recognised, but as concerns about dangerous emissions grow, South Africa also needs to be a responsible global neighbour. Emissions reduction could have a significant impact on the South African economy and trade because SA is a major exporter of coal. Alternative means of producing energy such as renewable energy sources which have less impact on the environment have to be considered. A complete switch to these renewables is virtually impossible and could take a very long period to implement to such levels that the renewables contribution is significant. Therefore more efficient techniques to use coal in such a manner that the hazards associated with its combustion are eliminated or are brought down to acceptable levels should be formulated. This is where clean coal technologies come into play.

The International Energy Agency (IEA) estimates that renewables will only be able to provide less than 10% of overall energy demand in 30 years time and that includes hydro power. Therefore the negative environmental impact of current use of coal, with its inherent dreadful emissions, will persist until other forms of clean fuels such as hydrogen and renewables make a significant contribution. The solution being proposed by many researchers is to produce energy using the traditional fossil fuels like coal, but in a manner which will minimise emissions, like the much anticipated CCTs.

At present there are 53-55 billion tonnes of economically accessible coal reserves in South Africa (Bredell Report 1987) of this total, 220 million tonnes are produced annually, of which 69 million tonnes (high rank) are exported. Beneficiation of South African coals results in the generation of approximately 60 million tonnes of coal discard annually (DME, 2006), and this is projected to accumulate to well over a billion tonnes to date. The discards normally have a high ash and sulphur content. This is typical of most South African coal reserves, distinguished by high inertinite content which is considered to be an inert maceral with low combustion and gasification efficiencies. Poor ignition and burnout properties of the inertinite in the pulverised

discards combined with high ash content, nitrogen and sulphur pollutants, are all factors which contribute to the need for alternative clean coal technologies that will enhance boiler combustion efficiency with less expensive downstream processes. The coal discards' calorific value range from as low as 2.00 MJ/kg to 14.60 MJ/kg on air-dried basis and contain upto 40% carbon and 45% ash.

The world at large injects huge sums of research funds annually into new coal based technologies. In an endeavour to keep up with international statutes prescribed to coal combustion power generation companies on pollutants, Eskom (SA) and the South African National Energy Research Institute (SANERI) have engaged with the Coal Technology Research Group in the School of Chemical and Minerals Engineering from the North-West University, Potchefstroom (South Africa) to partake in an extensive research programme aimed at economically utilising the coal discards and low grade coals with minimal unfavourable environmental impact. The research mainly focuses on clean coal technologies like FBC which can handle solids more efficiently, favour the removal of ash resulting from the combustion of high ash coals, handle sorbents for oxides of sulphur removal and reduce nitrogen oxides (NO_x) by the chars formed in situ.

The South African government continues to investigate and encourage options for the utilisation of coal discard stockpiles. Power generation using raw discards combustion in a fluidised bed combustor is regarded as a suitable alternative. This is the major motive behind the government's support for current techno-economic investigations on power production from coal discards.

This has also led to high interest and enthusiasm on the reduction of nitrogen oxides emission research and other pollution related works. This proposed research study seeks to address the reaction kinetics of NO using chars derived from typical South African discard coals, which have a high ash and inertinite content.

1.4 Objectives of the investigation

The aim of the investigation was to develop an understanding of the reaction kinetics of high ash chars derived from inertinite-rich coal discards with nitric oxide so as to provide information for the development of fluidised bed technology for power generation. To achieve this goal the following was

performed:

- characterisation of typical South African inertinite-rich high ash coals and the respective chars.
- evaluation of the reaction kinetics of nitric oxide with different chars under isothermal conditions, at temperatures ranging from 750°C to 900°C at atmospheric pressure using a thermogravimetric analyser.
- comparison the reaction kinetics of the different chars with nitric oxide and relate to the coal characteristics.

The research is directed toward the understanding of NO reaction kinetics with typical low grade (discards) South African coal chars under FBC conditions.

1.5 Scope of study

In an endeavour to achieve the specified objectives, a distinct scope of this study had to be formulated. The scope of this dissertation is presented schematically in Figure 1.1. Basically, the research is divided into three major focus areas, these encompass; coal/char characterisation, NO-char reaction in a TGA and the reaction rate modelling.

- Chapter 1 gives an overview of the background, motivating elements of the investigation and a concise outline of the objectives of the research work.
- A literature survey is given in Chapter 2, detailing work from relevant publications in order to give an in-depth understanding of subject matter fundamentals, covering coal/char characterisation, NO production from coal/char and its subsequent reduction by char or carbonaceous materials, and reaction rate modelling.
- The characterisation of parent coals and the subsequent chars is presented in Chapter 3. The description of the charring apparatus and procedure is also given. Proximate and ultimate analysis together with petrographic, minerological and carbon dioxide micropore surface area analyses were conducted.

- Experimental procedure, apparatus (TGA) and the reagents used are given in Chapter 4.
- Chapter 5 presents the results obtained from the NO-char reactions, subsequent data analyses and discussion. The effect of temperature and NO concentration is demonstrated. An appropriate reaction rate model is selected and evaluation of the associated parameters is carried out.
- General conclusions from the study are deduced and laid out in Chapter 6, of which contributions made to the knowledge base in this regard is considered as a milestone in typical South African low grade coal utilisation and the simultaneous reduction of nitric oxide in focus. Based on the results obtained, recommendations for future work are suggested.

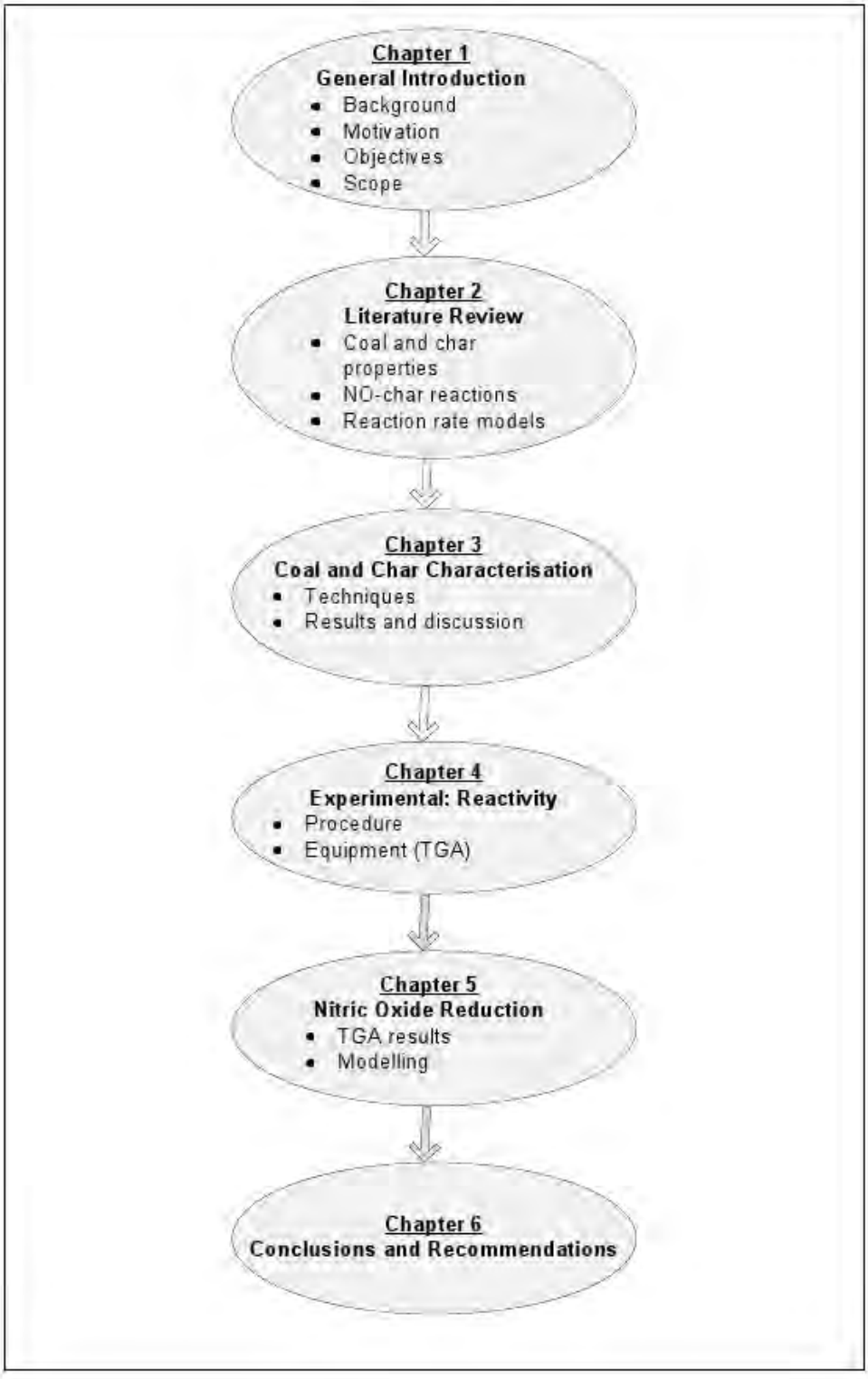

Figure 1.1: Scope of the study

CHAPTER 2

Literature Review

2.1 Introduction

The major objective of this chapter is to give a literature review on the characterisation of coals and chars, and an overview of the formation and reduction of nitric oxide under fluidised bed combustion conditions. Mechanisms and reaction rate models associated with char gasification are also reviewed.

2.2 Coal and char properties

The major properties of coal and char which have an influence on combustion, and the subsequent NO production and reduction are well documented in literature. These comprise chemical properties which include volatile matter content, initial carbon content (often referred to as rank of coal), and ash with its composition (Li *et al.,* 1998). The type and quantity of minerals, pore structure or surface morphology of the chars and petrographic properties have also been linked to char reactivity of NO reduction.
Li *et al.* (1998) stated that the reaction rate of NO reduction by carbon is dependent on the type of carbon and operation conditions.
Volatile matter is dependent on the macerals in the coal, it increases from

inertinite, vitrinite to liptinite and has a marked effect on the properties of chars formed. The liberation of volatiles during pyrolysis affects the char porosity and subsequently the overall reactivity of the chars (Li *et al.*, 1998). A high volatile content renders enhanced combustion efficiency due to the rapid combustion of the volatiles.

The effect of minerals (type and content) in coal or char towards nitrogen oxides reduction has been restricted largely to the catalytic aspects of the type and/or quantity of the minerals present. Illán-Gómez *et al.*, (1995a-f) conducted a series of investigations aimed at understanding the catalytic potential of various inorganic components inherently present or impregnated into carbonaceous materials. Their studies showed that potassium, calcium, copper, chromium, cobalt, nickel and iron possessed different catalytic abilities under various conditions.

Coal petrographic properties include vitrinite and total maceral reflectance, maceral and microlithotype compositions. Char petrographic attributes are characterised by total maceral reflectance and organic constituents comprising mainly of char carbon forms and partially reacted macerals (Du Cann, 2008).

Vitrinite reflectance increases uniformly with increasing coalification process, hence it is usually used as a measure of the extent of coalification, based on the scale of brown coal to anthracite (Berkowitz, 1985). Vitrinite reflectance is a reliable parameter since it is independent of the vitrinite content resulting in its common use as a rank indicator (Cloke and Lester, 1994). Reflectance readings taken on all organic components; liptinites, vitrinites and inertinites embodies the total maceral reflectance scan (Benfell, 2001; Kaitano, 2007; Du Cann, 2008 and Everson, 2008b). During pyrolysis or combustion, high temperatures tend to produce more thick-walled char particles and also networks are present in chars derived from lower rank coals which are linked to the coal aromaticity, and increase with coal rank (Cloke and Lester, 1994). Bend and co-workers, (1992) reported that the charring process produced hollow single-chambered optical anistropic chars and multi-chambered optical isotropic chars. The effect of petrographic properties on combustion and gasification reactivity is widely covered in literature (Thomas *et al.,* 1989; Mendez *et al.*, 2003; Biswas *et al.,* 2007; Hodge *et al.*, 2010).

2.3 Nitric oxide formation and reduction

Oxides of nitrogen comprise of nitric oxide (NO), nitrogen dioxide (NO_2) and nitrous oxide (N_2O). NO and NO_2 are collectively known as NO_x (Hill and Smoot, 2000) and NO makes up the major proportion of NO_x in fluidised bed combustion (FBC). NO_2 mostly emanates from the post combustion oxidation of NO in the atmosphere. FBC operated at low temperatures (750-900°C) has produced relatively low NO_x emissions (Johnsson, 1994; Chen *et al.*, 2001; Tomita, 2001), and also provide optimum conditions for the capture of SO_x using limestone and dolomite (Armesto *et al.*, 2003; Basu, 2006). Under FBC conditions the source of nitrogen oxides is the fuel-bound nitrogen (Köpsel and Halang, 1997; Chen *et al.*, 2001; Glarborg *et al.*, 2003). The use of FBC has been gradually increasing in both capacity and numbers over the past decades. However, the relatively low combustion temperatures employed in FBC increases the emission of N_2O compared to other combustion systems, nitrous oxide emitted from conventional boilers is approximately 5 ppm compared to fluidised bed combustors where the N_2O emissions are in the range of 15 to 200 ppm (Johnsson, 1994; Li *et al.*, 1997; Chen *et al.*, 2001; Armesto *et al.*, 2003; Glarborg *et al.*, 2003).
There are three basic ways in which nitric oxide can be formed (Köpsel and Halang, 1997; Hill and Smoot, 2000; Normann *et al.*, 2008):

- *Thermal* NO: is formed due to the gas phase reaction between molecular oxygen (O_2) and nitrogen (N_2) in the atmosphere at temperatures exceeding 1500°C . The reaction is depicted by the Zeldovich mechanism:

$$N_2 + O \rightleftharpoons NO + N \tag{2.1}$$

$$N + O_2 \rightleftharpoons NO + O \tag{2.2}$$

$$N + OH \rightleftharpoons NO + H \tag{2.3}$$

- *Prompt* NO: is formed from the reaction between molecular nitrogen and hydrocarbon radicals, which produce a nitrogen radical which subsequently reacts with oxygen.

- *Fuel* NO: this is formed due to the oxidation of coal-bound nitrogen. This is the reaction responsible for the formation of nitrogen oxides under fluidised bed combustion (Johnsson, 1994).

2.3.1 Nitric Oxide (NO)

The conversion of coal bound nitrogen (fuel-N) to nitric oxide is quite complex (Johnsson, 1994; Chen *et al.*, 2001). The process involves a primary step of devolatilisation, where organically bound nitrogen is partitioned into volatile-nitrogen (volatile-N) and char-nitrogen (char-N). The nitrogen in the volatile stream is known to exist as NH_3, HCN and tar-nitrogen (Johnsson, 1994; Chen *et al.*, 2001). Volatile-N and Char-N is oxidised to either NO or N_2O, and simultaneously partly reduced to N_2. A simplified overall reaction scheme illustrating the main formation and reduction of NO paths that takes place in a fluidised bed combustor is given in Figure 2.1 (Johnsson, 1994).

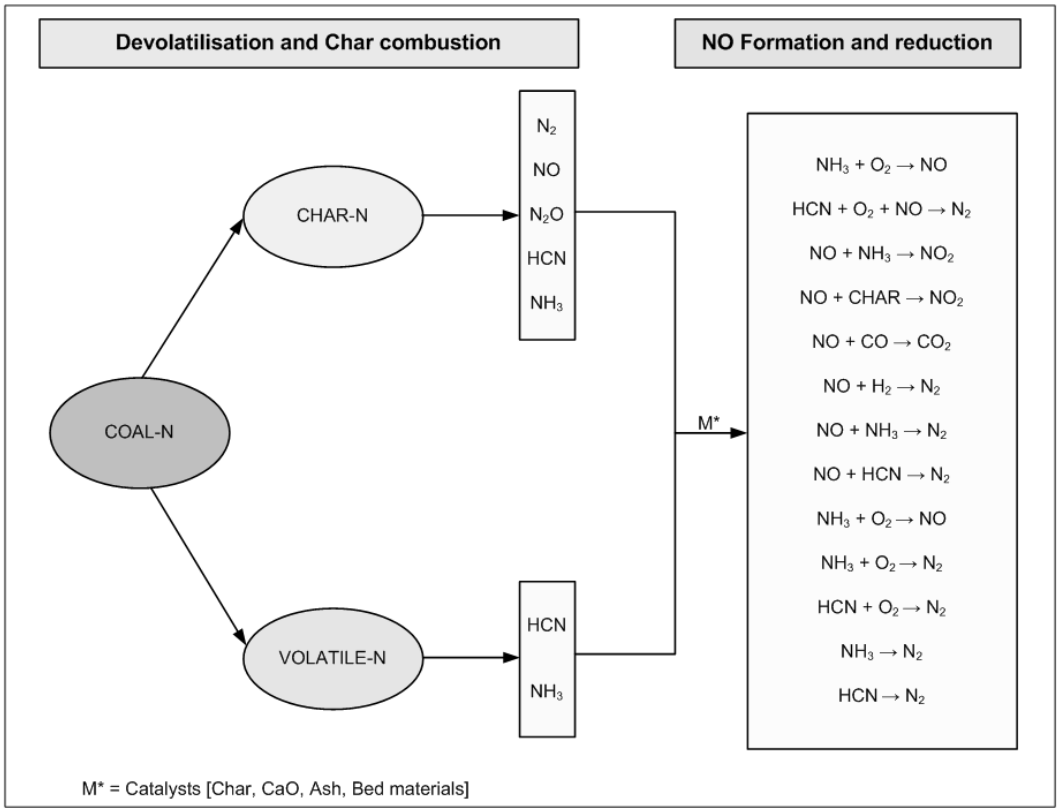

Figure 2.1: Simplified reaction scheme for NO formation and reduction (Adapted from Johnsson, 1994)

2.3.2 NO-Char Reactions

Nitric oxide (NO) produced during fluidised bed combustion can be heterogeneously reduced *in-situ* by the carbonaceous solid intermediates formed

during burnout (Aarna and Suuberg, 1997; Köpsel and Halang, 1997). The non-catalytic reduction of NO by char formed *in-situ* is considered to be the most important reaction of NO destruction (Furusawa *et al.*, 1985). The NO-carbon reaction is complex, involving initially the chemisorption and desorption of surface complexes.

Several aspects of these reactions are not well known; for instance, the nature of active sites by which the carbon can reduce NO to N_2 is still not well understood (Lazaro *et al.*, 1996; Aarna and Suuberg, 1997). Some evidence is available which suggests that these sites are different from those involved in gasification by oxygen. Aarna and Suuberg (1997) arrived at this conclusion by comparing the annealing behaviour towards NO and O and on the unusual result that many graphites exhibit higher surface-area-normalised reactivity towards NO than do several more disordered carbons.

Yamashita and Tomita (1993) reported that the presence of carbon-oxygen complexes on the char surface enhances the reactivity of NO with carbon. The formation of N_2 from the C-NO reaction can be attributed to the reaction between surface nitrogen species $C(N)$ and gaseous NO (Kyotani and Tomita, 1999).

$$2C() + NO \longrightarrow C(N) + C(O) \tag{2.4}$$

$$C(N) + NO \longrightarrow N_2 + C(O) \tag{2.5}$$

The $C()$ in Equation (2.4) denotes a carbon free site and $C(O)$ indicates a surface carbon-oxygen complex. Chambrion *et al.*, (1997) illustrated that the presence of $C(O)$ enhances the char reactivity towards NO. Depending on the severity of the reaction conditions, the O atom from NO either remains as $C(O)$ on the carbon surface or desorbs as CO (Kyotani and Tomita, 1999). Teng *et al.*, (1992) indicated that the overall non-stoichiometric reaction mechanism could be summarised as follows:

$$NO + C + C(O) \longrightarrow CO + CO_2 + N_2 + C(O)' \tag{2.6}$$

where $C(O)'$ indicates a carbon oxide surface product that might be different from the initial reactant $C(O)$ carbon surface oxide. NO is reduced to N_2, and both CO and CO_2 are also products of the reduction reaction. The products of the NO-carbon reaction are generally found to be N_2, CO and CO_2 (Teng *et al.*, 1992; Johnsson, 1994; Li *et al.*, 1997; Chen *et al.*, 2001). The overall

reactions can be expressed as follows:

$$C + 2NO \longrightarrow CO_2 + N_2 \tag{2.7}$$

$$C + NO \longrightarrow CO + \frac{1}{2}N_2 \tag{2.8}$$

$$CO + NO \longrightarrow CO_2 + \frac{1}{2}N_2 \tag{2.9}$$

Teng *et al.*, (1992) and Li *et al.*, (1997) pointed out that the reaction depicted by Equation (2.9) above is a catalytic reaction (catalysed by carbon), based upon the observation that NO reduction by carbon is enhanced in the presence of CO. The reactions, Equation (2.7) and Equation (2.8), are carbon consuming. Furusawa *et al.* (1985) studied both carbon consuming reactions and the catalytic reaction by measuring the material balances over the FBC temperature range. The findings showed that at low temperatures (994-1078K), the quantity of CO produced was stoichiometrically equal to the molar amount of NO reduced and to the molar amount consumed. The catalytic reaction, Equation (2.9), becomes the overall reaction scheme. At higher temperatures (1120-1194K), the molar amount of CO_2 formed was found to be less than that represented by the catalytic reaction, Equation (2.9), implying that the carbon consuming reactions become significant. This implies that the carbon consuming reactions dominates the reduction of NO as the temperature increases.
Kyotani and Tomita (1999) simulated the chemisorption of two NO molecules on the carbon surface as depicted in Figure 2.2(a) and the subsequent desorption of the formed surface species as shown in figure 2.2(b) using an ab initio molecular orbital theory calculation.

NO-carbon reactions basically follow first order reaction kinetics with respect to NO concentrations (Li *et al.*, 1998).

2.4 Nitric Oxide Reduction in Fluidised Bed Combustion

Fluidised bed combustion has emerged as an environmentally attractive technique for combusting coal (Liu *et al.*, 1999), primarily due to the low temperature used, ranging from 750-900°C. The easiest way to suppress NO emissions in coal combustion is to decrease the combustion temperature (Chen

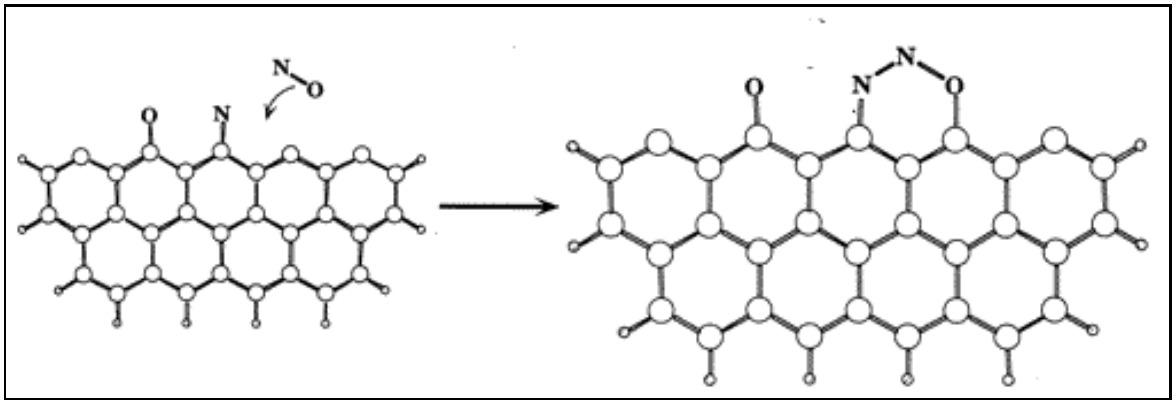

(a) Chermisorption of two NO molecules on carbon surface

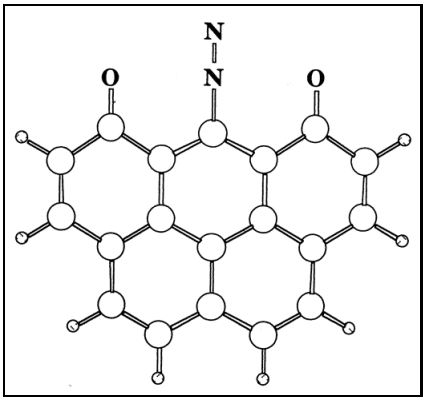

(b) N_2 desorption from the carbon surface

Figure 2.2: A diagram adapted from Kyotani and Tomita, (1999) illustrating the chemisorption of NO and desorption of the N_2 molecule

et al., 2001; Tomita, 2001), thus when FBC is operated at relatively low temperatures it hinders the formation of thermal-NO. The main advantages of using FBC as outlined by Basu (2006) are:

- Low emission of NO is a major attractive feature of both bubbling fluidised bed combustors (BFBC) and circulating fluidised bed combustors (CFBC).
- The ability of sulphur removal *in situ*.
- Fuel flexibility; the ability to burn a variety of fuels without major amends and drawbacks on performance.
- High combustion efficiency; combustion efficiency of CFBC is generally in the range of 97,5-99.5% and that of BFBC is from 90.0-98.0%.

2.4.1 Factors affecting nitrogen oxides emission

Factors affecting the rate of nitrogen oxides emission in FBC include the combustion conditions, coal related factors and the combustor design (Thomas, 1997; Chen *et al.*, 2001; Gungor, 2009). The overall emission level of nitrogen oxides is determined by the importance of formation and *in-situ* destruction processes (Furusawa *et al.*, 1985; Matos *et al.*, 1990). The purpose of nitrogen oxides controlling technologies is either to decrease NO_x formation by moderating combustion temperature or to enhance the reduction of NO_x formed.

Combustion factors

Combustion factors may be split into two, (1) combustor design and size (Chaiklangmuang *et al.*, 2002), and (2) combustion conditions used (Li *et al.*, 1998).
There are quite a number FBC technologies employed - bubbling, circulating, pressurised, as well as the size of the combustor for controlling NO_xemission (Chen *et al.*, 2001). These technologies include low-NO_x burners, overfire air (air staging), tangential burner firing, reburning (fuel staging), flue gas recirculation and boiler load. The underlying principle in combustor designs is to create a fuel-rich primary zone where devolatilisation takes place (Chaiklangmuang *et al.*, 2002). This favours the conversion of nitrogen in the volatiles to

N_2 and the low temperature does not favour the production of thermal-NO_x. If the combustor is large enough to give a residence time of several seconds, then the NO initially formed in the fluidised bed is reduced by carbon at the top of the bed. The secondary or tertiary treatment of flue gases involves the use of additives such as ammonia, urea and cyanuric acid (Harding *et al.*, 1996), in selective catalytic reduction (SCR) and selective non-catalytic reduction (SNCR).

Nitric oxide emission increases with increasing excess air ratio (Mann *et al.*, 1992; Shen *et al.*, 2003) and the conversely, low excess air and air staging reduce NO emissions (Johnsson, 1994). Nitric oxide emanates from both volatile and char-nitrogen combustion, and as the combustion progresses char becomes the reductant of NO. Operating conditions in FBC like fuel type (or coal rank), excess air, limestone feed, pressure, air staging, boiler load with respect to nitrogen oxides emission are contradictory (Chen *et al., 2001*). This arises due to different FBC technologies, size of combustor and the complex formation and destruction of NO. Mirek *et al.* (2007) showed that the shape of the air nozzles used for fluidisation in CFBC has a marked impact on the reduction of nitrogen oxides.

Coal related factors

Coal attributes that are most likely to influence the formation of nitrogen oxides during combustion are; (1) coal structure, this includes rank and volatile matter present, (2) char structure and reactivity, (3) total nitrogen content and (4) nitrogen functionality in the coals (Kambara *et al.*, 1993; Liu *et al.*, 1999), its subsequent conversion to volatile nitrogen species and char nitrogen.

Kurose *et al.* (2001a) and Kurose *et al.* (2001b) carried out studies on the effect of moisture on coal combustion characteristics and found that the contribution of thermal-NO_x to the total NO_x drastically decreased with increasing moisture content and on the other hand the emission of fuel-NO_x increases. Also, increase in moisture results in an increase of unburned fraction and a decrease of conversion ratio to NO_x.

Chaiklangmuang *et al.* (2002), pointed out that the volatile matter content of coal plays an important role in determining nitrogen oxides emission. In unstaged burners the NO formed tends to increase with the volatile matter content, but in staged burners the NO formed tends to decrease with increasing volatile content. The major part of the NO formed is released from

the char nitrogen during the later stages of combustion.
Quartenary nitrogen is converted to NH_3, and nitrogen in the form of pyridine and pyrrole is partly converted to HCN (Kambara *et al.*, 1993).

2.5 Char kinetics

The total reaction rate for the gas-char reaction depends on the intrinsic surface reaction r_s and structure of the char particles (structure factor $f(X)$). Intrinsic properties of different chars have been related to char reactivity and also kinetic behaviour by different investigators (Takarada *et al.*, 1985). Reaction rates are influenced by a number of variables which include particle size and distribution, mineral matter content of char (Köpsel and Halang, 1997; Zhao *et al.*, 2003), char porosity and pretreatment, partial pressure of reactant gases and temperature. These variables have a complex and obscure impact on char reactivity. Thus the reaction rate expression can be presented as follows (Lu and Do, 1992):

$$\frac{dX}{dt} = r_s(T, C)f(X) \tag{2.10}$$

There are three main factors affecting the intrinsic reactivity of chars derived from coal (Takarada *et al.*, 1985):

- Chemical composition that particularly affects the imperfections of the carbon structure (active sites).
- The coal ash content which may provide the catalytic effects.
- The rank of the coal which determines the pore size and structure.

The determination of these properties (characterisation) is very important in reaction kinetics investigations. The reactivity of the chars has been observed to increase as the rank of coal decreases. Some investigators (Hayhurst and Lawrence, 1997; Köpsel and Halang, 1997; Lissianski *et al.*, 2001; Zhao *et al.*, 2002) have also observed the catalytic effects of iron, calcium, sodium, potassium and magnesium on the reactivity of chars. De-ashed chars are normally used to annihilate the catalytic effects of metal constituents in chars. This is done by washing the chars in an acid, usually hydrochloric acid. Köpsel and Halang (1997) deduced that ash has a positive influence with regard to the reduction of nitrogen oxides.

In calculating reactivity R (s^{-1}), some investigators (Teng *et al.*, 1997; Ollero *et al.*, 2002) working on gasification experiments have used Equation (2.11)

$$\mathrm{R} = -\frac{1}{\mathrm{m} - \mathrm{m_{ash}}}\frac{\mathrm{dm}}{\mathrm{dt}} = \frac{1}{1 - \mathrm{X}}\frac{\mathrm{dX}}{\mathrm{dt}} \tag{2.11}$$

where m is the mass of the char, $\mathrm{m_{ash}}$ is the mass of the ash, X is the degree of conversion given by Equation (2.12)

$$\mathrm{X} = \frac{\mathrm{m_\circ} - \mathrm{m_t}}{\mathrm{m_\circ} - \mathrm{m_{ash}}} \tag{2.12}$$

of which $\mathrm{m_\circ}$ represents the initial mass of the dried and pyrolysed sample and m_t is the mass of the sample at any given time t during the course of the reaction.

2.6 Reaction rate models

Models often used for coal combustion and/or gasification include the homogeneous model, shrinking core model and the random pore model which was also used by Kaitano (2007) on gasification of char that is rich in inertinite and has a high ash content. Li *et al.*, (1999) carried out a kinetics study of NO-char in a TGA and proposed a new model by considering the contribution from different carbon-oxygen surface complexes during the reaction. Wang *et al.*, (2005) also used a TGA to investigate the reactions of graphon and coal char (carbonaceous materials) with NO, $\mathrm{O_2}$ and $\mathrm{NO} + \mathrm{O_2}$ using a method of direct nonlinear regression of the kinetic equation to obtain the kinetic parameters from the TG curve of carbon gasification in various atmospheres. Sun *et al.*, (2009) performed isothermal experiments in a drop-tube furnace (DTF) and compared the results of NO-char kinetics with those carried out in a TGA, a random pore model (RPM) was used to describe the results.

2.6.1 Homogeneous model

The homogeneous model is also referred to as the progressive-conversion model. The reactant gas is envisioned as entering and reacting right through a porous core at all times with different reaction rates at different zones within the particle. The solid reactant is converted continuously all over the

particle (Fogler, 1992), however, this is most likely achievable for very slow char conversion reactions. The reaction rate expression is given by:

$$X = 1 - e^{-kt} \tag{2.13}$$

2.6.2 Shrinking core model

The shrinking core model is also known as unreacted core model. It states that the reaction between the gas and the solid takes place on the outer edges of the particle (Fogler, 1992). As the exterior film of the particle reacts, the region of reaction moves into the solid. In this case, the particle may uniformly shrink as the solid is converted to gaseous products or may retain its original size by entirely leaving behind converted material and inert solids, referred to as ash in coal combustion. This implies that at any given time there is a non-reacted core remaining as the carbonaceous particle continues to shrink in size. According to Lu and Do (1992), the shrinking core model for spherical particles with surface reaction controlling its structure factor is given by:

$$\mathrm{f(X)} = \frac{\mathrm{S_o}\,(1-\mathrm{X})^{\frac{2}{3}}}{(1-\varepsilon_o)} \tag{2.14}$$

Everson *et al.*, (2005, 2006a and 2006b) have successfully used the model for predicting coal conversion kinetics. However, the shortcoming of the shrinking core model is that it does not account for structural changes like surface area and porosity occurring during char reaction, it only incorporates the initial porosity and surface area.

2.7 Nitric oxide-char reaction rate models

This section focuses on the kinetic models employed by researchers that have worked on NO-char reactions.

2.7.1 Direct non-linear regression

Wang *et al.*, (2005) investigated the kinetics of carbon reactions with NO, O_2 and NO+O_2 using thermogravimetric analysis. They applied direct non-linear

regression of the kinetic equation to obtain the kinetic parameters. This either involved a single-process mechanism or a two-process mechanism.
The theoretical considerations made by Wang and co-workers (2005) for kinetic calculations from the thermogravimetric data oftenly emanates from the basic kinetic equation

$$\frac{\mathrm{dX}}{\mathrm{dt}} = \mathrm{Ae}^{-\frac{\mathrm{E}}{\mathrm{RT}}}\mathrm{f(X)} \tag{2.15}$$

where X is degree of conversion, t is time, A is frequency factor, E is the apparent activation energy, T is the absolute temperature and R is the molar gas constant, where the function $\mathrm{f(X)}$ is dependent on the assumed reaction mechanism. For carbon oxidation

$$\mathrm{f(X)} = (1 - \mathrm{X})^{\mathrm{n}} \tag{2.16}$$

where n is the reaction order.
Substituting Equation (2.16) into Equation (2.15), the kinetic equation in the form of Equation (2.17) is obtained.

$$\frac{\mathrm{dX}}{\mathrm{dt}} = \mathrm{Ae}^{-\frac{\mathrm{E}}{\mathrm{RT}}}(1 - \mathrm{X})^{\mathrm{n}} \tag{2.17}$$

Equation (2.17) is additive for several independent parallel processes and can be expanded for p different processes.

$$\left(\frac{\mathrm{dX}}{\mathrm{dt}}\right)_{\mathrm{tot}} = \sum_{\mathrm{p}} \frac{\mathrm{dX_p}}{\mathrm{dt}} = \sum_{\mathrm{p}} \mathrm{A_p e}^{-\frac{\mathrm{E_p}}{\mathrm{RT}}}(1 - \mathrm{X_p})^{\mathrm{n_p}} \tag{2.18}$$

Wang *et al.*, (2005) then considered the time step small enough for derivatives to be replaced by differences. The rearranged expression then led to the recurrence form

$$(\mathrm{X_i})_{\mathrm{tot}} = \sum_{\mathrm{p}} \mathrm{X_{p,i-1}} + \sum_{\mathrm{p}} \mathrm{A_p e}^{-\frac{\mathrm{E_p}}{\mathrm{RT_{i-1}}}}(1 - \mathrm{X_{p,i-1}})^{\mathrm{n_p}}(\mathrm{t_i} - \mathrm{t_{i-1}}) \tag{2.19}$$

Equation (2.19) enabled Wang and fellow workers (2005) to construct a theoretical thermogravimetric curve and to evaluate kinetic parameters $\mathrm{A_p}$, $\mathrm{E_p}$ and $\mathrm{n_p}$ for overlapping processes from thermogravimetric data by non-linear regression.

2.7.2 Computational modelling

For computational modelling Aarna and Suuberg (1997) used least-squares regression over 24 data sets obtained from NO reduction by coal char by applying Equation (2.20). This is also reported by Jones *et al.*, (1999).

$$\mathrm{R_{NO}} = 2.6 \cdot 10^{4} \exp\left(\frac{-15900}{\mathrm{T}}\right) \mathrm{A_E P_{NO} mols^{-1}} \tag{2.20}$$

$\mathrm{A_E}$ is the char external surface area ($\mathrm{m^2 g^{-1}}$ and $\mathrm{P_{NO}}$ is the partial pressure of NO (atm). Jones *et al.*, (1999) also pointed out that the rate of NO reduction by carbon has also been determined from Equation (2.21)

$$\mathrm{R_{NO}} = \alpha_{\mathrm{NO}} \mathrm{Z_{NO}} \mathrm{A_p} \tag{2.21}$$

where α_{NO} is the reaction probability of the NO molecule, $\mathrm{Z_{NO}}$ is the collision number per time and per unit area and $\mathrm{A_p}$ is the surface area of the reacting particle. The reaction probability (α_{NO}) is given by Equation (2.22)

$$\alpha_{\mathrm{NO}} = 1.82 \exp\left(\frac{-15000}{\mathrm{T}}\right) \tag{2.22}$$

2.7.3 Random pore model

Application of the random pore model on NO-carbon reactions has been reported in literature (Gray and Do, 1993; Lu and Toh, 1993; Li *et al.*, 1997; Sun *et al.*, 2009). These studies applied the random pore model or modified random pore model derived by Bhatia and Perlmutter (1980), and Galavas (1980). They independently derived a more rigorous model based on the assumption that the volume enclosed by the moving pore and reaction surfaces is randomly distributed in the char. Both sets of researchers approached their derivations differently.

This model addresses the issue of structural changes that takes place within the char particle during the course of the reaction. It is a model that consists of randomly intersecting cylindrical pores. For simplicity of surface area and porosity calculations the capillaries are perceived to be uniform. This assumption, however, limits the model's applicability since chars have a wide pore size distribution. The NO-carbon reaction rate is expressed as

$$\frac{dX}{dt} = \frac{r_s (1 - X) S_\circ \sqrt{1 - \psi \ln(1 - X)}}{(1 - \varepsilon_\circ)} \tag{2.23}$$

where ψ is the structural parameter and X is the carbon conversion. A detailed application of the random pore model is presented in Chapter 5.

CHAPTER 3

Coal and Char Characterisation

3.1 Introduction

This chapter focuses on the characterisation of the parent coals and the respective chars and results thereof. Several detailed characterisation techniques were employed. The origin of the coal samples is given in Section 3.2, while the char preparation procedure and instruments used are given in Section 3.3. The techniques used for characterisation are outlined in Section 3.4. The characterisation results and the subsequent discussion which form an integral part of this chapter are presented in Section 3.5; it includes petrographic (organic composition and reflectance properties), chemical and physical structural characteristics. A summary of characterisation results is given in Section 3.6.

3.2 Origin of coal samples

The six low grade coal samples used in this study were supplied by Eskom which is South Africa's sole power utility company. The samples were obtained from different coal sites around South Africa. The chosen low grade samples were characterised by high ash content and were rich in inertinites.

These are the typical factors that limit their application in conventional pulverised fuel combustion.

3.3 Char preparation: pyrolysis at 900°C

A photograph and schematic presentation of the packed bed reactor system shown on Figure 3.1 was used for preparing chars. It consists of a vertical tubular furnace mounted on a high precision analytical balance supported by a tripod stand. Nitrogen gas was introduced into the reactor at a specified flow rate by means of a control unit.
The parent coal used for preparing chars was received in various particle sizes ranging from fine powder to particles with approximately 5 cm diameter. The char samples were prepared by heating the respective parent coals in an inert nitrogen atmosphere at a constant heating rate of $20°C{\cdot}min^{-1}$ up to a temperature of 900°C. The final temperature (900°C) was then held isothermally for 60 minutes. A final constant weight signified that almost all the volatiles have been driven off. One millimetre char particles were then sieved and stored in an airtight container under nitrogen atmosphere.

3.4 Characterisation techniques

3.4.1 Chemical analysis

The proximate and calorific value determinations, total sulphur and ultimate analysis were conducted by the South African Bureau of Standards (SABS) Mineral Laboratory, Richards Bay. Procedure or methods employed are shown on Table 3.1.

3.4.2 Physical Structural Analysis

The physical structural analysis was carried out only on char samples. The Micromeritics ASAP 2020 Accelarated Surface Area and Porosimetry analyser was used to measure the micropore surface area of chars by applying the carbon dioxide adsorption technique at 273K. This equipment has the capability of measuring pore sizes ranging from 4 to 5000Å (Gregg and Sing,

(a) A photograph of a packed bed reactor

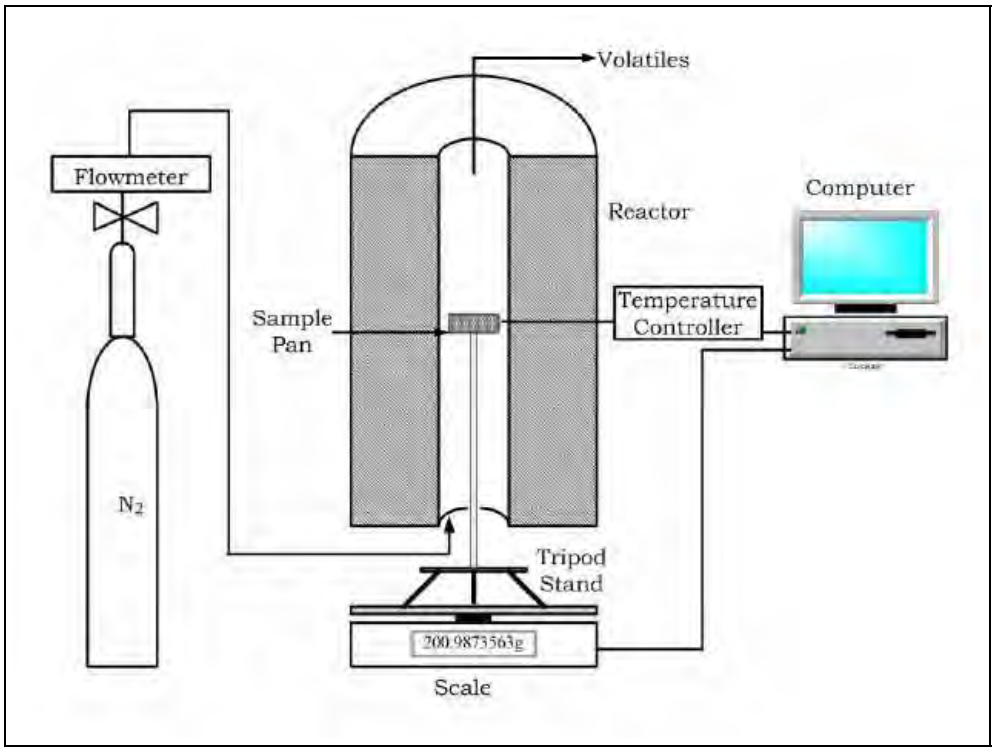

(b) Schematic presentation of a packed bed reactor system

Figure 3.1: A photograph and schematic representation of the packed bed reactor system

Table 3.1: Analytical methods used

Proximate Analysis	Method	**Ultimate Analysis**	Method
Sample preparation	SABS 0135:1997	Carbon	ASTM D 5373
Moisture content	SABS Method 925	Hydrogen	ASTM D 5373
Ash content	SABS ISO 1171:1997	Nitrogen	ASTM D 5373
Volatile matter	SABS ISO 562:1998	Hydrogen	ASTM D 4239 1997
Fixed Carbon	By Difference	Oxygen	Calculated
Gross calorific value	SABS ISO 1928:1995		

1982; Stanley-Wood and Lines, 1992). Carbon dioxide was adsorbed onto the char surface at 273K.
Before the gas adsorption experiments, the chars were degased under a vacuum in order to eliminate surface adsorbed species like moisture and/or condensed volatiles, which might hinder the adsorbate accessibility. Degassing was perfomed at ambient temperatures.
The Micromeritics ASAP 2020 makes use of two independent vacuum systems, one for degasing the sample and the other is reserved for sample analysis, this allows degasing and analysis to run concurrently without the delay inherent in typical single vacuum system analysers.

3.4.3 Petrographic Analysis

Petrographic analysis was undertaken by Petrographics SA in Pretoria (Du Cann, 2008). Coal petrology comprises of microscopic examination of coals/chars together with the interpretation of the analytical data to provide valuable information regarding organic composition, maturity and the associations of the organic matter with minerals contained in the coals or chars (Tsai, 1982; Kabe *et al.*, 2004). The coal and char samples were milled to a particle size of -2.5mm for the petrographic analysis. A polished block was examined under a reflected light microscope and macerals (and char carbon forms) were identified under an immersion medium by their relative reflectance, morphology and colour.

- *Preparation*
  The petrographic block for each coal or char sample was prepared and

polished as prescribed in the guidelines of the ISO 7402-2, 1985 standard, and then examined under a reflected light microscope.

- *Reflectance*
  Vitrinite reflectance was done only on the parent coal samples. Total maceral reflectance scan measurements were conducted on both coal and char samples in accordance with the ISO Standard 7404-5, 1994. A total random reflectance scan was done on each sample with a total of 250 reflectance readings being obtained on all macerals with respect to coal samples and carbon forms in case of chars, over the polished surface of the petrographic block.

- *Organic Analysis*
  A quantitative analysis of the organic constituents in coal (macerals) and char (carbon forms) samples was performed. The respective proportions (volume percentage) of the macerals and char carbon forms were determined on the basis of a point-count procedure (500 point-count) according to the method set out in the ISO Standard 7404-3, 1994.

The microscopic components of the coal and char samples were assessed by attributes of their colour, reflectance, degree of anisotropy, size, morphology, the extent of devolatilisation and porosity.

3.4.4 X-ray Diffraction Analysis (XRD)

The XRD analysis was done at the laboratories of the Department of Geology at Pretoria University (courtesy of Dr. Sabine Verryn). The back loading method was used for preparation of the char samples prior to the XRD analysis. A PANalytical X'Pert Pro powder diffractometer combined with a X'Celerator detector with variable divergence and receiving slits with Fe filtered Co-K α radiation was used for the XRD analysis of the chars. X'Pert Highscore Plus software was used to identify the phases. The relative phase quantities (as weight %) were estimated using the Rietveld method (Autoquan Program).

3.5 Results and Discussion

3.5.1 Chemical Analysis

The comparison between coals and the respective chars' proximate, ultimate and gross calorific value results is outlined on Table 3.2 and Figure 3.2. Both coal and char composition covers a wide spectrum, with ash content of the parent coals ranging from 37% while the char counterparts had 49% and above. In retrospect, all six coal and char samples had high ash content. Figure 3.2(a) presents a comparison of the volatiles between the coals and the subsequent chars. Fixed carbon variations of the parent coals coupled with the char comparisons is presented on Figure 3.2(b). Gross calorific values of the coals and chars are shown on Figure 3.2(c), it is apparent that the chars have a slightly lower gross calorific value than the parent coals. This is attributed to the energy of the volatile stream liberated during char preparation. The ultimate analysis reveals that the coals had approximately 1% nitrogen bound in the coal and ranging from 0.03 to 0.8% in the respective char samples. It is generally known that this is the nitrogen responsible for the formation of nitrogen oxides during fluidised bed combustion (Johnsson, 1994). Figure 3.2(d) illustrates the ash content in coal and the respective chars.

Table 3.2: Proximate and ultimate analysis results for coal and char samples

		Coal						**Char**					
		A2	D1	D3	E1	E3	F1	A2	D1	D3	E1	E3	F1
Proximate Analysis (db)	(wt)												
Ash	(%)	48.7	41.6	37.0	39.7	38.6	47.1	62.0	54.2	49.0	52.2	57.5	63.7
Volatiles	(%)	20.7	20.7	21.5	20.5	20.0	19.6	3.8	3.2	4.0	3.4	2.0	3.1
Fixed Carbon	(%)	30.6	37.7	41.5	39.8	41.4	33.3	34.2	42.6	47.0	44.4	40.5	33.2
Gross Calorific Value	($MJ \cdot kg^{-1}$)	14.5	15.1	16.4	18.2	17.0	14.8	12.1	14.8	16.1	15.7	14.3	12.6
Ultimate Analysis (ad)													
Carbon	(%)	35.6	40.3	43.9	45.6	43.8	37.4	33.4	42.4	46.1	43.1	33.2	30.0
Hydrogen	(%)	2.9	3.0	3.2	2.9	2.9	2.3	0.9	1.0	1.1	0.8	0.9	0.8
Nitrogen	(%)	0.9	0.9	1.0	1.0	1.0	1.0	0.3	0.7	0.8	0.03	0.6	0.6
N/C		0.03	0.02	0.02	0.02	0.02	0.03	0.010	0.017	0.017	0.001	0.018	0.02
Total Sulphur	(%)	1.6	0.6	0.4	1.6	1.1	1.9	1.4	0.6	0.5	1.8	2.3	2.2
Oxygen (by diff.)	(%)	11.2	15.9	16.8	10.1	13.9	11.1	1.2	0.1	0.9	1.0	5.7	2.1

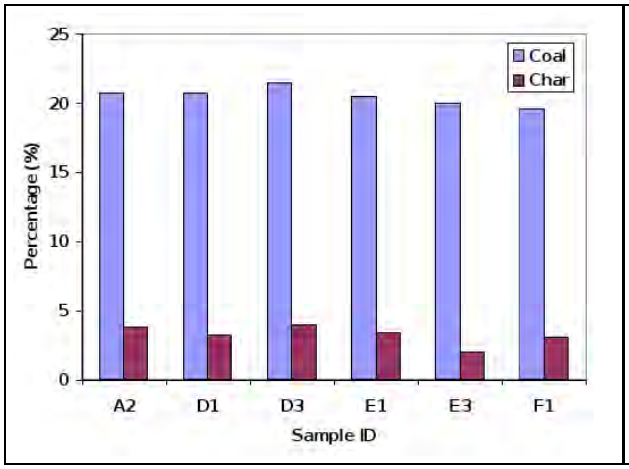

(a) Reduction of volatiles from the parent coals to the subsequent chars (db)

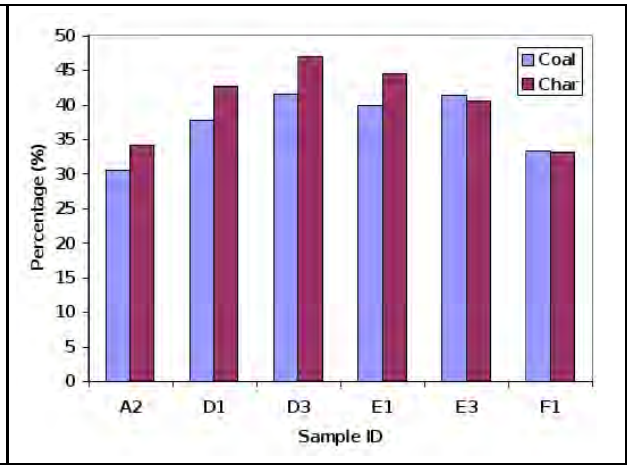

(b) Fixed carbon in the parent coals and the produced chars (db)

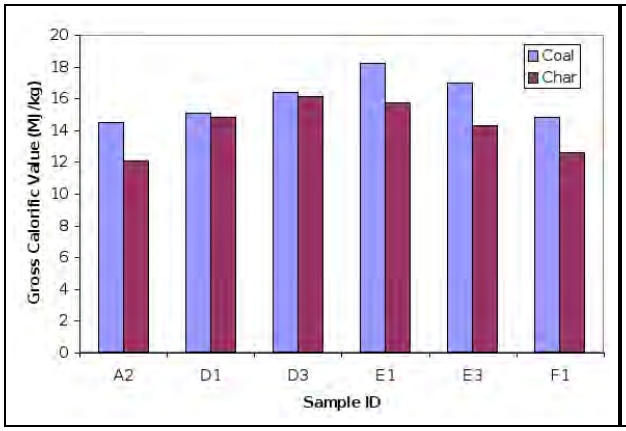

(c) Gross calorific values of coal and respective char samples (db)

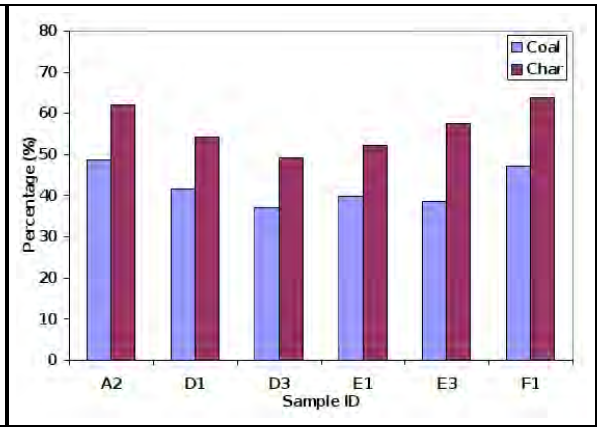

(d) Ash content of the parent coals and the formed chars (db)

Figure 3.2: Comparison of parent coals with respective chars

3.5.2 Physical Structural Analysis Results

The Dubinin-Radushkevich surface area equation (S_{D-R}) (Yang, 1987) was applied to calculate the total surface area. The results of the carbon dioxide Dubinin-Radushkevich micropore surface area (S_{D-R}) and monolayer pore volume are displayed on Table 3.3. Char D1 exhibits the highest micropore surface area and monolayer pore volume. Char F1 has the least value for both micropore surface area and mono layer pore volume, it is also characterised by the highest ash content amongst the six chars. There is no defined trend of the surface area of the chars when linked with other char characteristics.

It is given in literature that carbon dioxide gives a better characterisation of small microporosity whose diameter is less than 2nm (Walker *et al.*, 1988) as compared to nitrogen adsoption (Garrido *et al.*, 1987). This is due to the faster diffusion of carbon dioxide into finer micropores at 273K than nitrogen diffusion at 77K (Walker *et al.*, 1988; Garrido *et al.*, 1987). Carbon dioxide has been frequently used to measure surface areas of coals and chars (Alvarez and Borrego, 2007; Borrego and Alvarez, 2007).

Table 3.3: Carbon dioxide char micropore surface area S_{D-R} (Dubinin-Radushkevich) and monolayer pore volume.

		Char ID					
		A2	D1	D3	E1	E3	F1
Micropore surface area	($m^2 \cdot g$)	128.65	249.98	235.47	119.70	112.14	102.17
Monolayer pore volume	($m^3 \cdot g$)	28.163	54.722	51.545	26.204	24.548	22.366

3.5.3 Petrographic Analysis

Results of the petrographic characteristics of the six original parent coals and the subsequent chars are presented, including; organic composition which encompasses maceral and microlithotypes analyses, carbominerite and minerite analyses on parent coals and the carbon form analysis on the chars. Reflectance properties which includes vitrinite reflectance (on parent coals only) and total maceral reflectance scans (on both coals and chars) are also given.

Reflectance Properties

According to the ISO 11760 - 2005 Classification of Coals, the obtained vitrinite random reflectance data implied that the six original parent coals were characterised as bituminous, Medium Rank D to C coals, with mean random reflectance of vitrinite values ranging from 0.58% to 0.78% Rr.
The total mean scan reflectances (Rsc) had shifted dramatically from values of about 1% in parent coal towards substantially higher ranges of above 4% of reflectance in chars as depicted on Table 3.4. The shift in reflectance is clearly illustrated on the reflectance histograms of the parent coals placed adjacent to the histograms of the respective chars as shown in Figure 3.3 to Figure 3.5. Kaitano (2007) and Everson *et al.*, (2008b) also observed a similar transition in reflectance for chars that were also prepared at 900°C.
Principal evaluation of the general reflectance of organic components showed that carbon-rich particles had acquired hugely varying levels of reflectance as a result of the charring process. Increasing reflectance denotes increasing molecular ordering, which has a great influence on the combustion and gasification performances of coal/char structures (Du Cann, 2008).

Table 3.4: Major reflectance properties of coal and char samples

	Coal						**Char**					
	A2	D1	D3	E1	E3	F1	A2	D1	D3	E1	E3	F1
Vitrinite, Rr(%)	0.72	0.58	0.58	0.78	0.68	0.68						
σ(%)	0.098	0.075	0.085	0.095	0.086	0.086						
Mean scan values, Rsc (%)	1.09	1.14	1.10	1.46	1.45	1.29	5.02	4.84	5.00	5.45	5.06	5.18
Range reading, Rsc(%)	0.1-2.4	0.1-2.1	0.2-1.9	0.2-2.5	0.3-2.6	0.3-2.3	3.6-6.5	2.0-6.6	1.7-6.6	3.3-7.4	3.0-6.9	3.1-7.4
σ (%)	0.502	0.388	0.392	0.467	0.475	0.435	0.543	0.744	0.725	0.872	0.716	0.799

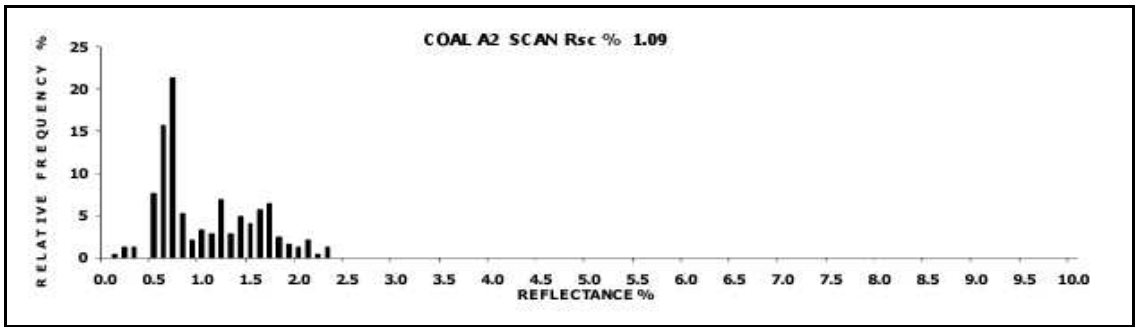

(a) Total reflectance scan for coal A2

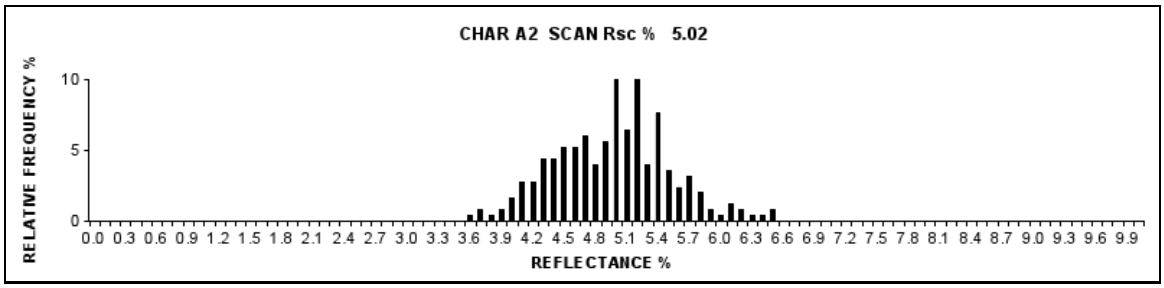

(b) Total reflectance scan for char A2

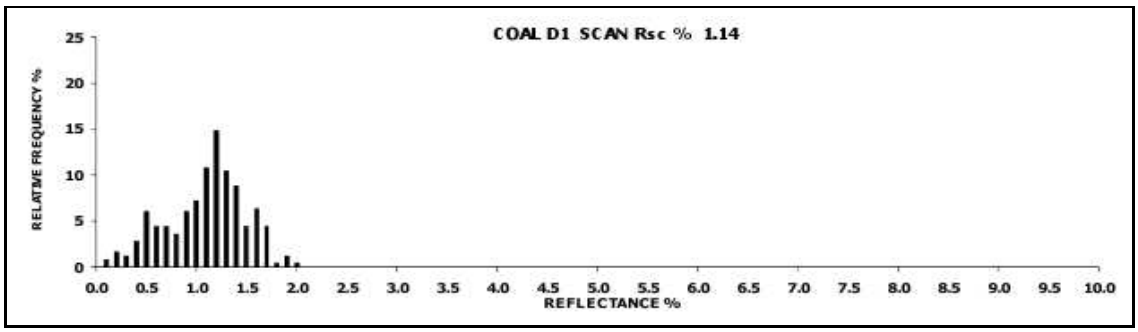

(c) Total reflectance scan for coal D1

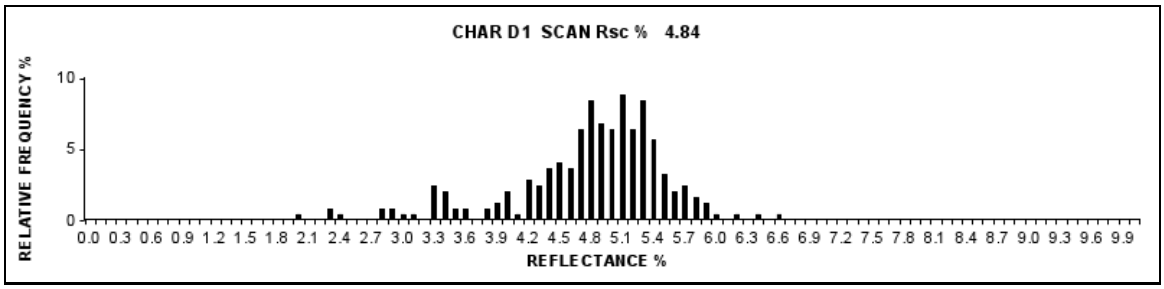

(d) Total reflectance scan for char D1

Figure 3.3: Total reflectance scan histograms for coal and char; A2 and D1

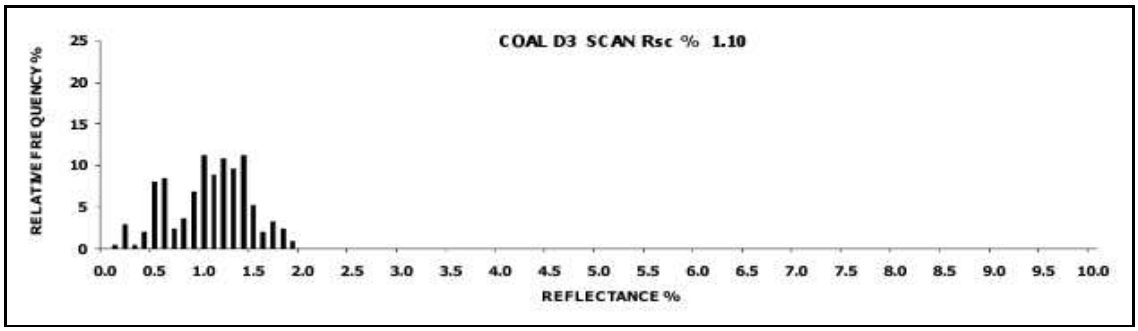

(a) Total reflectance scan for coal D3

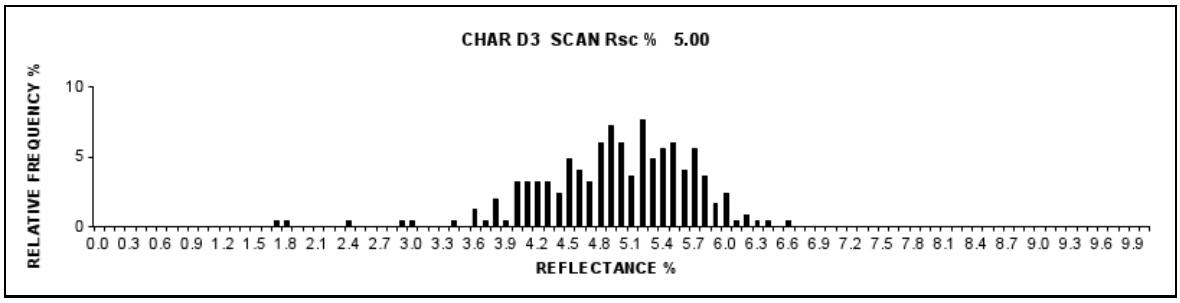

(b) Total reflectance scan for char D3

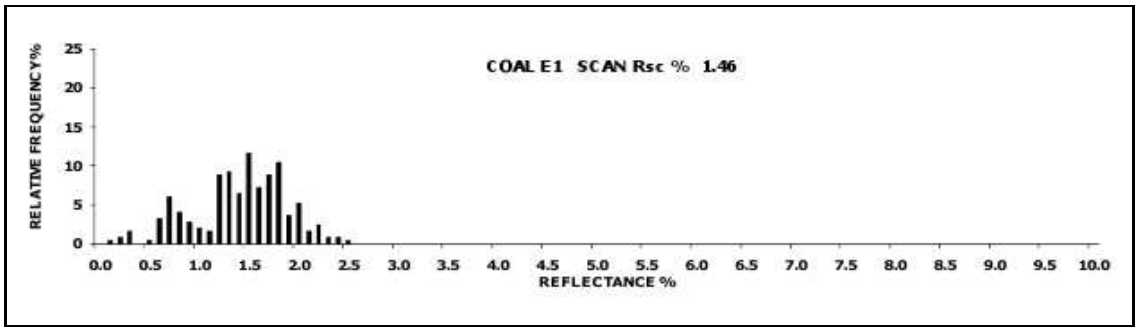

(c) Total reflectance scan for coal E1

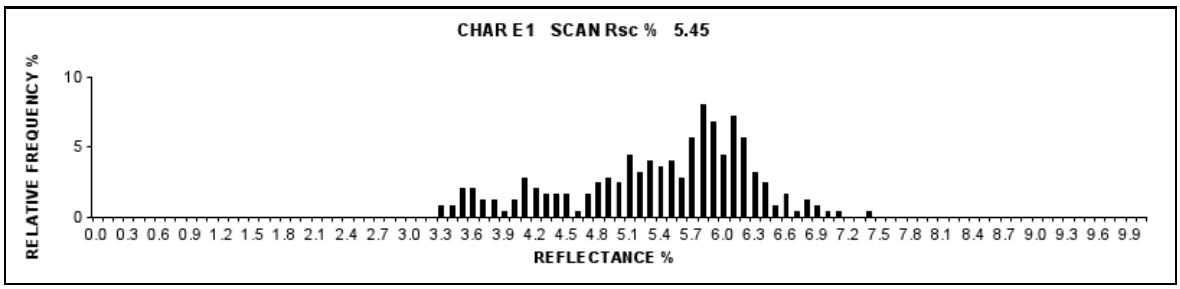

(d) Total reflectance scan for char E1

Figure 3.4: Total reflectance scan histograms for coal and char; D3 and E1

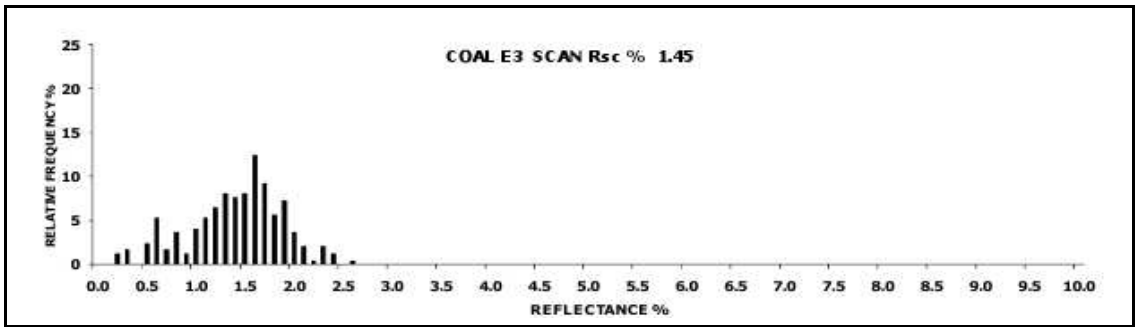

(a) Total reflectance scan for coal E3

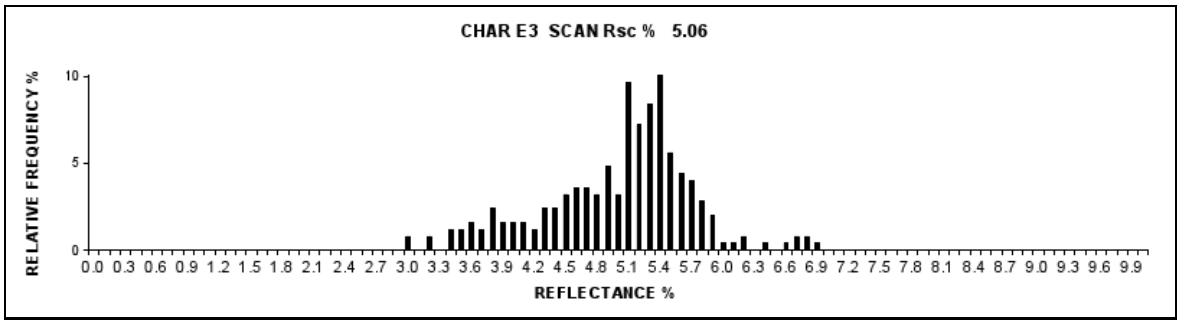

(b) Total reflectance scan for char E3

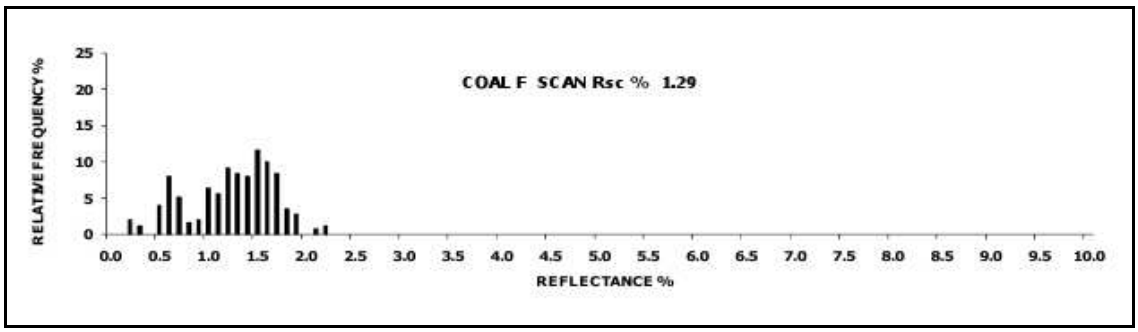

(c) Total reflectance scan for coal F1

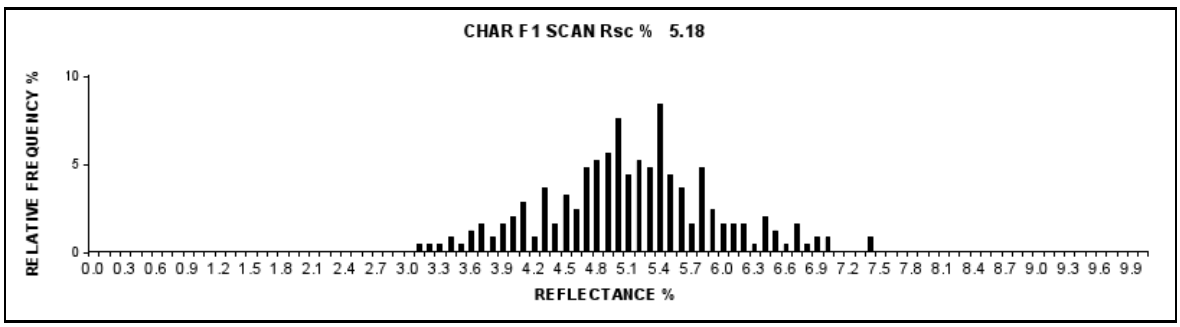

(d) Total reflectance scan for char F1

Figure 3.5: Total reflectance scan histograms for coal and char; E3 and F1

Organic Composition

Maceral Composition (Coal)

The maceral compositions of parent coals were established by point-count analysis and then expressed by volume percentage on mineral matter basis (mmb). The results presented on Table 3.5 show that coals had generally low vitrinite content (with the exception of A2). The liptinites varied between 2% and 3% (mmb), while the total inertinite content was as high as 66%, hence the coals were described as inertinite-rich. Coal D3 and E3 had the least amount of visible mineral matter, whereas coal A2 had the highest.

Microlithotype and Carbominerite Analysis (Coal)

Results in Table 3.6 show that relative amount of "pure" vitrinite, which is the mono-maceral vitrite (that is vitrinite >95%) was very low in many instances (< 8%), with the exception of coal A2. The inertite contents, collectively refering to "pure" inertinite particles, banded tissue and "detrital", varied significantly, the lowest amount being observed in coal A2 and above 23% in other coal samples. Generally, the intermediate maceral/maceral mixtures ranged from 11% to 18%. Carbominerites were most abundant in coal A2 and less common in coal E1.

Char Carbon Forms (Char)

When bituminous rank coal is heated to temperatures exceeding 350°C, vitrinites, liptinites and some inertinites begin to soften, become plastic and expand while the rest of the inertinites remain largely unchanged. Reactives-rich components in bituminous coal increase in volume on heating to form cellular structures producing porous chars which then provide greatly increased surface areas for reactions to take place. However most inertinites (inert and reactive), particularly fusinites do not soften, degasify nor develop into porous structures, but form quite dense chars which are more difficult to ignite and also tend to have low burn-off rates.

The carbon form analysis proposed by Du Cann (2008) and Everson *et al.*, (2008b) given in Appendix B, was used in this investigation with minor modifications. Table 3.7 shows that the six char samples constituted very different mixtures of partially reacted coal macerals, "char", "coke" and inorganic matter. Categories of carbon-form components observed are given. Figure 3.6 to Figure 3.8 show photomicrographs of the char carbon form categories encountered. It should be noted that these photomicrographs are not spe-

Table 3.5: Maceral composition of coal samples (volume %, mmb)

	Vitrinite			Liptinite			Inertinite							Total	Visible
	VIT[a]	PV	TV	S/R/C	ALG	TOTL	RSF	ISF	F/SEC	MIC	R INT	I INT	TOTI	Reactives	Minerals
Coal ID	(%)	(%)	(%)	(%)	(%)	(%)	(%)	(%)	(%)	(%)	(%)	(%)	(%)	(%)	(%)
A2	26	2	28	2	0	2	2	9	2	1	2	9	25	34	45
D1	10	0	10	3	0	3	11	17	1	2	9	18	58	33	29
D3	13	0	13	2	0	2	10	17	2	1	9	23	62	34	23
E1	14	0	14	3	0	3	8	12	2	1	10	20	53	35	30
E3	7	1	8	3	0	3	9	11	2	1	18	25	66	38	23
F1	8	0	8	2	0	2	11	17	1	1	10	15	55	31	35

Total Reactives = Vitrinite(VIT) + Reactive Semifusinite(RSF) + Reactive Inertodetrinite(R INT)

[a]See Appendix A for explanation of abbreviations.

Table 3.6: Microlithotype and carbominerite analysis of coal samples

Coal ID	Mono-macerals (%)		Intermediate maceral/maceral mixtures (%)				Carbominerite (%)	Minerite (%)
			Bi-macerals			Tri-macerals		
	Vitrite[b]	Inertite	Clarite	Durite	Vitrinertite	Trimacerite		
A2	19	7	3	0	4	7	33	27
D1	7	27	1	8	5	3	31	18
D3	5	38	1	5	6	3	23	19
E1	6	36	1	6	7	4	18	22
E3	7	43	1	5	5	2	26	11
F1	4	24	0	3	4	4	27	34

[b]See Appendix A for explanation of terms.

Table 3.7: Outline of classification system for char carbon forms (volume %, mmb)

Category		Char carbon form (Volume %) (mmb)	Maceral precursor	Photomicrograph (Fig)	Char ID					
					A2	D1	D3	E1	E3	F1
A	1.[b]	Dense char with frequent tiny pores	(from vitrinite)	3.6(a)	6	7	10	8	6	8
		Dense char with frequent tiny pores	(from inertinite)	3.6(b)	5	20	23	24	21	13
	2.	Char networks: fine walled more open networks	(from reactives)	3.6(c) (above)	7	10	6	6	4	5
	3.	Char networks: thicker walled more open networks	(from reactives)	3.6(c) (below)	16	17	17	13	16	13
B	7.	Isotropic thick walled “coke”	(from vitrinite)	3.6(d); 3.6(e)	10	1	2	3	3	3
D	12.	Partially reacted macerals (from coal)		3.6(f);3.7(a); 3.7(b) & 3.7(c)	2	2	2	1	4	2
E	13.	Inorganic matter (from coal)			55	43	40	45	46	56
		Total			100	100	100	100	100	100

Group A & B: Very highly reflecting, oxidation restricted

Group C: Relatively low reflecting, displaying oxidation rims

Group D: Low reflecting, little or no change

Anistropic: Exhibiting optical properties of different values when viewed under crossed nicols

Isostropic: Exhibiting optical properties that are the same in all directions when viewed under crossed nicols

[b]See Appendix B for the full outline of classification system for char carbon forms

cific to a given char but rather give an overview or features observed on any of the six chars;

- *Char forms (Category A1)*
  These carbon forms incorporate the "char" that greatly retained the parent coal maceral structure but with some very fine pores, emanating from both coal vitrinites and inertinites.
  1. *Char forms from coal vitrinites*: these carbon forms often displayed frequent tiny open gas pores but not well developed considerably larger devolatilasation vesicles, Figure 3.6(a) depicts the photomicrograph displaying this effect.
  2. *Char forms from coal inertinites*: These carbon forms shown by the photomicrograph in Figure 3.6(b) emanated from inertinites in the parent coal which had neither softened, expanded nor "opened up" to any appreciable limit on charring, to a large extent keeping their initial coal maceral shape and form. These carbons were usually pitted with tiny open pores, giving the same porosity.

- *Char networks (Category A2 & A3)*
  These char forms encompass char networks exhibiting differing extents of porosity. Those networks that had emanated from reactives-rich coal were fine walled and had "opened up" to varying degrees, giving high internal surface areas as depicted on the top half of Figure 3.6(c). Inerts-rich parent coal particles were the precursors to the thicker walled and less porous networks as illustrated on the lower half of Figure 3.6(c).

- *Coke forms (Category B7)*
  These developed mainly from vitrite, which is a pure or almost pure form of vitrinite in the parent coal.
  1. The vitrinites and other reactive coal macerals soften and degasify when they are heated during the charring process, subsequently creating pores in the process. As the evolved gases within the pores increase in volume, the softening walls expand and the materials expand in volume and surface area (Figure 3.6(d)).
  2. The "coke" in the char samples was denoted by isotropic forms exhibiting well-developed devolatilisation vesicles and frequent thick "coke" walls which were also frequently pitted with very fine-sized open pores. This is shown by the photomicrograph in Figure 3.6(e).

- *Oxidation effects (Category C8-10)*
  No indications of oxidation were observed on any of the six chars. Oxidation features are symbolised by dark rims and zones on particle edges and also around gasification pores.

- *Unreacted coal (Category D11)*
  Material unaffected by heat, with vitrinites exhibiting typical bituminous Medium Rank C reflectance levels, was not experienced in the set of six chars.

- *Partially-reacted macerals (Category D12)*
  Basically, the material in this class was of the reflectance levels above those of the parent coal vitrinites, but relatively lower than those of the fully charred constituents. Partially-reacted macerals have intermediate reflectivities ranging approximately from 1-4% Rr. In this instance, devolatilisation was limited and porosity relatively poorly developed. Photomicrographs illustrated in Figures 3.6(f); 3.7(a); 3.7(b) and 3.7(c) denote the partially-reacted macerals.

- *General condition of the chars*
  The chars were marked with a common feature of cracks (Figure 3.7(d)), fissures (Figure 3.7(e)) and deteriorated organic materials. Figure 3.7(f) depicts inertodetrinites showing passive deflagration and disintergration. These features are attributable to thermal stress fracturing and were common to all the six chars.

- *Visible minerals from parent coal*
  A substantial quantity of inorganic substances were observed to be present in the chars. Figure 3.8(a) shows fine inertinite particles associated with clay minerals from carbominerite in the parent coal, while Figure 3.8(b) potrays the remains of carbonates intergrown in inertinite.

Char D3 had the highest reacted macerals while char F1 displayed the least reacted macerals. Char D3 exhibited the highest frequent tiny gas pores from vitrinite while char E1 had dominating frequent tiny gas pores emanating from inertinite. Char D1 was observed to have the most abundant char networks with char F1 having the least in that regard. Char A2 was deduced to be having the most Isotropic coke, on the other hand it also had huge amounts of visible minerals although not as much as char F1 which had the most of the visible minerals. Partially reacted organic materials were mostly

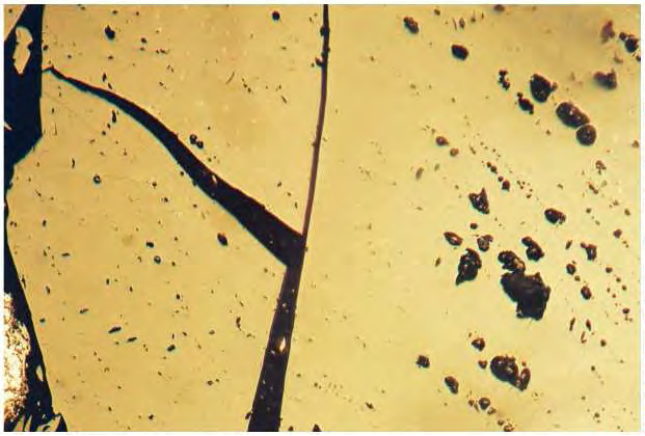

(a) Category A1: Dense char with frequent tiny gas pores - from vitrinite which displays no major change in original parent coal maceral structure

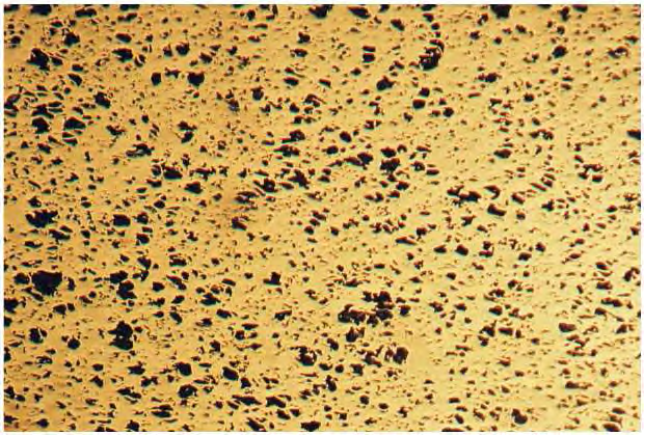

(b) Category A1: Dense char from inertinite which has not "opened up" and increased in porosity

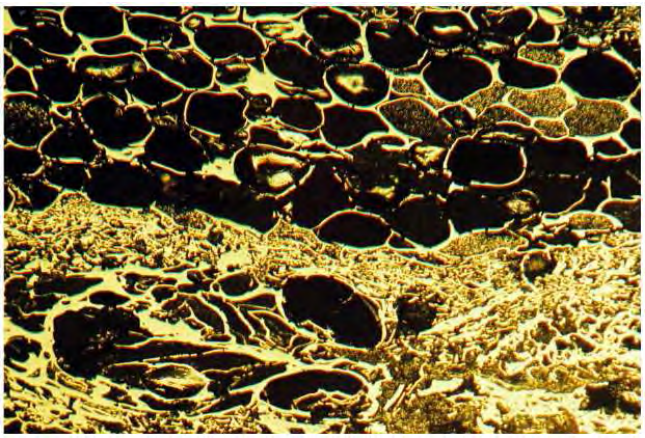

(c) Category A2: Fine walled char networks from reactives-rich coal macerals (above); Category A3: relatively thicker walled from inert coal macerals (below)

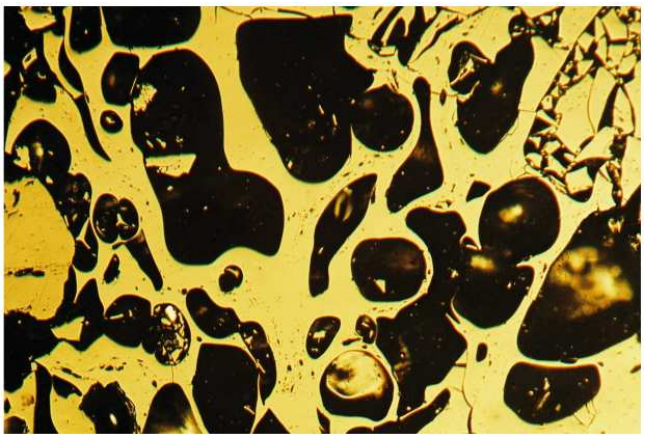

(d) Category B7: Isotropic "coke" from vitrinite in the parent coal with well-developed devolatilisation pores

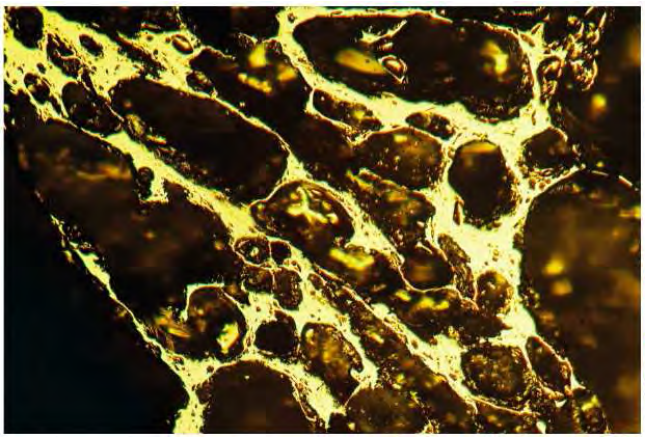

(e) Category B7: Highly porous isotropic “coke” formed from reactives

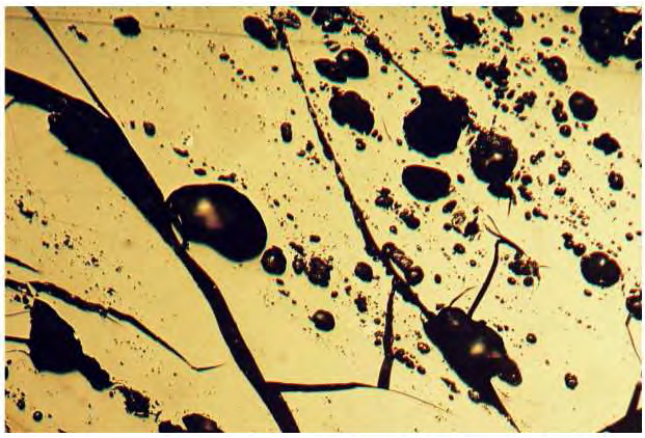

(f) Category D12: Partially reacted vitrinite due to restricted devolatilisation

Figure 3.6: Photomicrographs of char form analysis (magnification=2×10^5)

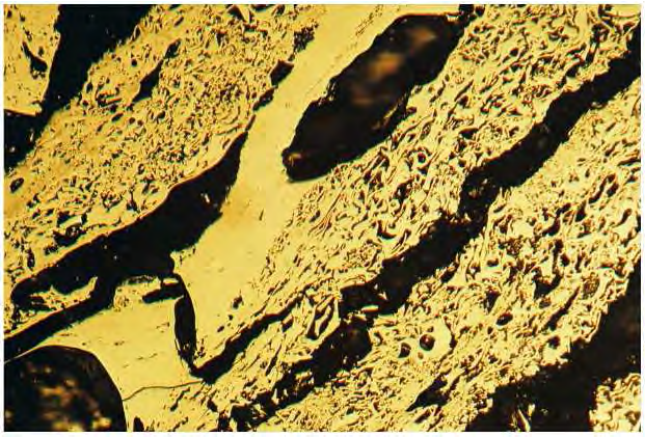

(a) Category D12: Partially reacted particle showing thermal stress fractures but little change in maceral structure and limited gas pore formation

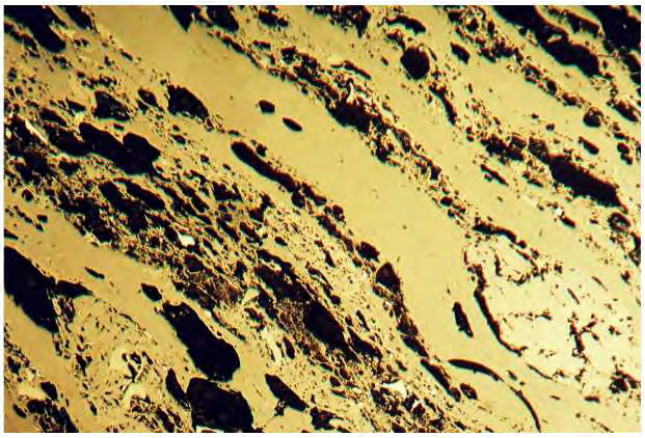

(b) Category D12: Maceral bands with fine clay inclusions displaying little change in structure

(c) Category D12: Fusinite showing deformation due to compression but had no increase in porosity

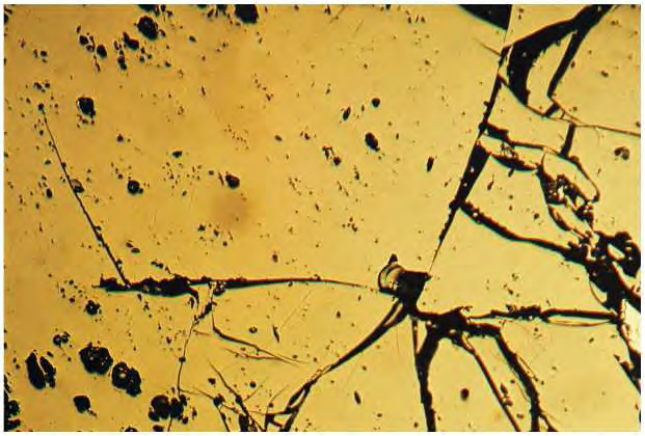

(d) Extensive cracking in vitrinite but little change in maceral structure

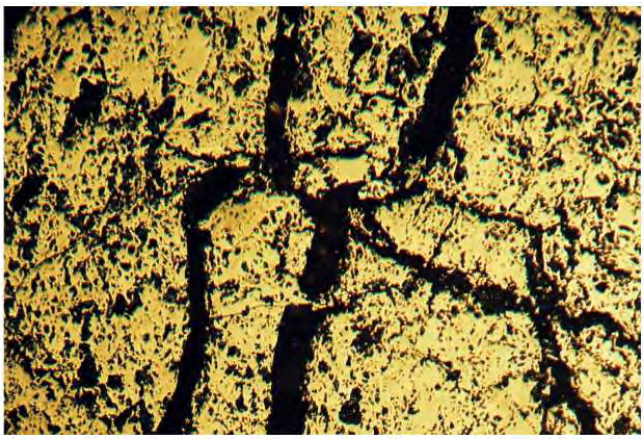

(e) Char from inertinite displaying severe fissuration

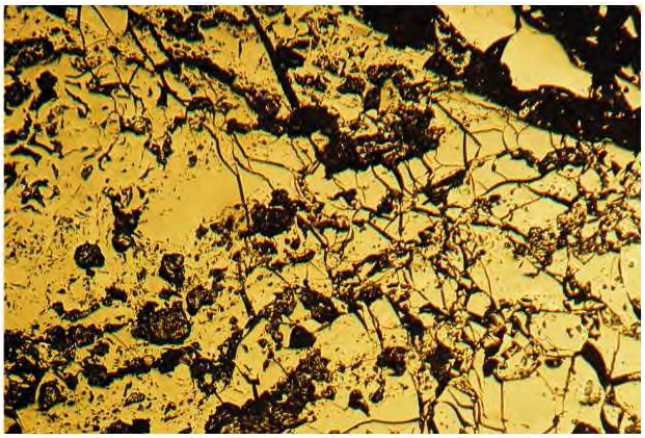

(f) Inertodetrinites showing "passive deflagration" and disintegration giving rise to increased surface area

Figure 3.7: Photomicrographs of char form analysis (magnification=2×10^5)

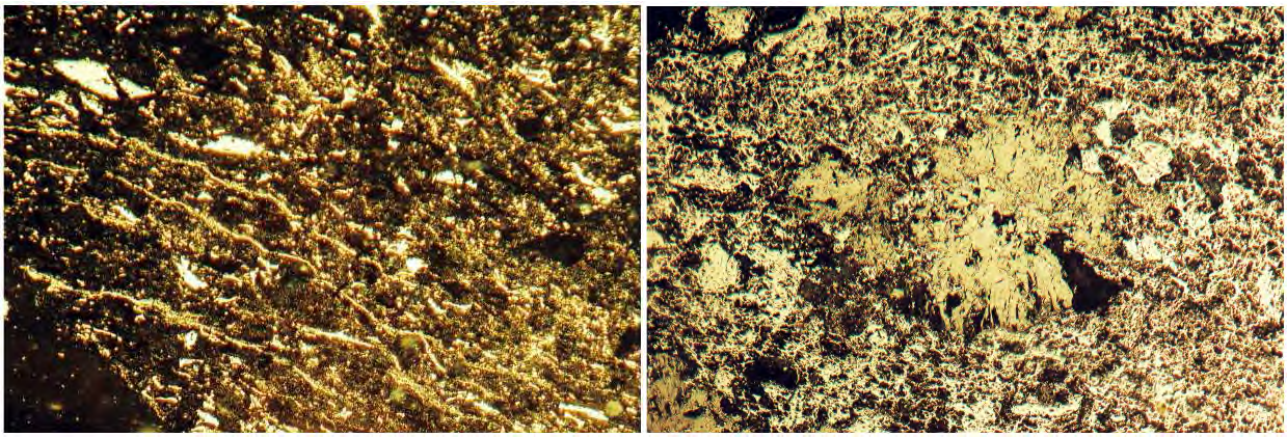

(a) Fine inertinite particles associated with clay minerals from carbominerite in the parent coal

(b) The remains of carbonates inter-grown in inertinite

Figure 3.8: Photomicrographs of char form analysis (magnification=2×10^5)

noticed in char E3 with the least amount being found in both char A2 and E1. No unreacted coal macerals were encountered in this set of six samples. Reactive macerals comprise of total vitrinite, total liptinite, reactive semifusinite and reactive inertodetrinite while the inert macerals consist of inert semifusinite, fusinite/secretinite, micrinite and inert inertodetrinite. The char carbon forms derived from reactive macerals consist of char network from reactives, isotropic coke and dense char vitrinites. On the other hand, char carbon forms emanating from inert macerals comprised of char networks from inerts and dense char from inertinite.

The comparisons between the parent coal macerals and the subsequent char carbon form derivatives are expounded in Figures 3.9 and 3.10. Figure 3.9(a) portrays the comparison between the parent coal vitrinite and the “dense char with frequent tiny gas pores” emanating from vitrinites. It is apparent that this char carbon form is not produced in pronounced ratios from the parent coal vitrinite in sample A2 as compared to other samples. The parent coal inertinite and the respective dense char with frequent tiny gas pores are illustrated in Figure 3.9(b). More open fine walled char carbon networks emanating from the total parent coal reactives are depicted in Figure 3.9(c). Parent coal inert macerals with successive thicker walled more open char carbon network from inerts comparison are presented in Figure 3.9(d). Parent coal reactive and inert macerals are compared with respective char carbon forms in Figure 3.10(a) and 3.10(b) respectively.

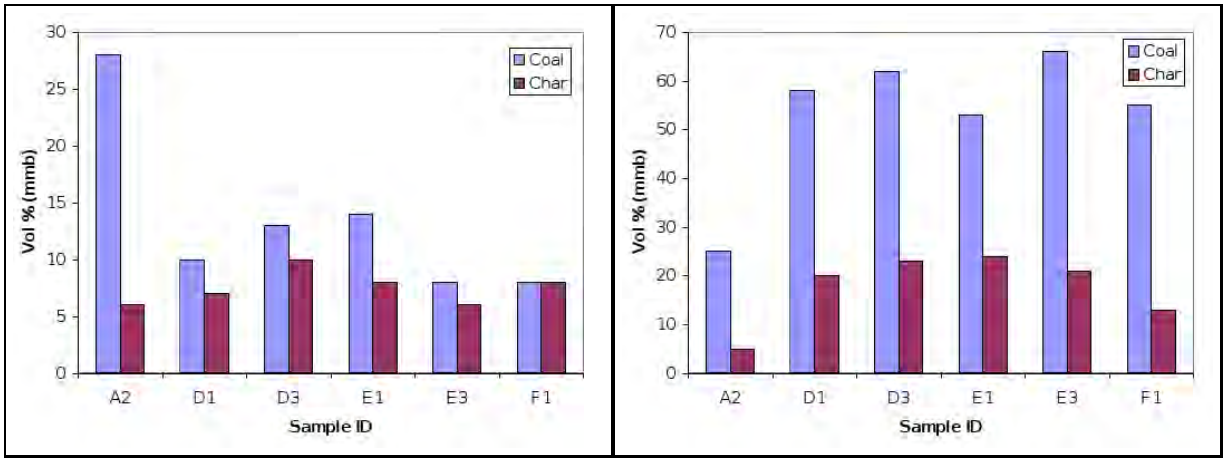

(a) Parent coal vitrinite and the subsequent dense char with frequent tiny gas pores

(b) Parent coal inertinite and the respective dense char with frequent tiny gas pores

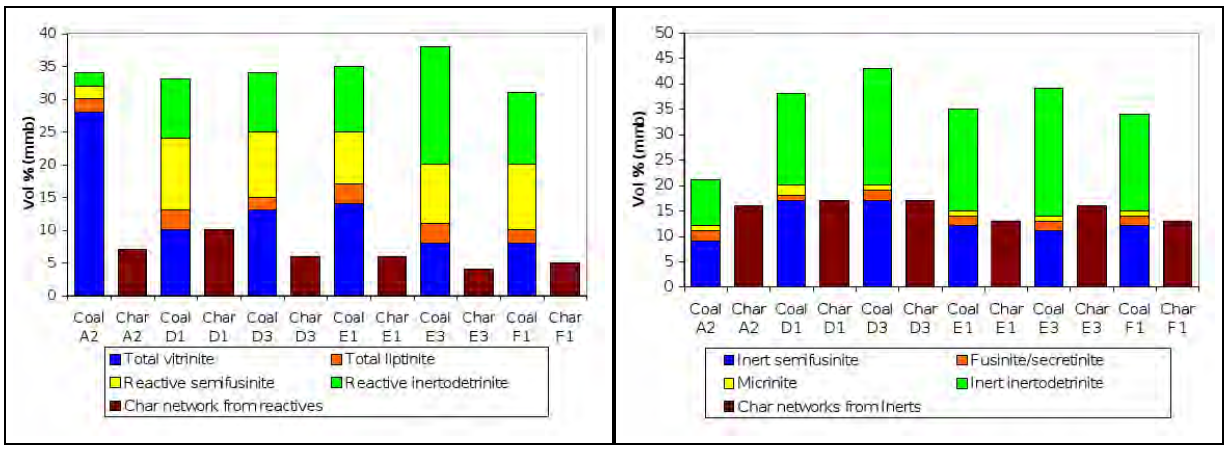

(c) Total parent coal reactives and more open fine walled char carbon network emanating from the total reactives

(d) Parent coal inert macerals with successive thicker walled more open char carbon network

Figure 3.9: Comparison of the macerals in parent coals with the respective char carbon form derivatives

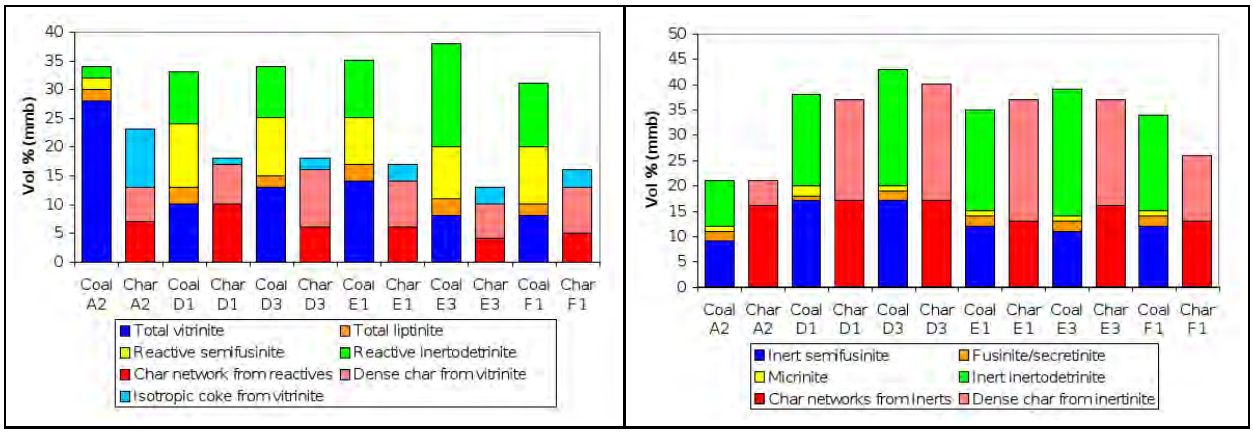

(a) Comparison of the parent coal reactives with the subsequent char carbon form derivatives

(b) Total inert macerals in parent coals compared with the total successive char carbon forms

Figure 3.10: Comparison of the parent coal macerals with the successive char carbon forms

3.5.4 XRD Analysis Results

Various minerals that are present in parent coals and the respective chars are presented in Table 3.8. It is apparent that the charring process changed the mineralogical composition of the samples. The results show that kaolinite which is a part of the clay group comprising of hydrous aluminium silicate is generally high in the coal samples, quartz was also predominantly detected in coal. Quartz, cristobalite and microcline were commonly in the char samples.

Kaolinite is a clay mineral with the chemical composition $Al_2Si_2O_5(OH)_4$. Kaolinite undergoes a series of phase transformations upon thermal treatment. Endothermic dehydroxylation (or alternatively, dehydration) begins at 550-600°C to produce disordered metakaolin, $Al_2Si_2O_7$, but continuous hydroxyl loss ($-OH$) has been observed up to 900°C and has been attributed to gradual oxolation of the metakaolin (Bellotto *et al.*, 1995). This is what caused the predominant kaolinite in parent coal samples not to be detected at all in the six char samples that were prepared at 900°C. Metakaolin is percieved to be a complex amorphous structure that retains some longer-range order due to stacking of its hexagonal layers (Bellotto *et al.*, 1995).

Cristobalite mineral is a high temperature polymorph of quartz, implying

that it has the same empirical formula, SiO_2, but a different crystalline structure. This could be the explanation for its pronounced detection in the six chars and its total absence in the parent coal samples. Calcite and pyrite/pyrrhotite were obtained to a lesser extent. These may be problematic to the operation of pulverised fuel combustion.

Table 3.8: XRD mineral proportions of coal and char samples

Mineral Abundance (weight %)	Mineral source in "coal/char"	Sample ID Coal A2	Char A2	Coal D1	Char D1	Coal D3	Char D3	Coal E1	Char E1	Coal E3	Char E3	Coal F1	Char F1
Calcite	$CaCO_3$	1.4	0.2	0.9	0.2	0.8	0.1	2.3	0.9	1.8	0.4	1.3	0.3
Dolomite	$CaMg(CO_3)_2$	1.9		0.7		1.6		1.3		1.8		1.3	
"Char/Coal"	Carbon-rich coal	51.5	75.1	47.5	78.7	54.1	79.3	61.9	72.9	64.6	83.3	64.4	79.1
Gypsum	$CaSO_4 2H_2O$	1.4		13.2		0.7		1.0		1.8		1.2	
Kaolinite	$Al_2Si_2O_5(OH)_4$-clay	27.7		19.1		22.7		19.1		22.3		21.7	
Muscovite	$KAl_2[(OH)_2\|AlSi_3O_{10}]$-mica group	4.7		3.2		6.6		2.3		1.6		2.1	
Pyrite/pyrrhotite	partial transformation of pyrite (FeS_2)	0.7		0.2		0.2		0.8		0.7		1.1	
Quartz	SiO_2	9.7	14.3	14.3	14.7	12.7	12.6	10.9	13.1	4.9	7.1	6.2	7.3
Rutile	TiO_2	0.1		0.4		0.4		0.3		0.2		0.2	
Siderite	$FeCO_3$	0.9		0.6		0.2		0.2		0.1		0.6	
Cristobalite	SiO_2		3.6		2.6		2.2		2.4		3.7		3.7
Illite	$KAl_2(AlSi_3)O_{10}(OH)_2$		2.8		0.6		1.0		1.8		0.8		2.2
Alpha iron/ferrite	$\alpha - Fe$		0.1		0.3		0.5		1.1		0.4		0.4
Microcline	$K(AlSi_3O_8)$		1.1		1.9		2.6		4.8		2.3		3.7
Oldhamite	$Ca, Mg)S$		0.9		0.9		1.2		1.8		1.3		1.8
Sodalite	$Na_8[Cl_2\|Al_6Si_6O_{24}]$		0.0		0.0		0.3		0.2		0.2		0.1
Troilite	FeS		1.9		0.2		0.2		1.1		0.5		1.5

3.6 Main findings

- The six parent coals had ash content (% by mass, dry basis) ranging from 37.0% to 47.1%, while the respective chars were characterised as high ash products with ash yields ranging from 49% to 63.7% (db).
- The volatile matter yields in parent coals were in the range of 19.6% to 21.5% (dry basis), while the respective chars had volatiles between 2.0% and 4.0% also on dry basis. Even though significant devolatilisation took place during char formation, most of the char carbon forms did not increase in porosity to any great extent.
- Vitrinite reflectance values of the parent coal ranged from 0.58% to 0.78% Rr, hence the coal samples are characterised as bituminous, medium rank C to D according to the ISO 11760 - 2005. The parent coal total maceral reflectance scans had values ranging from 1.09% to 1.46% Rsc. The charring process substantially shifted the overall total mean scan reflectance to values within the narrow range from 4.84-5.45% Rsc.
- The organic constituents of the majority of the coals were inertinite-rich with the exception of coal A2.
- Chars formed at 900°C, parent coal reactive macerals formed minor proportions of isotropic “coke” and fine char networks while some vitrinites and the majority of the coal inertinites exhibited a marked increase in reflectance levels.
- Regarding the general condition of the parent coals and the respective chars; the coal samples had a general “fresh” appearance, with frequent micro-fissures in macerals. Cracks, fissures and deteriorated organic material was a common feature in all the six chars. These characteristics are attributable to thermal stress fracturing coupled with passive deflagration.
- Looking at the physical structural attributes of the chars, the carbon dioxide micropore surface area calculated using the Dubinin-Radushkevich equation (S_{D-R}), ranged from 102.17-249.98$m^2 \cdot g^{-1}$ while the monolayer pore volume ranged from 22.37-54.72$m^3 \cdot g^{-1}$. Char D1 and D3 exhibited a greater surface area and monolayer pore volume compared to rest of the chars.

- XRD analysis revealed that kaolinite and quartz are generally very high in the coal samples and on the other hand quartz, cristobalite and microcline are predominantly detected in the char samples. A close look at both parent coals and the chars showed that the mineral components vary within a small range amongst the six samples.

CHAPTER 4

Experimental: Nitric Oxide-Char Reaction

4.1 Introduction

Experimental apparatus and reagents with respect to experimental procedure and conditions for reactivity determination are discussed in this chapter. A description of the thermal analysis equipment and technique used is given, followed by the specifications of reagents used. Experimental procedures are outlined while the experimental programme is presented at the end.

4.2 Thermogravimetry

4.2.1 Thermogravimetric analyser (TGA)

In this study the Thermax 700 thermogravimetric analyser supplied by Thermo Scientific was used for determination of reactivity of the chars with nitric oxide (NO). The weight loss of the char sample was continuously measured using a very sensitive balance that detects the slightest movements on the balance. The weighing mechanism has high accuracy, it is capable of detecting and recording mass changes in the range of 0.001 mg. The mass is

instantaneously recorded during the course of the reaction and the mass-temperature-time data acquisition is enabled by software (supplied by the TGA manufacturer) which logs it onto the computer. Thermogravimetry has been used by a number of researchers for coal and/or char conversion experiments (Teng *et al.*, 1997; Li *et al.*, 1999; Ollero *et al.*, 2002; Wang *et al.*, 2005; Kaitano, 2007; Everson *et al.*, 2008a; Sun *et al.*, 2009; Ren *et al.*, 2010).

A photograph of the Thermax700 TGA supplied by Thermo Scientific is presented in Figure 4.1(a) while the schematic illustration of the TGA system and accessories is shown in Figure 4.1(b). The TGA equipment consists of a microbalance, furnace, gas supply system, mass flow controllers and a data logging system. The Thermax700 TGA can operate up to 1700°C at atmospheric pressure. The flow of inert or reactant gas to the reactor (furnace) is regulated by the mass flow controllers.

4.2.2 Thermax700 TGA specifications

A summary of the Thermax700 TGA specifications are presented on table 4.1.

Table 4.1: Thermax700 TGA Specifications

Parameter	**Specification**
Maximum mass capacity	100 g
Maximum sample volume	35 mℓ
Temperature range	Ambient-1700°C
Sensitivity/resolution	1μg
Thermocouple	B or K type
Heating rate	0.1-100$^oC\cdot$ min^{-1}

(a) A photograph of the Thermax700 TGA

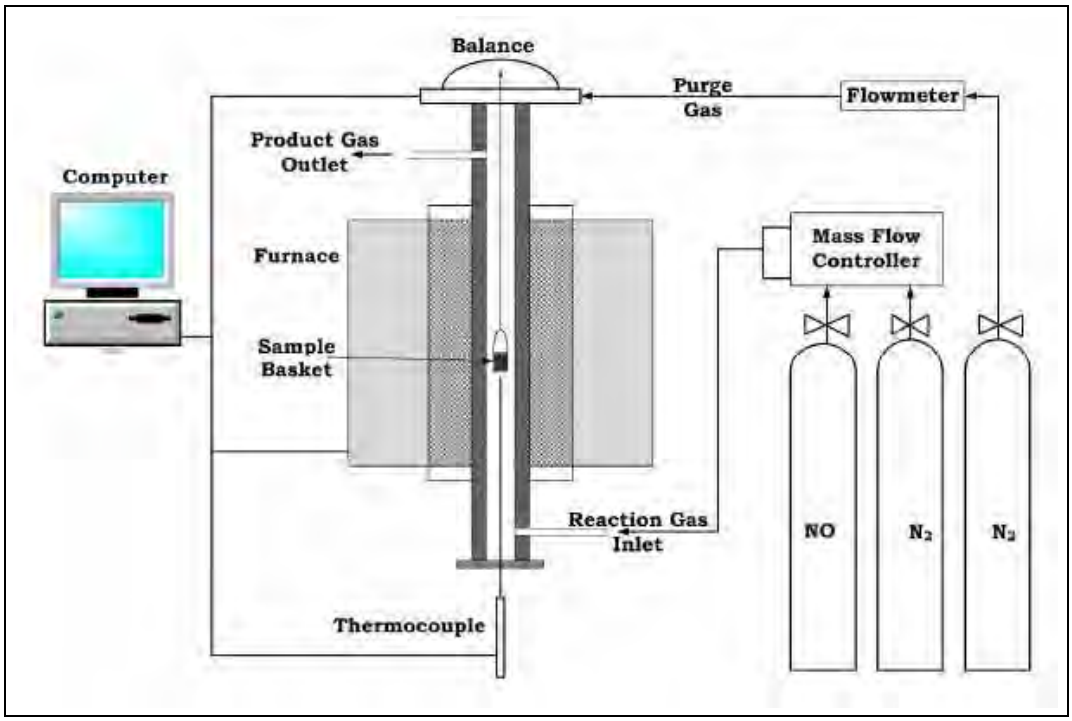

(b) Schematic presentation of the TGA system

Figure 4.1: A photograph of Thermax700 TGA and a schematic presentation of the system.

4.3 Chemical reagents

Nitric oxide, nitrous oxide and nitrogen are the gases that were used in the experiments with chars derived from six different low grade coals.

4.3.1 Gases

The gases used in the nitrogen oxides reduction experiments were supplied by Afrox (South Africa). The grade and the purity of gases is given on Table 4.2. Ultra-high purity (>99.999%) nitrogen was used as the purge and balance gas.

Table 4.2: Specifications of Gases used in the Experiments

Gas	**Grade**	**Purity**
Nitric Oxide (NO)	Mixture of NO and N_2	5% NO (v/v)
Nitrogen (N_2)	Ultra-high purity	$\geq$99.999%

4.3.2 Coal chars

Six low grade coal samples that were pyrolysed to prepare chars as described in Chapter 3. Characterisation of the coals and the respective chars is also given in Chapter 3.

4.4 Experimental procedure

The chars used for the experimental work were prepared as outlined in Chapter 3; a 100 mg sample consisting of 1 mm diameter particles was used for thermogravimetric analysis. A gas flowrate of 500 ml·min^{-1} was applied in all the experimental runs which were carried out. The operation procedure can be summarised as follows:

- All the required parameters on the TGA were set and then the empty sample basket was tared on the microbalance.

- A char sample of approximately 100 mg was weighed on a top loading balance with a 0.001mg degree of accuracy.
- The sample was then loaded into the TGA furnace and degassed by flushing inert ultra high purity nitrogen gas through the system for 10 minutes.
- The data logging programme was started which automatically enabled the char sample to be heated at a preset constant heating rate of $20^{o}C{\cdot}min^{-1}$ up to the specified isothermal temperature (750.0; 787.5; 825.0; 862.5 or 900.0°C), some volatiles and moisture were lost during this period.
- After ascertaining that there is no observable mass change at the stipulated isothermal temperature, the reaction gas (NO) was then introduced.
- The reaction was allowed to proceed until there was no apparent weight change on the heated sample symbolising that the reaction has reached completion and only an uncombustible residue (ash) was remaining.

4.5 Experimental Programme

Thermogravimetry experiments were conducted in order to evaluate the reaction kinetics of nitric oxide with the six chars. This enabled the determination of the effect of temperature and NO concentration on char reactivity, and the deduction of a suitable model for the reaction. Table 4.3 gives the operation conditions and parameters employed to achieve the respective objectives. The reaction data which include temperature, weight and time were automatically logged onto the computer with the aid of the software provided by the TGA supplier. The data was then exported to an Excel spreadsheet for further processing.

Table 4.3: Experimental Parameters and Conditions

Reaction variable	Condition
Reaction	NO-char reaction in nitrogen atmosphere
Sample mass (mg)	100($\pm$2)
Char particle diameter (mm)	1
Reaction temperature (°C)	750.0; 787.5; 825.0; 862.5; 900.0
Flowrate (ml·min^{-1})	500
Gas compositions (v/v % NO)	1.25; 2.0; 3.0; 5.0
Pressure (kPa)	87.5
Chars	Prepared at 900°C
Heating rate	20°C·min^{-1} up to the isothermal temperature

CHAPTER 5

Results and Discussion: Nitric Oxide Reduction

5.1 Introduction

Experimental results of the nitric oxide reaction with the six chars are presented. The chars were prepared as outlined in Section 3.3.1. The experiments were conducted in a thermogravimetric analyser (Section 4.2.1) using the specific conditions and parameters outlined on Table 4.3.
The primary goal of this chapter is to determine the reactivity of 1.25 % (v/v) to 5% (v/v) NO reduction by six different chars at temperatures ranging from 750-900°C, confirm model appropriateness and deduce quantitave data (parameters) with regard to the reactivity of the chars.
Li and co-workers (1999) used a concentration of 0.92% (v/v) and 5.00% (v/v) while Wang *et al.*, (2005) reacted carbonaceous materials with 0.5 to 2.5% (v/v) NO. Similar concentrations of NO were adapted in this investigation, even though relatively higher than those experienced in fluidised bed combustion.

5.2 Thermogravimetry Results

5.2.1 Typical Experimental Results

The diagram depicted in Figure 5.1 illustrates typical raw experimental results from the Thermax700 TGA at 900°C, 87.5 kPa and 1.25% NO (v/v), of which mass is presented as a function of time. At the initial stages of reaction there is a rapid decline in mass and as the reaction progresses the decrease in mass slows down up to an equilibrium point where no significant mass change is observed. The equilibrium position on the reaction trajectory indicates the ash remained in the sample, this correlated with the proximate analysis of the chars even though a maximum deviation of ±2% of the mass was observed.

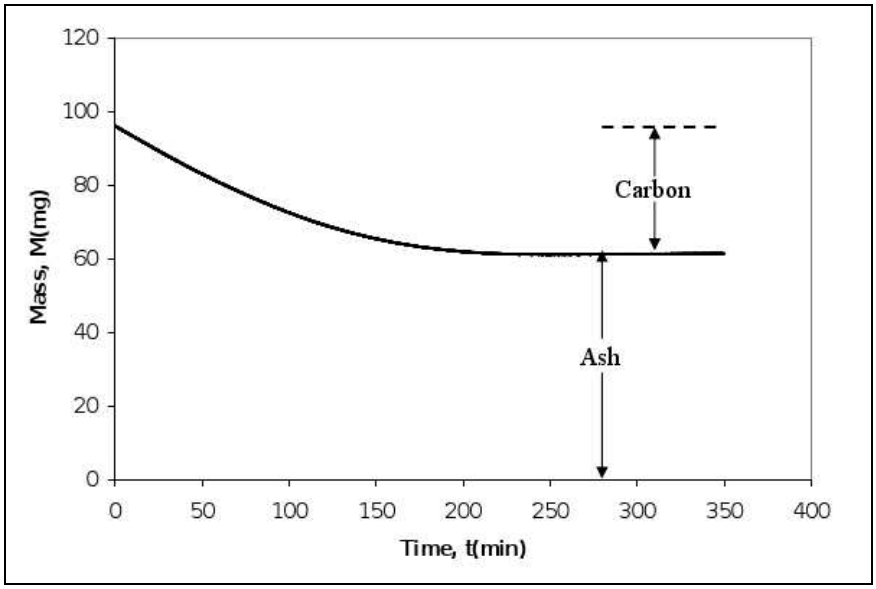

Figure 5.1: TGA raw experimental results of char A2 obtained at 900°C using 1.25% NO.

The char conversion transformation with time is conveniently expressed on ash free basis such that the observed mass decrease is attributed to the conversion of carbonaceous material. This approach has been adopted and implemented with great success by a variety of researchers working on gas-char kinetics (Wang *et al.*, 2005; Kaitano, 2007; Everson *et al.*, 2008a; Sun *et al.*, 2009). The outcome from such a typical calculation enables significant and quantitative comparisons of conversion rates of the carbon containing

compounds and the subsequent modelling. The characteristics of structural properties like porosity and surface area are a result of the presence of ash. Catalytic properties are also due to the minerals in ash embedded in the char matrix, in the form of carbon/mineral associations.
The nitric oxide reduction by char experimental results were normalised on ash free basis according to Equation (5.1);

$$X = \frac{m_o - m_t}{m_o - m_{ash}} \tag{5.1}$$

where X denotes fractional conversion of carbon, m_o is the initial mass of char, m_t is mass of char at any given time (t) and m_{ash} is mass of ash. Figure 5.2 illustrates typical normalised results obtained from the experimental data of 1.25% NO with char A2 at 900°C. For modelling purposes, 20 experimental conversion data points were used.

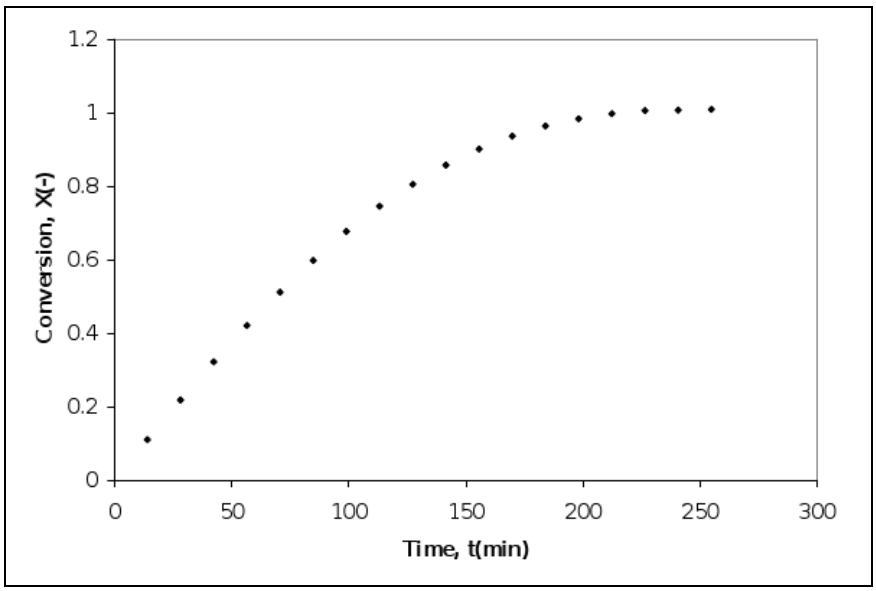

Figure 5.2: Conversion of char A2 at 900°C by 1.25% NO

5.2.2 Effect of operating conditions on NO-char reactivity

Temperature

In Figure 5.3 the effect of temperature on nitric oxide reduction rate by char is illustrated. The rate of reaction distinctly increased with increasing temperature with respect to all the chars as clearly depicted by Figure 5.3(a)

to 5.3(f). The relative increase in reaction rate (carbon conversion) with increasing temperature is in conformity with Arrhenius type kinetics. Similar results on the influence of temperature on the NO-char reaction were also obtained by Li *et al.* (1998) and Sun *et al.* (2009).

Nitric oxide concentration

The effect of nitric oxide composition [1.25% to 5% (v/v)] at 900°C and 87.5 kPa on char conversion is presented in Figure 5.4. From the illustrations in Figures 5.4(a) to 5.4(e), it is apparent that the rate of carbon conversion increases with increasing nitric oxide concentration as envisaged with the reaction trends and profiles similar for all the chars. The results are in concurrence with those of Wang *et al.*, (2005).

Influence of char properties

In Figure 5.5 the effect of char properties at 900°C exhibited by the six chars with 1.25% NO is shown. Char A2 displayed the fastest reaction rate followed by char D1 and E3 while char E1 took the longest time for the reaction to reach completion. Char E1 is characterised by very low N/C ratio (Table 3.2) and high mean total random reflectance of scan as shown on Table 3.4. Sample A2 is characterised by high vitrinite content in the parent coal when compared with other samples (Table 3.5). Char D1 displayed the highest CO_2 surface area (S_{D-R}) while char F1 had the lowest, as indicated on Table 3.3. On analysis of the effect of the modified reactive maceral index (RMI*) on reactivity is given in Section 5.4, for this purpose, the parameter t_f (lumped reaction rate) evaluated from the random pore model is used.

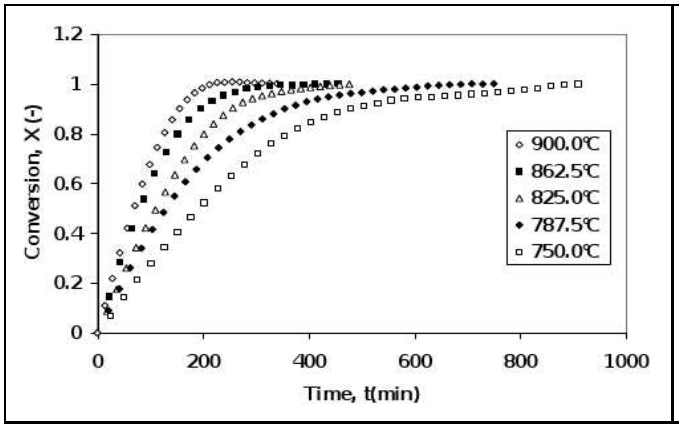

(a) Effect of temperature on 1.25% NO and char A2 reaction

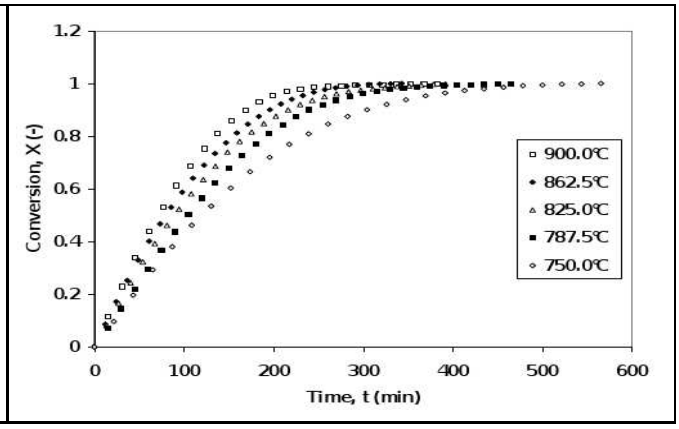

(b) Effect of temperature on 1.25% NO and char D1 reaction

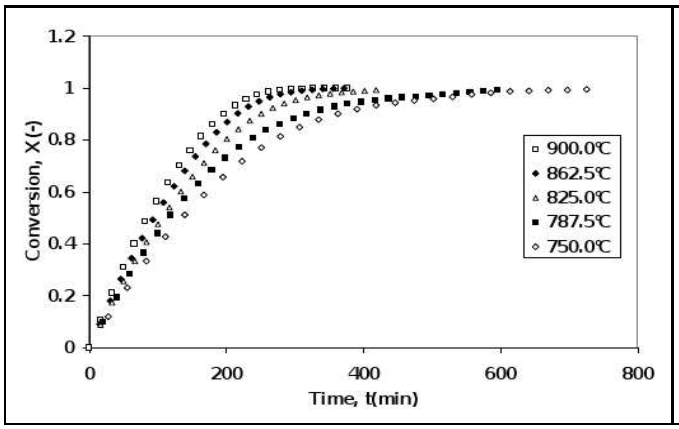

(c) Effect of temperature on 1.25% NO and char D3 reaction

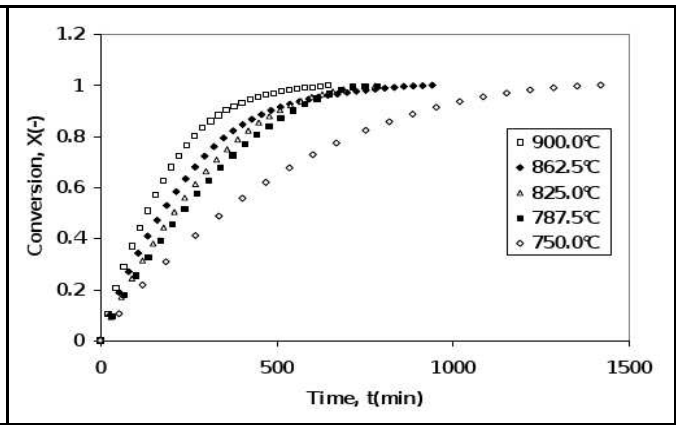

(d) Effect of temperature on 1.25% NO and char E1 reaction

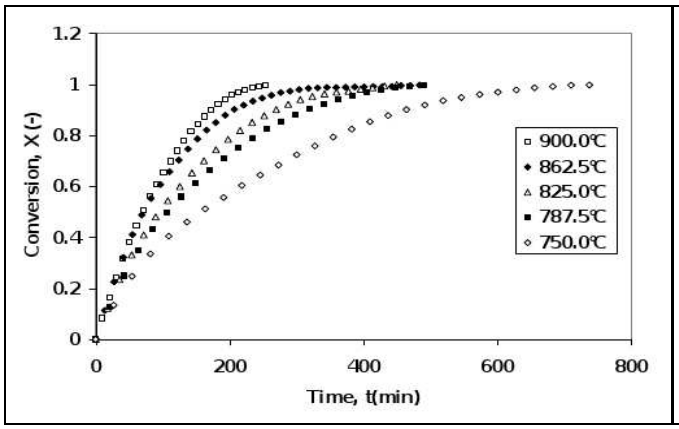

(e) Effect of temperature on 1.25% NO and char E3 reaction

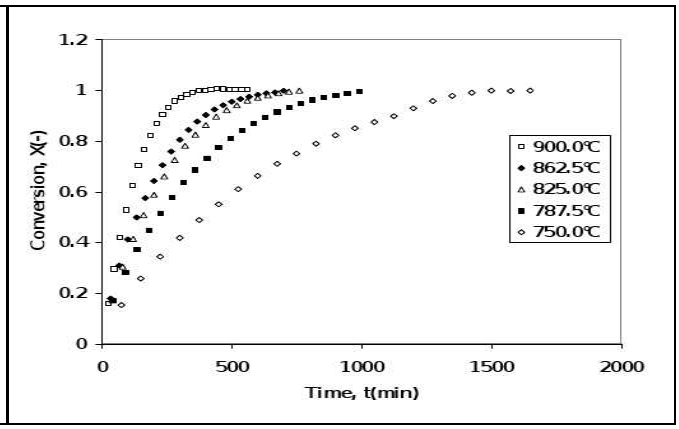

(f) Effect of temperature on 1.25% NO and char F1 reaction

Figure 5.3: Effect of temperature on NO-char reaction using 1.25% NO at 87.5kPa

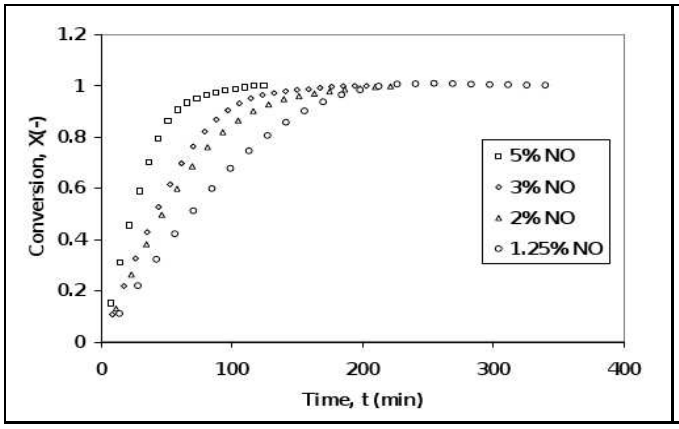

(a) Effect of NO concentration on char A2 reaction at 900°C

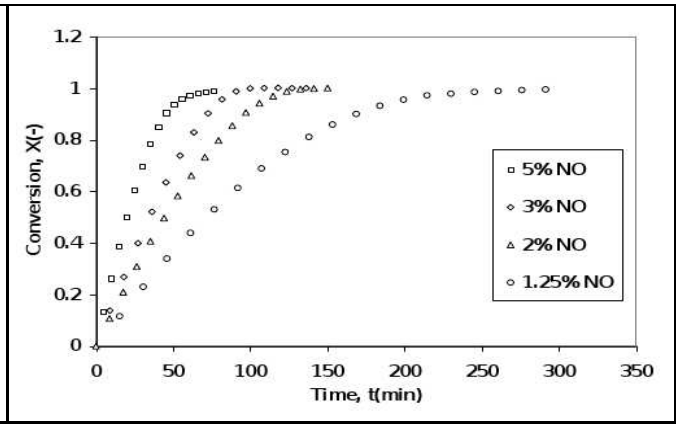

(b) Effect of NO concentration on char D1 reaction at 900°C

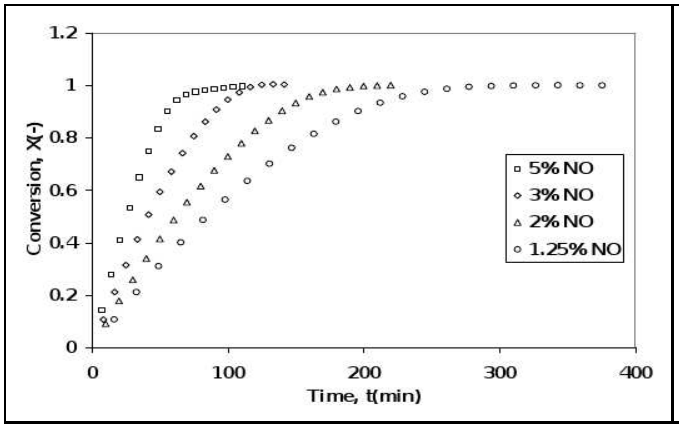

(c) Effect of NO concentration on char D3 reaction at 900°C

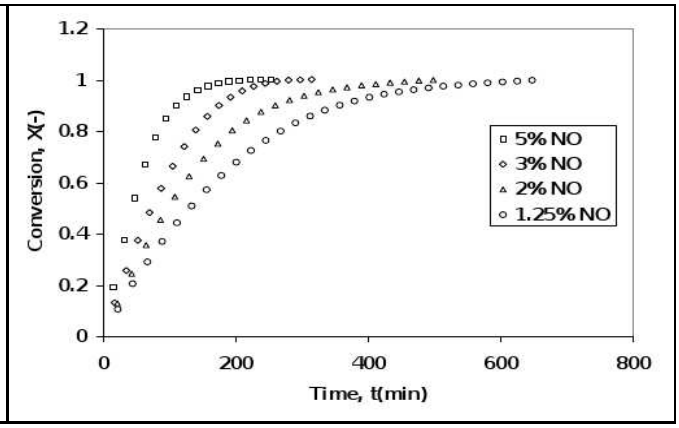

(d) Effect of NO concentration on char E1 reaction at 900°C

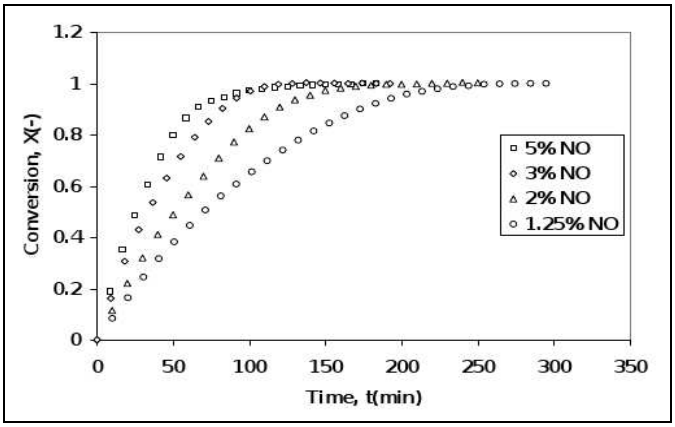

(e) Effect of NO concentration on char E3 reaction at 900°C

Figure 5.4: Effect of NO concentration on NO-char rate of reaction at 900°C and 87.5kPa

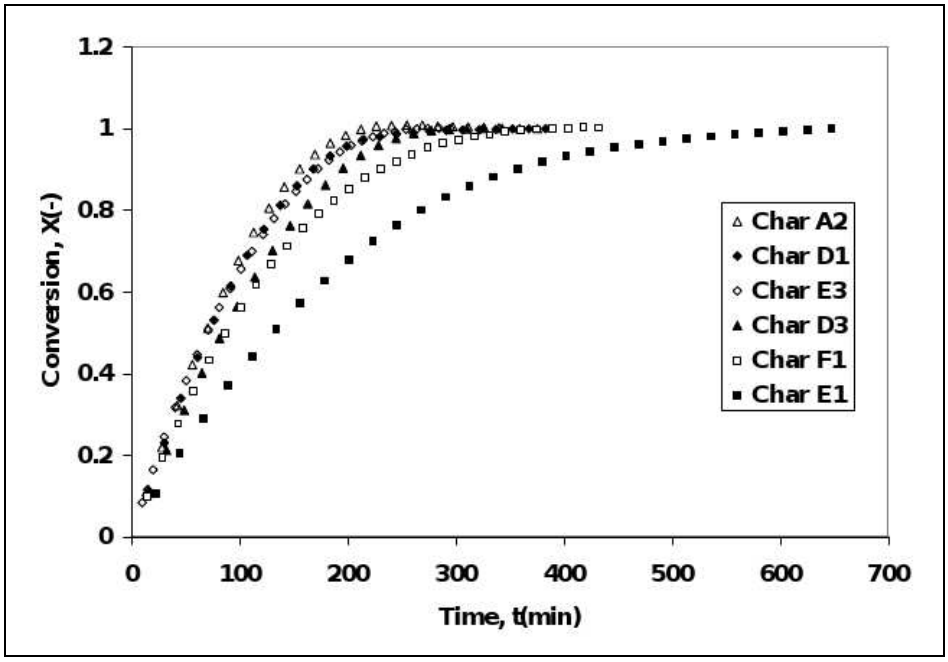

Figure 5.5: Effect of char properties on NO-char reactivity at 900°C and 87.5 kPa using 1.25% NO

5.3 Reaction rate modelling: NO-Char Reaction

The mathematical modelling of the NO-char experimental results is presented in this section. Some models commonly used for gas-char reaction are briefly discussed in Section 2.7. The random pore model (RPM) which is introduced in Section 2.7.3 was applied to model the NO-char kinetics. The RPM was also used by other researchers working on nitric oxide reduction by chars (Gray and Do, 1993; Lu and Toh, 1993; Li *et al.*, 1997; Sun *et al.*, 2009).

5.3.1 Random Pore Model

The introduction to this model is given in Section 2.7. The fundamental equation for the random pore model describes the reaction rate as a function of conversion inside a porous particle with a constant gas composition throughout the particle that has no pore diffusional effects (regime I: chemical reaction controlled) and also characterised by a dimensionless structural parameter. The structural parameter (ψ) may be deduced from calculations based on initial structural properties of the char which includes the surface

area, porosity and pore length. In this investigation it will be obtained by a regression procedure described below.
An overall reaction rate model is used for evaluation of regime I kinetics, the intrinsic kinetics, the structural changes which encompass the surface area dependency on char properties and reaction conditions to be addressed. The equations and respective derivatives are discussed in the next section and the application for the analysis of results presented in the subsequent sections.

Model equations

According to Bhatia and Perlmutter (1980), the overall rate expression is given by equation 5.2;

$$\frac{\mathrm{dX}}{\mathrm{dt}} = \frac{\mathrm{r_s}\,(1-\mathrm{X})\,\mathrm{S_o}\sqrt{1-\psi\ln(1-\mathrm{X})}}{(1-\varepsilon_o)} \tag{5.2}$$

where ψ is the structural parameter attribute of the initial char structure and elucidated as:

$$\psi = \frac{4\pi \mathrm{L_o}\,(1-\varepsilon_o)}{\mathrm{S_o^2}} \tag{5.3}$$

The Equation (5.2) can be expressed in terms of the the dimensionless parameter as depicted in Equation (5.4);

$$\frac{\mathrm{dX}}{\mathrm{d}\tau} = (1-\mathrm{X})\sqrt{1-\psi\ln(1-\mathrm{X})} \tag{5.4}$$

where

$$\tau = \frac{\mathrm{r_s S_o t}}{1-\varepsilon_o} \tag{5.5}$$

Expressions for carbon conversion X presented in terms of time t or dimensionless time τ (implicit and explicit) attained by the integration of Equations (5.2) to (5.4) would be given as discussed by Kaitano (2007) and Everson *et al.* (2008a):
In terms of time t;

$$\mathrm{t} = \frac{2(1-\varepsilon_o)}{\mathrm{r_s S_o}\psi}\left(\sqrt{1-\psi\ln(1-\mathrm{x})}-1\right) \tag{5.6}$$

In terms of dimensionless time τ;

$$\tau = \frac{2}{\psi}\left(\sqrt{1-\psi\ln(1-\mathrm{x})}-1\right) \tag{5.7}$$

and explicitly it is expressed as;

$$\mathrm{X} = 1-\exp\left[-\tau\left(1+\frac{\psi\tau}{4}\right)\right] \tag{5.8}$$

The time factor, $\mathrm{t_f}$ (lumped reaction rate) defined as;

$$\mathrm{t_f} = \frac{\mathrm{r_s S_\circ}}{1-\varepsilon_\circ} \tag{5.9}$$

Expressing Equation (5.8) in terms of time t leads to the derivation of Equation (5.10);

$$\mathrm{X} = 1-\exp\left[-\mathrm{t_f t}\left(1+\frac{\psi\mathrm{t_f t}}{4}\right)\right] \tag{5.10}$$

Kaitano (2007) and Everson *et al.* (2008a) proposed that the reduced time expression is given by $\frac{\mathrm{t}}{\mathrm{t_x}}$, of which $\mathrm{t_x}$ denotes the time taken for fraction X conversion, being the upper limit for reliable results. This leads to the attainment of the expression illustrated by Equation (5.11), which is independent of parameters appearing before the square root in Equation (5.6) except for ψ. In Equation (5.11) the term $\mathrm{t_{0.9}}$ represents the time taken for 90% conversion of char, hence this expression makes it possible for the structural parameter (ψ) to be determined from the experimental data.

$$\frac{\mathrm{t}}{\mathrm{t_{0.9}}} = \frac{\sqrt{1-\psi\ln(1-\mathrm{X})}-1}{\sqrt{1-\psi\ln(1-0.9)}-1} \tag{5.11}$$

Based on the discussed model expressions, it should be noted that;

$$\frac{\mathrm{t}}{\mathrm{t_{0.9}}} = \frac{\tau}{\tau_{0.9}} \tag{5.12}$$

Intrinsic reaction rate equation $\mathrm{r_s}$ given by Equation (5.13) based on the $\mathrm{n^{th}}$ order power rate relationship was applied.

$$\mathrm{r_s} = \mathrm{k_{so}}\exp\left(-\frac{\mathrm{E}}{\mathrm{RT}}\right)\mathrm{p^n} \tag{5.13}$$

Validation Procedure

The determination the chemical controlled model requires the estimation of structural parameter ψ (Equation (5.3)) and time factor t_f (Equation (5.9)). Bhatia and Perlmutter (1980) pointed out that the structural parameter can be evaluated from BET results and image analysis. However the non-uniform pore size distribution, surface area and pore volumes estimates from BET measurements pose major limitations towards this approach because of the approximations needed to describe the non-uniformity of the pore sizes and, furthermore, the accuracy of pore size estimates within the micro-pore range. In this study, these limitations were overcome by fitting Equation (5.11) by regression with the unknown structural parameter to corresponding experimental results as proposed by Kaitano (2007) and Everson *et al.* (2008a). An upper limit of 90% conversion was used. The uncertainty of the experimental conversion results which are normally asymptotic towards the end of the reaction is eliminated. The validation of the structural model involved plotting dimensionless time $\left(\frac{t}{t_{0.9}}\right)$ against conversion (X) as illustrated in Figure 5.6. This enabled the structural parameter (ψ) to be calculated by regression with the use of experimental results obtained at different operating conditions. The second regression calculation was then carried out using the regressed value for the structural parameter using Equation (5.10) with real time conversion results with t_f being the unknown parameter. With the t_f evaluated from experimental results at various gas concentrations or partial pressures and temperatures, the intrinsic reaction rate parameters were evaluated using the logarithmic form of Equation (5.13) to produce Equation 5.14.

$$\ln t_f = -\frac{E}{RT} + n \ln p + \ln(k'_{so}) \tag{5.14}$$

where

$$k'_{so} = \frac{k_{so}}{1 - \varepsilon_o} \tag{5.15}$$

Isothermal experimental results were used for the evaluation of reaction order parameter n through linear regression procedure involving a plot of $\ln(t_f)$ against $\ln(p)$. The activation energy E was also determined through linear regression by plotting $\ln t_f$ against $1/T$ at a constant partial pressure.

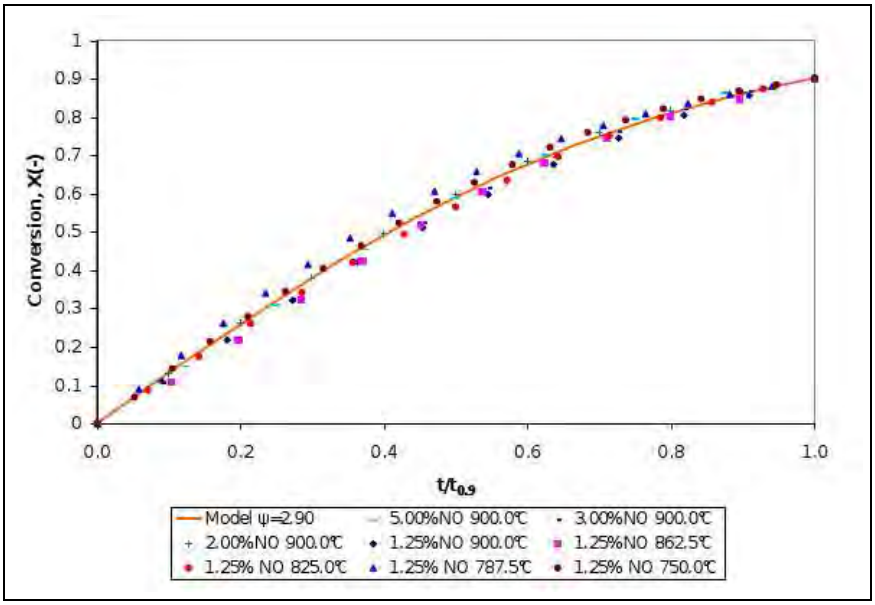

Figure 5.6: Dimensionless plot for experimental data of char A2

5.3.2 Results and discussion

An evaluation of the intrinsic kinetic parameters was done and subsequently used to validate the model. The process involved the determination of the time factor parameter (t_f) for each given experiment. This was followed by the evaluation of the activation energy (E), order of reaction (n) with respect to nitric oxide partial pressure by applying the n^{th} order power rate law and the Arrhenius equation (Section 5.4).

Structural parameter (ψ)

The structural parameter characteristic of the initial char structure was evaluated by using Equation (5.3), through the procedure discussed in Section 5.3.1. The results are presented on Table 5.1.
The values of structural parameter (ψ) range are given on Table 5.1 Chars E1, E3 and F1 had structural parameter of 1.7, 1.1 and 0.7 ($\psi < 2$) respectively, implying that the reaction rates of the chars with NO do not display a maximum when plotted against char conversion and that pore coalescence was the principal structural mechanism. On the other hand chars A2, D1 and D3 had structural parameter of 2.9; 3.1 and 3.0 ($\psi > 2$) respectively

meaning that pore growth coupled with coalescence characterised the structural mechanism (Bhatia and Perlmutter, 1980). This outcome signifies that the initial fine pore char network established during pyrolysis treatment (Everson *et al.*, 2008b), experienced only pore growth during pyrolysis (Bhatia and Perlmutter, 1980) and that the char structure before the reaction with nitric oxide was in such a state that pore coalescence occurred during the NO-char reaction. Therefore the NO-char reaction is kinetically controlled, even at 900°C, according to the random pore model despite the low porosity of the chars. Sun *et al.*, (2009) also used the random pore model on the NO-char reaction to determine the structural parameters. They found the values of ψ which range from 4.3 to 36, while Li *et al.* (1997) obtained a structural parameter value of 7.96.

Table 5.1: Structural parameter (ψ) of the chars.

		Char					
		A2	D1	D3	E1	E3	F1
Structural parameter	(ψ)	2.9	3.1	3.0	1.7	1.1	0.7

Model fitting

The reaction conditions employed to obtain experimental results used for model evaluation and successive determination of kinetic parameters are presented on Table 4.3. The choice of conditions was limited to those used in fluidised bed operation.
The comparison of the random pore model with experimental results for char conversions are shown in Figure 5.7 and Figure 5.8 for the effect of temperature on 1.25% NO, and NO concentration at 900°C respectively. It is apparent that the model displayed a good fit with the experimental char conversion of the chars.

Time factor, t_f (Lumped reaction rate)

The time scale parameter (t_f) was calculated by using Equation (5.10) through regression for each given experiment, using the respective structural parameters (ψ) which were determined as outlined in Section 5.4. The calculated

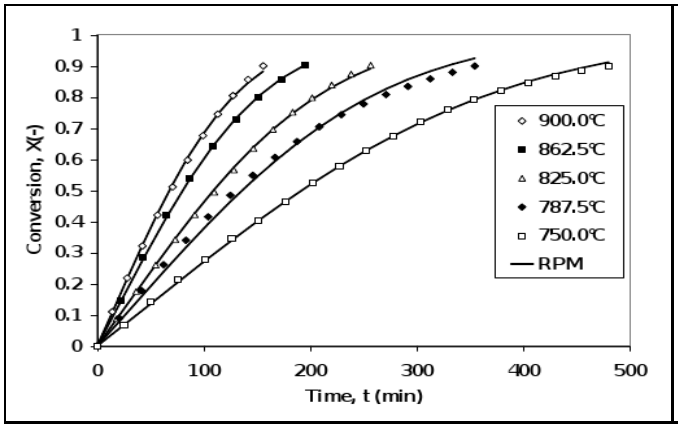

(a) Effect of temperature on 1.25% NO and char A2 reaction using ψ=2.90

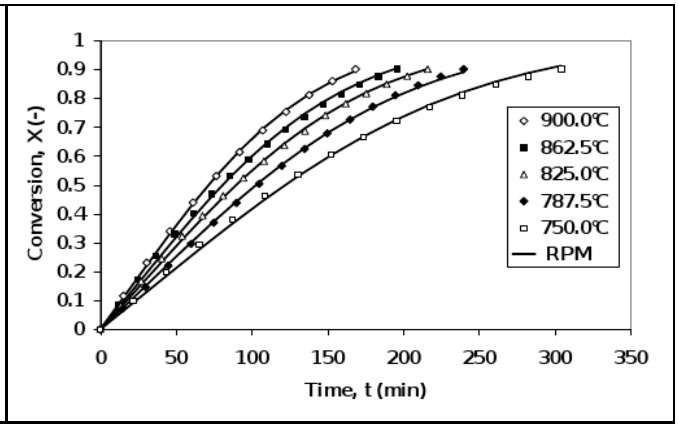

(b) Effect of temperature on 1.25% NO and char D1 reaction using ψ=3.07

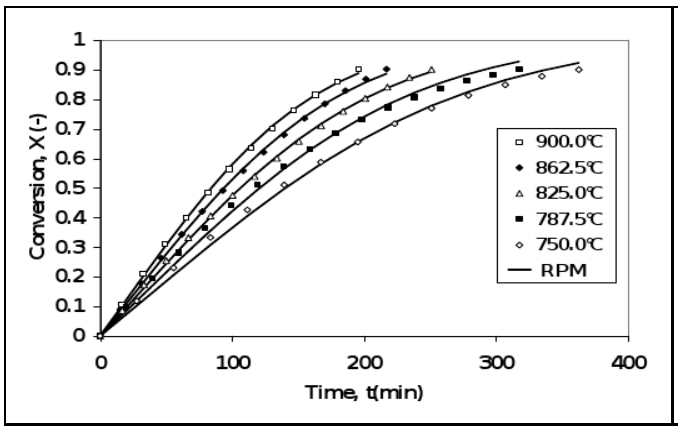

(c) Effect of temperature on 1.25% NO and char D3 reaction using ψ=2.95

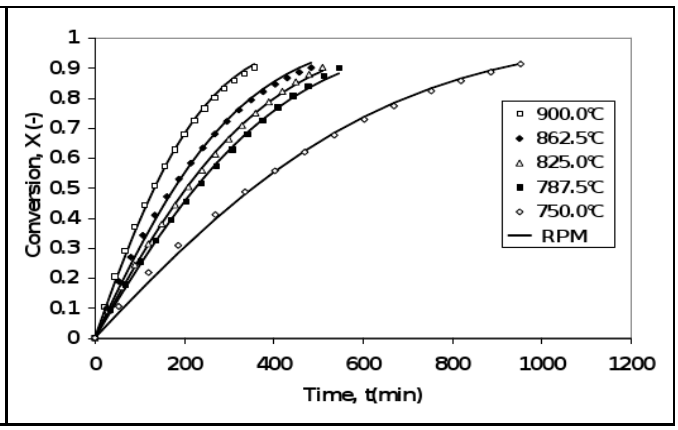

(d) Effect of temperature on 1.25% NO and char E1 reaction using ψ=1.66

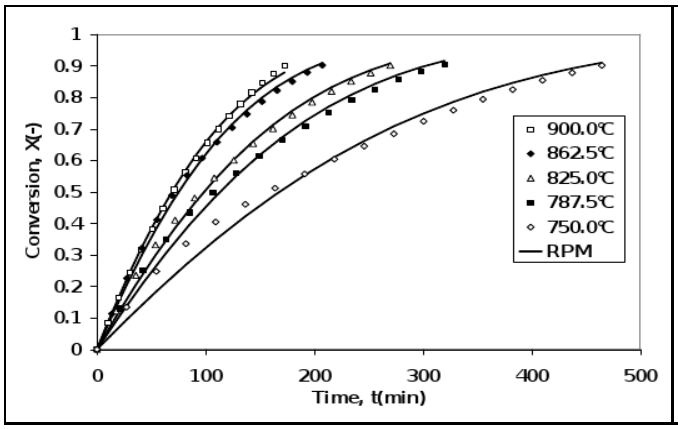

(e) Effect of temperature on 1.25% NO and char E3 reaction using ψ=1.14

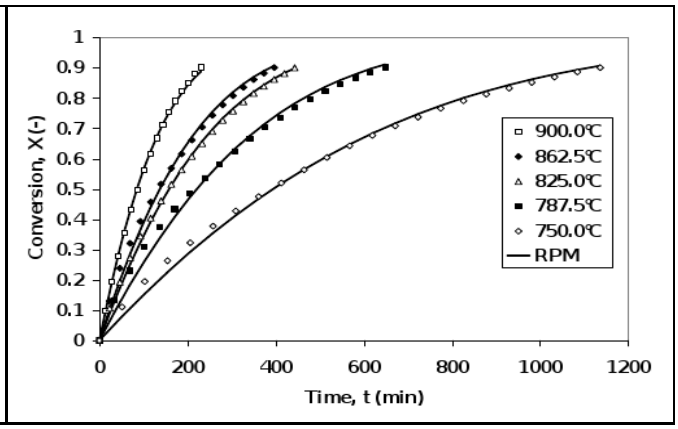

(f) Effect of temperature on 1.25% NO and char F1 reaction using ψ=0.70

Figure 5.7: The random pore model for 1.25% NO reaction with chars up to 90% conversion

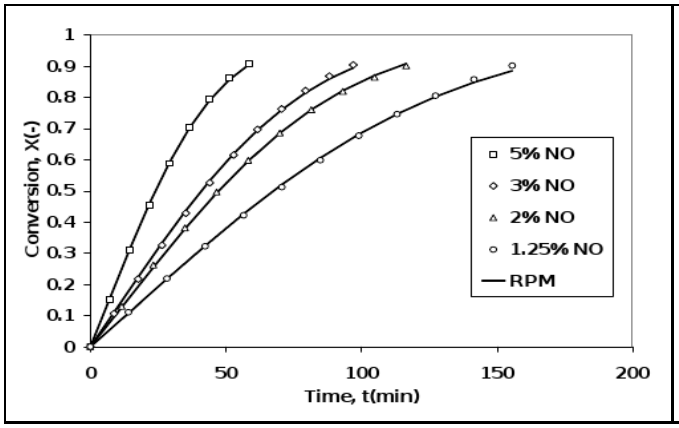

(a) Effect of NO concentration on char A2 reaction rate at 900°C using ψ=2.90

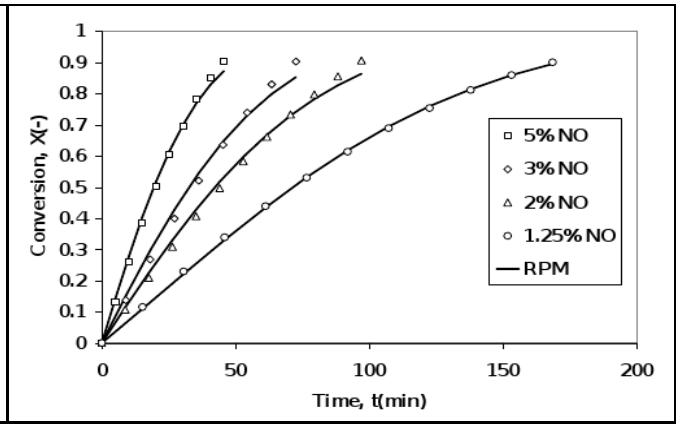

(b) Effect of NO concentration on char D1 reaction rate at 900°C using ψ=3.07

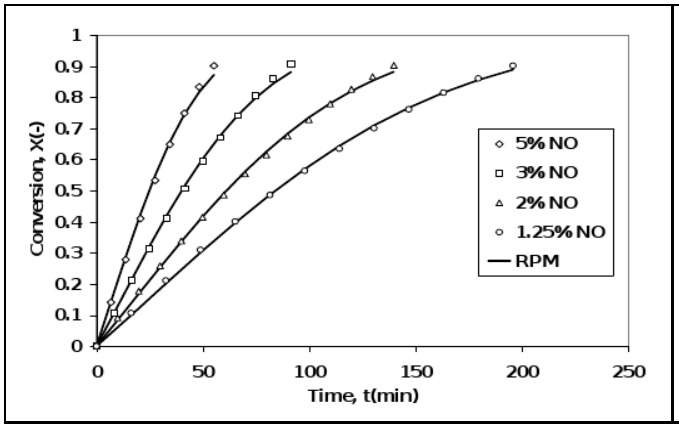

(c) Effect of NO concentration on char D3 reaction rate at 900°C using ψ=2.95

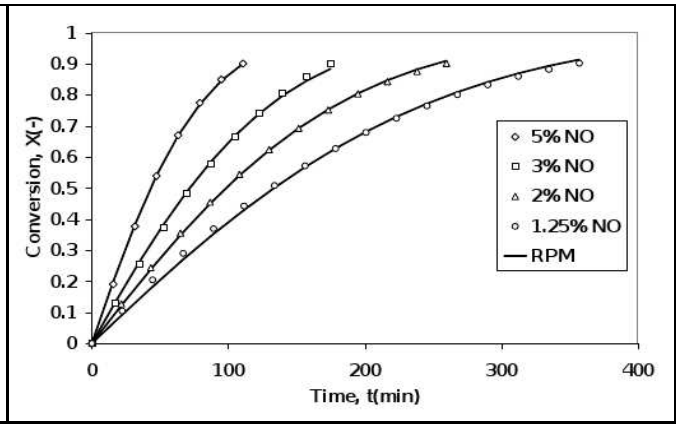

(d) Effect of NO concentration on char E1 reaction rate at 900°C using ψ=1.66

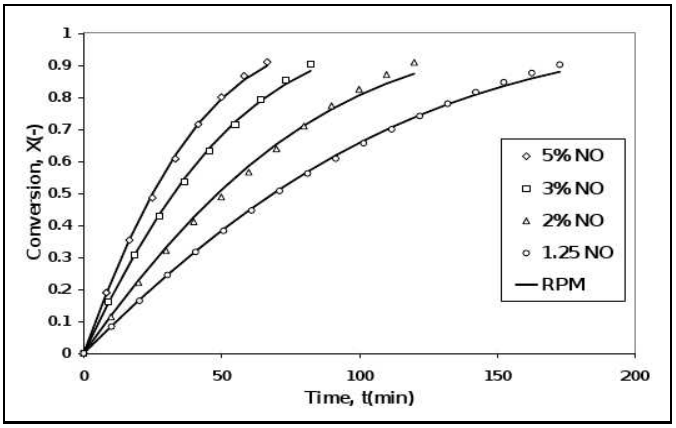

(e) Effect of NO concentration on char E3 reaction rate at 900°C using ψ=1.14

Figure 5.8: Model fittings of experimental data at various NO concentrations at 900°C and 87.5kPa.

values are presented on Table 5.2, which shows that the time factor increased with increase in temperature and NO partial pressure as expected.

Table 5.2: Time factor t_f values obtained at 87.5kPa

		t_f values ($\times 10^{-3}$ min^{-1})					
Temp (°C)	%NO	A2	D1	D3	E1	E3	F1
750.0	1.25	2.64	4.10	3.60	1.59	3.53	1.64
787.5	1.25	3.73	4.86	4.18	2.50	5.23	2.82
825.0	1.25	4.65	5.57	4.75	2.74	6.02	3.95
862.5	1.25	6.33	6.19	5.38	3.15	7.87	4.72
900.0	1.25	7.45	7.00	6.00	4.21	8.58	7.32
900.0	2.00	10.7	13.1	8.26	5.72	12.1	-
900.0	3.00	12.4	17.1	12.6	7.84	18.1	-
900.0	5.00	21.1	28.6	20.4	13.0	23.6	-

Activation energy

The activation energy was evaluated by using Equation (5.14), achieved by plotting $\ln t_f$ against $\frac{1}{T}$ of which a straight line with a gradient of $-\frac{E_a}{R}$ is produced. The activation energies calculated from the plots shown on Figure 5.9(a) to 5.9(f) are given on Table 5.3. The value of activation energies ranged from 34 kJmol^{-1} to 94 kJmol^{-1}.

The values of the activation energies agree with results obtained at low temperatures and published by Matos *et al.* (1990), Lu *et al.* (1992), Li *et al.* (1998) and Li *et al.* (1999) and Wang *et al.* (2005). It was established that two temperature regimes for reactivity exist with a distinctive change in the activation energy due to a change in the rate-determining step involving surface complexes. It was reported by Li *et al.* (1999) that at high temperatures the activation energy (118 kJmol^{-1}) is much higher than that in the low temperature regime (52 kJmol^{-1}) with a break point (Arrhenius plot) at approximately 700°C. The low activation energy at low temperatures was established to be a result of slow desorption of surface complexes which determines the overall rate (Li *et al.,* 1998).

Table 5.3: Apparent activation energies evaluated at 750-900°C

		Char					
		A2	D1	D3	E1	E3	F1
Activation energy	($kJmol^{-1}$)	69.6	35.0	34.0	58.4	58.6	94.4
Correlation coefficient, r^2		0.9939	0.9965	0.9993	0.9425	0.9648	0.9694

Order of reaction

The reaction order (n) with respect to nitric oxide partial pressure was evaluated by using Equation (5.14). Figure 5.10(a) to Figure 5.10(e) were obtained through plotting $\ln(t_f)$ as a function of $\ln(P_{NO})$ at 900°C and a pressure of 87.5kPa. The partial pressure dependence (n) was evaluated directly from the gradient of the linear plots. The results are tabulated on Table 5.4, showing that the order of reaction with respect to nitric oxide is close to 1 (0.7-1.0) which conforms to results widely reported in literature (Matos *et al.*, 1990; Lu *et al.*, 1992; Illán-Gómez *et al.*, 1993; Li *et al.*, 1998).

Table 5.4: Order of reaction values obtained at 900°C and 87.5kPa

	Char					
	A2	D1	D3	E1	E3	F1
Order of reaction	0.7	1.0	0.9	0.8	0.8	-
Correlation coefficient, r^2	0.9688	0.9842	0.9931	0.9899	0.9862	-

5.4 Relationship between reactivity and maceral index

To predict the reaction behaviour of nitric oxide with char, quite a number of coal and char characteristics (petrographic, mineral effects etc) were correlated with the reactivity parameters. The modified maceral index gave a meaningful correlation with the lumped reaction rate.
Indices have been used to predict combustion behaviour of coals and blends. Su *et al.* (2001) proposed maceral index (MI) to predict the combustion behaviour of coal based on 68 coals and blends. The proposed MI was evaluated

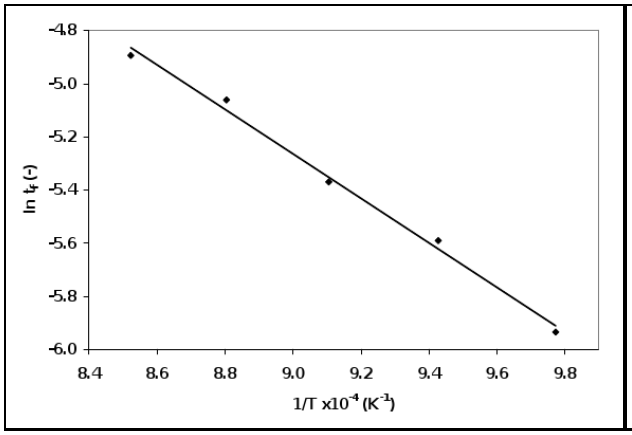

(a) Apparent activation energy determination of 1.25% NO reaction with char A2.

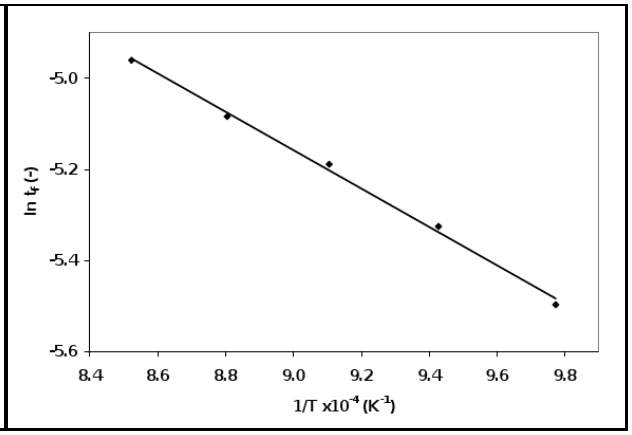

(b) Apparent activation energy determination of 1.25% NO reaction with char D1.

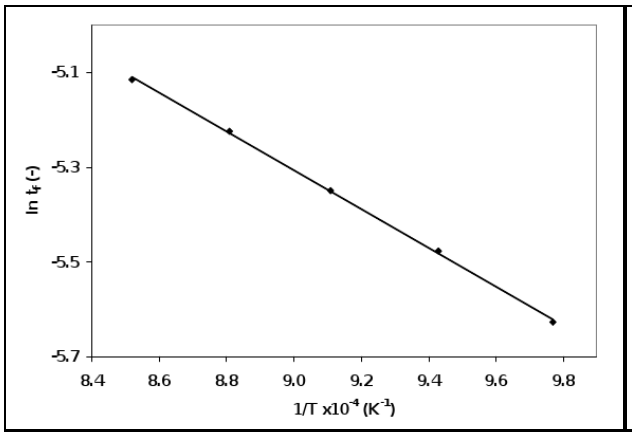

(c) Apparent activation energy determination of 1.25% NO reaction with char D3.

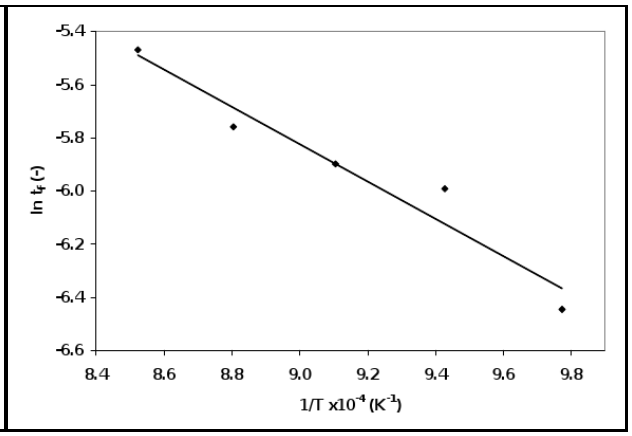

(d) Apparent activation energy determination of 1.25% NO reaction with char E1.

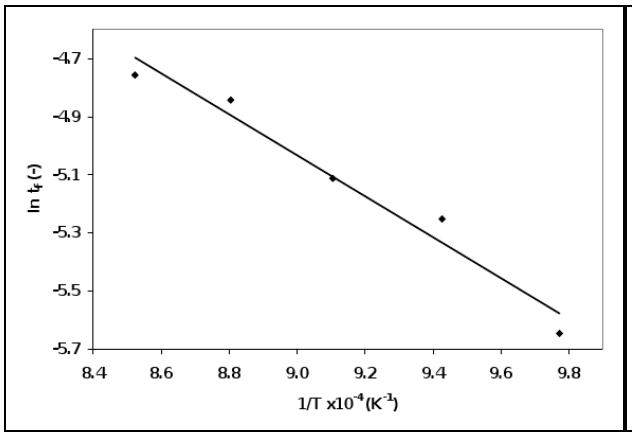

(e) Apparent activation energy determination of 1.25% NO reaction with char E3.

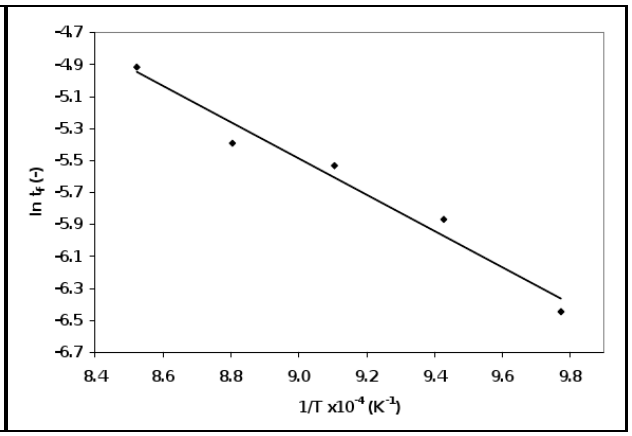

(f) Apparent activation energy determination of 1.25% NO reaction with char F1.

Figure 5.9: Apparent activation energy evaluation of 1.25% NO with chars at 87.5 kPa.

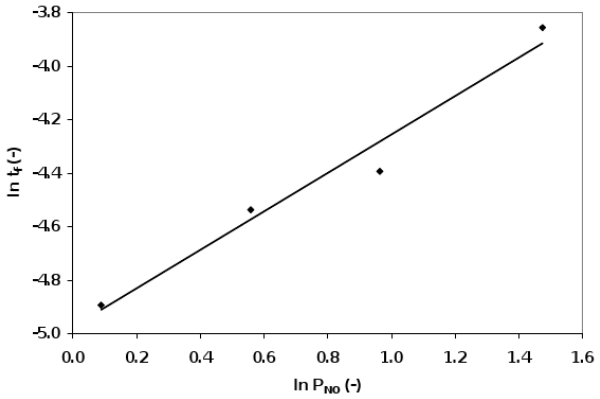

(a) Order of reaction evaluation for NO reaction with char A2 at 900°C.

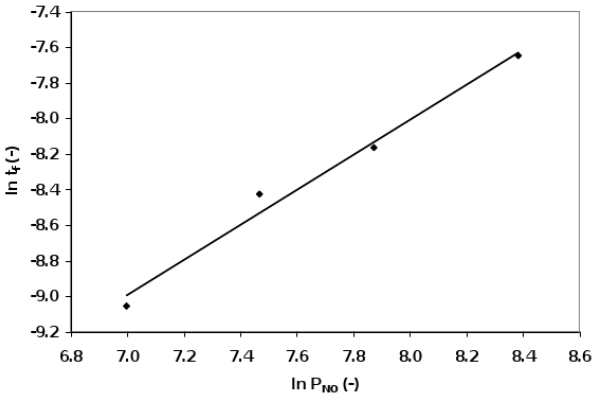

(b) Order of reaction evaluation for NO reaction with char D1 at 900°C.

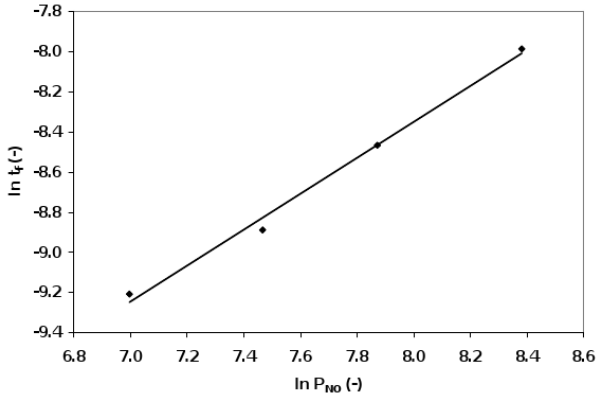

(c) Order of reaction evaluation for NO reaction with char D3 at 900°C.

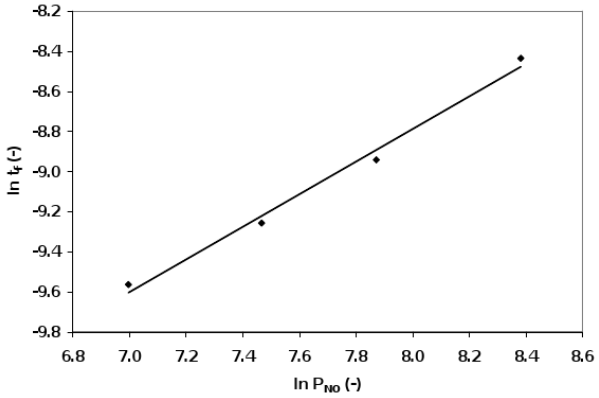

(d) Order of reaction evaluation for NO reaction with char E1 at 900°C.

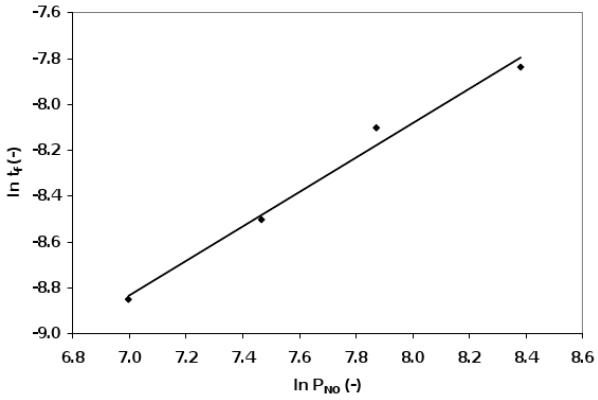

(e) Order of reaction evaluation for NO reaction with char E3 at 900°C.

Figure 5.10: Order of reaction evaluation for NO with chars at 900°C.

by using Equation 5.16;

$$\mathrm{MI} = \frac{\mathrm{L} + \frac{\mathrm{V}}{\mathrm{Rr}^2}}{\mathrm{I}^{1.25}} \left(\frac{\mathrm{CV}}{30}\right)^{2.5} \tag{5.16}$$

where L is the percentage by volume liptinite, mineral matter free (mmf); V is the percentage by volume vitrinite (mmf); I is the percentage by volume inertinite (mmf); Rr is the mean vitrinite reflectance; and CV is the gross calorific value of the coal, MJ·kg^{-1}.

Helle *et al.* (2003) modified the given index by adjusting the content of inertinite "I" to non-reactive content of inertinite "Inr" (inert semifusinite, fusinite/secritinite, micrinite and inert inertodetrinite) and hence coming up with reactive maceral index (RMI) evaluated by using the following expression;

$$\mathrm{RMI} = \frac{\mathrm{L} + \frac{\mathrm{V}}{\mathrm{Rr}^2}}{\mathrm{Inr}^{1.25}} \tag{5.17}$$

where lnr is the volume percentage of non-reactive inertinite on mineral matter free (mmf).

In this study the RMI was modified to predict the reaction behaviour of NO with the given chars on the basis of maceral analysis of the parent coals by adding the reactive component of the inertinite (Ir) to the total vitrinite as shown on Equation 5.17. The expression depicted by Equation (5.18) was used to determine the RMI* based on the results given on Table 5.5.

$$\mathrm{RMI}^* = \frac{\mathrm{L} + \frac{\mathrm{V+Ir}}{\mathrm{Rr}^2}}{\mathrm{Inr}^{1.25}} \tag{5.18}$$

The parameter Ir represents the percentage (by volume) of reactive content of the inertinite (reactive semifusinite and reactive inertodetrinite) on mineral matter free (mmf). The variations of the modified reactive maceral index (RMI*) with the time factor (t_f) are given in Figure 5.11. Although it is not empirically conclusive, the observed trend for values of RMI* ranging from 0.6 to 0.9 show that t_f increases almost linearly with increasing RMI* at temperatures ranging from 750°C to 862.5°C as illustrated in Figures 5.11(a) to 5.11(d). Coal A2 characterised by high vitrinite content falls out of the trend compared to the five coals with high inertinite content. At 900°C and RMI ranging from 0.6 to 1.2, an unsystematic linear relationship between t_f and RMI* is depicted in Figures 5.11(e) and 5.11(f).

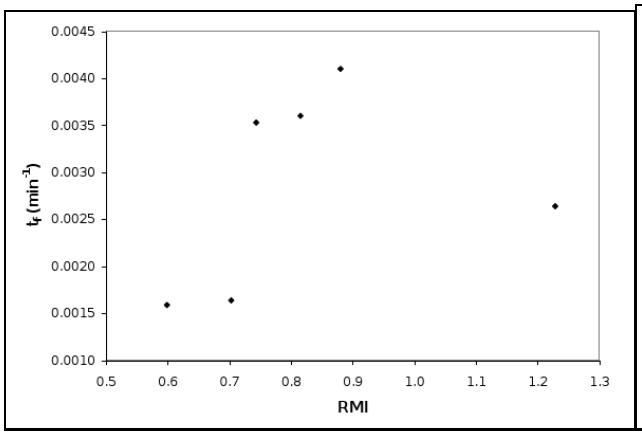

(a) Modified reactive maceral index variation with t_f values at 750°C using 1.25% NO.

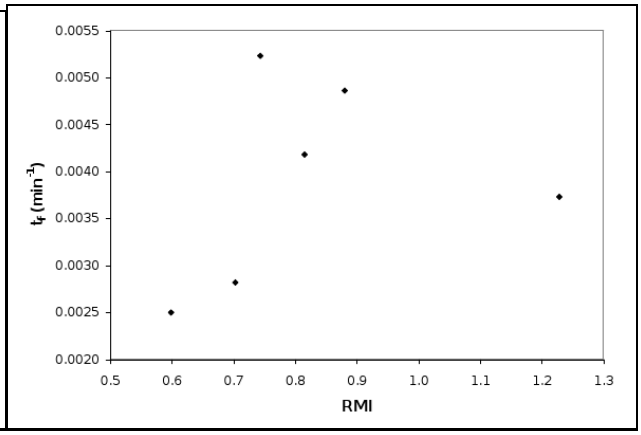

(b) Modified reactive maceral index variation with t_f values at 787.5°C using 1.25% NO.

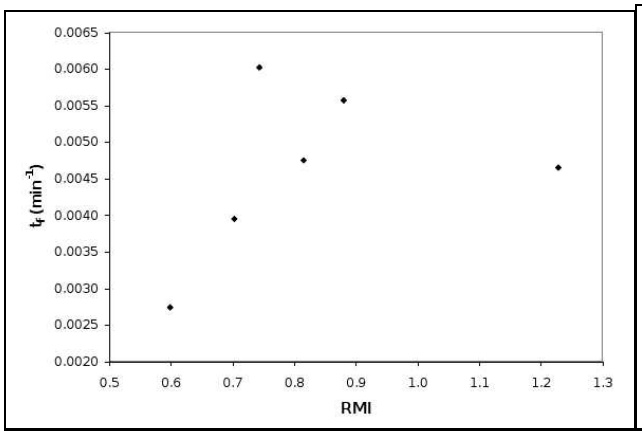

(c) Modified reactive maceral index variation with t_f values at 825°C using 1.25% NO.

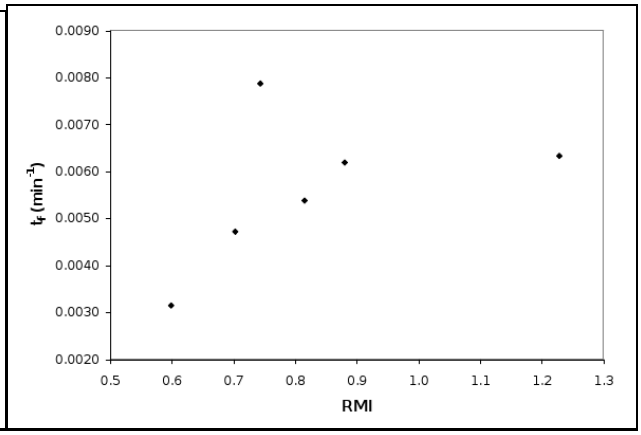

(d) Modified reactive maceral index variation with t_f values at 862.5°C using 1.25% NO.

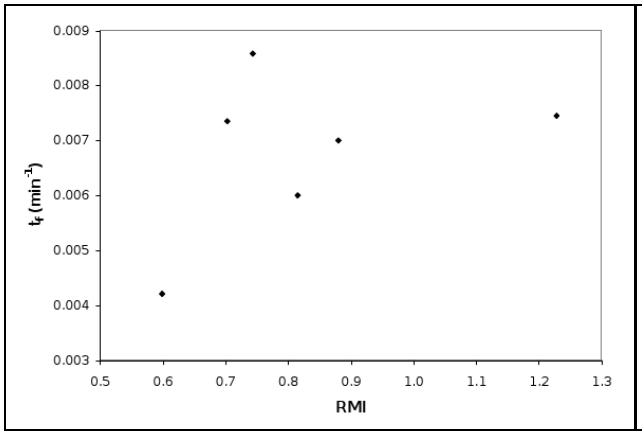

(e) Modified reactive maceral index variation with t_f values at 900°C using 1.25% NO.

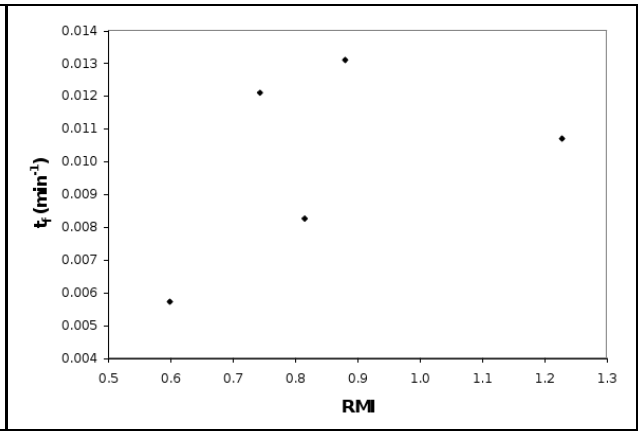

(f) Modified reactive maceral index variation with t_f values at 900°C using 2.0% NO.

Figure 5.11: Modified reactive maceral index (RMI*) variation with the lumped reaction rate (t_f)

Table 5.5: Results used to evaluate the modified reactive maceral index (RMI*) on mineral matter free (mmf).

Coal	Liptinite	Vitrinite	Inertinite (vol. %)		Rr	CV	RMI*
ID	(L) vol. %	(V) vol. %	Reactive (Ir)	Inert (Inr)	%	$MJ \cdot mol^{-1}$	
A2	51	4	7	38	0.72	28.26	1.22
D1	14	4	28	54	0.58	25.86	0.88
D3	16	3	25	56	0.58	26.03	0.82
E1	20	4	26	50	0.78	30.18	0.60
E3	10	4	35	51	0.68	27.69	0.74
F1	12	3	32	52	0.68	27.98	0.70

5.5 Main findings

- Table 5.6 summarises the kinetic parameters obtained and also furnishes the comparison of values obtained by other researchers.
- Initial intrinsic reactivity for the NO-char reaction increased significantly with both temperature and NO concentration.
- The evaluated apparent activation energy range from 34 $kJ \cdot mol^{-1}$ to 94.4 $kJ \cdot mol^{-1}$. These values are within the wide range published in literature.
- The reaction orders range from 0.7 to 1, in conformity with published results.
- The observed trend for the modified reactive maceral index ranging from 0.6 to 0.9 shows that t_f increases almost linearly with increasing RMI* at temperatures ranging from 750°C to 862.5°C. At 900°C for RMI* ranging from 0.6 to 1.2, an unsystematic linear relationship between t_f and RMI* is obtained. Coal A2 characterised by high vitrinite content falls out of the trend compared to the five coals with high inertinite content.

Table 5.6: Kinetic parameters evaluated for NO-char reaction.

	Reference	Carbon/ Char ID	Reactor	Temp range (K)	Structural parameter (ψ)	Activation energy (kJ/Mol)	P_{NO} kPa	Reaction order, n
1.	This study	A2 char	TGA	1023-1173	2.90	69.6	1.09	0.7
		D1 char	TGA	1023-1173	3.07	35.0	1.09	1.0
		D3 char	TGA	1023-1173	2.95	34.0	1.09	0.9
		E1 char	TGA	1023-1173	1.66	58.4	1.09	0.8
		E3 char	TGA	1023-1173	1.14	58.6	1.09	0.8
		F1 char	TGA	1023-1173	0.70	94.4	1.09	-
2.	Li *et al.* (1998)	Sub-bitu coal char	TGA	973-1173	7.96	120		1.0
3.	Lu *et al.* (1992)	Act carbon	TGA	973-1173	-	68.4	0.3-1.5	1.0
4.	Matos *et al.* (1990)	Coal char	FBC	848-1003	-	47		1.0
5.	Sun *et al.* (2009)	YB char	TGA	973-1173	4.3-10	116.8		
		SH char	TGA	973-1173	31.38-36.01	121.5		
6.	Wang *et al.* (2005)	Coal-char	TGA	303-1173	-	30-46		
		Graphon	TGA	303-1173	-	54-67		

CHAPTER 6

Conclusions and Recommendations

6.1 Conclusions

The six low grade coal chars with high ash and rich in inertinite were characterised and subsequent reactivity experiments carried out by using a thermogravimetric analyser under fluidised bed combustion conditions (750-900°C and 87.5 kPa).

- The six coals analysed and the respective char samples are characterised as high ash products with low calorific values and relatively low nitrogen content. Petrographically, the six parent coals have high total inertinite, low vitrinite content and extremely low liptinite composition.
- The vitrinite random reflectance data showed that the coal samples are classified as bituminous, Medium Rank C to D.
- The reactive parent coal macerals formed minor proportions of isotropic "coke" and fine char networks with respect to the chars formed at 900°C. Some of the vitrinites and a large portion of the coal inertinites exhibited greatly increased reflectance but still remained noticeable in original maceral form.
- The majority of the char carbon forms had not increased in porosity to any great extent even though marked devolatilisation had taken place.

- Significant devolatilisation coupled with marked complete maceral conversion occurred, consisting of a large fraction of dense char (low porosity) emanating from inertinite with a more pronounced reflectance.
- NO-char initial intrinsic reactivity increased markedly with increasing temperature.
- The fitting of the random pore model and the structural parameter characterising the pore behaviour during the NO-char reaction were evaluated by plotting char conversion against a reduced time parameter (real time/time for 90% conversion). This made it possible to approximate the structural parameter using results obtained at different temperatures.
- Some of the chars displayed structural mechanism marked with pore coalescence while others displayed pore coalescence in conjunction with pore growth.
- Low activation energies were obtained within the range 750 to 900°C which is attributed to the presence of a slow desorption (of surface complexes) rate determining step.
- Calculated values of apparent activation energies are within the wide range published in literature.
- The reaction was confirmed to be first order with respect to NO concentration, in conformity with values obtained in literature.
- The modified maceral index gave a linear relationship with t_f values for coals that had a predominantly high inertinite content, the coal with a substantial amount of vitrinite deviated from the correlation.

6.2 Recommendations

Based on the results of this study, the following recommendations are suggested for further investigation towards contributing and expansion of knowledge of clean utilisation of high ash discard coals with rich inertite content.

- An extensive characterisation needs to be conducted on the coal discard feed stocks and the respective chars in order to understand the

NO-char reaction attributes in depth. Advanced characterisation techniques such as ss-NMR, FTIR, LD-TOF MS, HRTEM and gas product analyses coupled with conventional characterisation methods can be used for molecular modelling to simulate char behaviour during NO-char reactions.

- Further studies incorporating various aspects influencing reactivity like particle size and pressure need to be undertaken.
- A study incorporating NO and a mixture of gases present in the FBC such as NO/O_2; NO/N_2O; NO/CO; NO/CO_2 or NO/SO_2 combinations should be carried out to shed more light on the effects of other gaseous species present.
- In order to understand the effect of macerals or char carbon forms, using maceral indices or otherwise, on NO reduction prediction large sample size with varying maceral compostions or different ranks need to be used.
- Further investigation needs to be directed towards nitrous oxide (N_2O) especially given that N_2O is a potent greenhouse gas, it has become a concern because of its link to climate change.

CHAPTER 7

References

AARNA, I. AND SUUBERG, E.M. (1997) A review of the kinetics of the nitric oxide-carbon reaction. *Fuel* **76** (6), 475-491.

AIHARA, T., MATSUOKA, K., KYOTANI, T. AND TOMITA, A. (2000) Mechanism of N_2 formation during coal char oxidation. *Proceedings of the Combustion Institute* **28**, 2189-2195.

ALVAREZ, D. AND BORREGO, A.G. (2007). The evolution of char surface area along pulverized coal combustion. *Energy & Fuels* **21**, 1085-1091.

ARMESTO, L., BOERRIGTER, H., BAHILLO, A. AND OTERO, J. (2003) N_2O emissions from fluidised bed combustion. The effect of fuel characteristics and operating conditions. *Fuel* **82**, 1845-1850.

AVRAMI, M. (1940) Kinetics of phase change: II Transformation-time relations for random distribution of nuclei. *Journal of Chemical Physics* **8**, 212.

BASU, P. (2006) Combustion and gasification in fluidized beds. New York: Taylor and Francis. 10-12.

BELLOTTO, M., GUALTIERI, A., ARTIOLI, G., AND CLARK, S.M. (1995) Kinetic study of the kaolinite-mullite reaction sequence. Part I: kaolinite dehydroxylation. *Phys. Chem. Minerals* **22**, 207-214.

BEND, S.L., EDWARDS, I.A.S. AND MARSH, H. (1992) The influence of rank upon char morphology and combustion. *Fuel* **71**, 493-501.

BENFELL, K.E. (2001) Assessment of char morphology in high-pressure pyrolysis and combustion. Doctoral Thesis. The University of Newcastle. Australia.

BERKOWITZ, N. (1985) The chemistry of coal. Amsterdam, New York.

BHATIA, S.K. AND PERLMUTTER, D.D. (1980) A random pore model for fluid-solid reactions: I. Isothermal, kinetic control. *AlChE Journal* **26** (3), 379-385.

BISWAS, S., CHOUDHURY, N., GHOSAL, S., MITRA, T., MUKHERJEE, A., SAHU, S.G. AND KUMAR., M. (2007) Impact of petrographic properties on the burning behavior of pulverized coal using a drop tube furnace. *Energy & Fuels* **21**, 3130-3133.

BORREGO, A.G. AND ALVAREZ, D. (2007). Comparison of chars obtained under oxy-fuel and conventional pulverized coal combustion atmospheres. *Energy & Fuels* **21**, 3171-3179.

CHAIKLANGMUANG, S., JONES, J. M., POURKASHANIAN, M. AND WILLIAMS, A. (2002) Conversion of volatile-nitrogen and char-nitrogen to NO during combustion. *Fuel* **81**, 2363-2369.

CHAMBRION, P., ORIKASA, H., SUZUKI, T., KYOTANI, T. AND TOMITA, A. (1997) A study of the $C - NO$ reaction by using isotopically labelled C and NO. *Fuel* **76** (6), 493-498.

CHEN, Z., LIN, M., IGNOWSKI, J., KELLY, B., LINJEWILE, T.M. AND AGARWAL, P.K. (2001) Mathematical modeling of fluidized bed combustion. 4: N_2O and NO_x emissions from the combustion of char. *Fuel* **80**, 1259-1272.

CLOKE, M. AND LESTER, E. (1994). Characterisation of coals for combustion using petrographic analysis. A review. *Fuel* **73**, 315-320.

DME. (2003) South Africa's mineral industry 2002/2003. Pretoria, South Africa, Government Printer.

DME. (2006) Digest of South African Energy Statistics. http://www.dme.gov.za/ [Date of access: 21 February 2009].

DU CANN, V.M. (2008). Test Report. PSA 2008-040. Petrographics SA.

EPA. (1998) Nitrogen oxides hazards. http://www.epa.gov/ [Date of access: 23 January 2008]

ESKOM. (2007) Annual Report. http://www.eskom.co.za/publications. [Date of access: 23 January 2008]

EVERSON, R.C., NEOMAGUS, H.W.J.P. AND KAITANO, R. (2005) The modeling of the combustion of high-ash coal-char particles suitable for pressurised fluidized bed combustion: shrinking reacted core model. *Fuel* **84**, 1136-1143.

EVERSON, R.C., NEOMAGUS, H.W.J.P. AND NJAPHA, D. (2006a) Kinetic analysis on non-isothermal thermgravimetric analyser results using a new method for the evaluation of the temperature integral and multi-heating rates. *Fuel* **85**, 418-422.

EVERSON, R.C., NEOMAGUS, H.W.J.P., KASAINI, H. AND NJAPHA, D. (2006b) Reaction kinetics of pulverised coal-chars derived from inertinite-rich coal discards: Gasification with carbon dioxide and steam. *Fuel* **85** (7-8), 1076-1082.

EVERSON, R.C., NEOMAGUS, H.W.J.P., KAITANO, R., FALCON, R. AND DU CANN, V.M. (2008a) Properties of high ash coal-char particles derived from inertinite-rich coal: II. Gasification kinetics with carbon dioxide. *Fuel* **87**, 3403-3408.

EVERSON, R.C., NEOMAGUS, H.W.J.P., KAITANO, R., FALCON, R., VAN ALPHEN, C. AND DU CANN, V.M. (2008b) Properties of high ash coal-char particles derived from inertinite-rich coal: I. Chemical, structural and petrographic characteristics. *Fuel* **87**, 3082-3090.

EUROPEAN COMMISSION. (2001) Directive 2001/80/EC on the limitation of emissions of certain pollutants into the air from large combustion plants.

FOGLER, H.S. (1992) Elements of chemical reaction engineering, 2^{nd} Edition. Prentice Hall, Englewood Cliffs, NJ. 838.

FURUSAWA, T., TSUNODA, M., TSUJIMURA, M. AND ADSCHIRI, T. (1985) Nitric oxide reduction in fluidized-bed combustion of coal. *Fuel* **64**, 1306.

GARRIDO, J., LINARES-SOLANO, A., MARTIN-MARTINEZ, J.M. AND MOLINA-SABIO, M. (1987) Use of N_2 vs. CO_2 in characterisation of activated carbons. *Langmuir* **3**, 76-81.

GAVALAS, G.R. (1980) A random capillary model application to char gasification at chemically controlled rates. *AlChE Journal* **26** (4), 577-585.

GLARBORG, P., JENSEN, A.D. AND JOHNSSON, J.E. (2003) Fuel nitrogen conversion in solid fuel fired systems. *Progress in Energy and Combustion Science* **29**, 89-113.

GRAY, P.G. AND DO, D.D. (1993) Modelling of the interaction of nitrogen dioxide with activated carbon II. Kinetics of reaction with pore evolution. *Chemical Engineering Communication* **125**, 109-120

GREGG, S.J. AND SING, K.S.W. (1982). Adsorption, surface area and porosity. Second edition. Academic Press. London.

GUNGOR, A. (2009) Prediction of SO_2 and NO_X emissions for low-grade Turkish lignites in CFB combustors. *Chemical Engineering Journal* **146**, 388-400.

HARDING, A.W., BROWN, S.D. AND THOMAS, K.M. (1996) Release of NO from the combustion of coal chars. *Combustion and Flame* **107**, 336-350.

HAYHURST, A.N. AND LAWRENCE, A.D. (1992). Emissions of nitrous oxide from combustion sources. *Progress in Energy Combustion Science* **18**, 529-552.

HAYHURST, A.N. AND LAWRENCE, A.D. (1997) Reduction of the nitrogen oxides NO and N_2O to molecular nitrogen in the presence of iron, its oxides, and carbon monoxide in a hot fluidized bed. *Combustion and Flame* **110**, 351-365.

HE, R., SUDA, T., TAKAFUJI, M., HIRATA, T. AND SATO, J. (2004). Analysis of low NO emission in high temperature air combustion for pulverised coal. *Fuel* **83**, 1133-1141.

HELLE, S., GORDON, A., ALFARO, G., GARCÍA, X. AND ULLOA, C. (2003). Coal blend combustion: link between unburnt carbon in fly ashes and maceral composition. *Fuel Processing Technology* **80**, 209-223.

HILL, S.C. AND SMOOT, L.D. (2000) Modeling of nitrogen oxides formation and destruction in combustion systems. *Progress in Energy and Combustion Science* **26**, 417-458.

HODGE, E.M., ROBERTS, D.G., HARRIS, D.J. AND STUBINGTON, J.F.(2010) The significance of char morphology to the analysis of high-temperature char-CO_2 reaction rates. *Energy & Fuels* **24**, 100-107.

IEO, 2009. (2009) International Energy Outlook 2009. http://www.eia.doe.gov/ [Date of access: 05 May 2010].

ILLÁN-GÓMEZ, M.J., LINARES-SOLANO, A., SALINAS-MARTINEZ DE LECEA, C. AND COLO, J.M. (1993) NO reduction by activated carbons. 1. The role of carbon porosity and surface area. *Energy & Fuels* **7**, 146-154.

ILLÁN-GÓMEZ, M.J., LINARES-SOLANO, A., RADOVIC, L.R. AND SALINAS-MARTINEZ DE LECEA, C. (1995a) NO reduction by activated carbons. 2. Catalytic effect of potassium. *Energy & Fuels* **9**, 97-103.

ILLÁN-GÓMEZ, M.J., LINARES-SOLANO, A., RADOVIC, L.R. AND SALINAS-MARTINEZ DE LECEA, C. (1995b) NO reduction by activated carbons. 3. Influence of catalyst loading on the catalytic effect of potassium. *Energy & Fuels* **9**, 104-111.

ILLÁN-GÓMEZ, M.J., LINARES-SOLANO, A., RADOVIC, L.R. AND SALINAS-MARTINEZ DE LECEA, C. (1995c) NO reduction by activated carbons. 4. Catalysis by calcium. *Energy & Fuels* **9**, 112-118.

ILLÁN-GÓMEZ, M.J., LINARES-SOLANO, A., RADOVIC, L.R. AND SALINAS-MARTINEZ DE LECEA, C. (1995d) NO reduction by activated carbons. 5. Catalytic effect of iron. *Energy & Fuels* **9**, 540-548.

ILLÁN-GÓMEZ, M.J., LINARES-SOLANO, A. AND SALINAS-MARTINEZ DE LECEA, C. (1995e) NO reduction by activated carbons. 6. Catalysis by transition metals. *Energy & Fuels* **9**, 976-983.

ILLÁN-GÓMEZ, M.J., LINARES-SOLANO, A., RADOVIC, L.R. AND SALINAS-MARTINEZ DE LECEA, C. (1995f) NO reduction by activated carbons. 7. Some mechanistic aspects of uncatalyzed and catalyzed reaction. *Energy & Fuels* **10**, 158-168.

JOHNSSON, J.E. (1994) Formation and reduction of nitrogen oxides in fluidized-bed combustion. *Fuel* **73** (9), 1398-1415.

JONES, J.M., PATTERSON, P.M., POURKASHANIAN, M. AND WILLIAMS A. (1999) Approaches to modelling heterogeneous char NO formation/destruction during pulverised coal combustion. *Carbon* **37**, 1545-1552.

KABE, T., ISHIHARA, A., QIAN, E.W., SUTRISNA, I.P. AND KABE, Y. (2004) Coal and coal-related compounds: structures, reactivity and catalytic reactions. Kodansha Elsevier.

KAMBARA, S., TAKARADA, T., YAMAMOTO, Y. AND KATO, K. (1993) Relation between functional forms of coal nitrogen and formation of NO_x precursors during rapid pyrolysis. *Energy & Fuels* **7**, 1013-1020.

KAITANO, R. (2007) Characterisation and reaction kinetics of high ash chars derived from inertinite-rich coal discards. Doctoral Thesis. North-West University, Potchefstroom, South Africa.

KÖPSEL, R.F.W. AND HALANG, S. (1997) Catalytic influence of ash elements on NO_x formation in char combustion under fluidized bed conditions. *Fuel* **76** (4), 345-351.

KUROSE, R., TSUJI, H. AND MAKINO, H. (2001a). Effects of moisture in coal on pulverized coal combustion characteristics. *Fuel* **80**, 1457-1465.

KUROSE, R., TSUJI, H. AND MAKINO, H. (2001b). Numerical simulation of pulverized coal combustion in a furnace. Effects of moisture in coal on combustion characteristics. *Transactions of the Japan Society of Mechanical Engineers. B* **67** (653), 210-218.

KYOTANI, T. AND TOMITA, A. (1999) Analysis of the reaction of carbon with NO/N_2O using ab initio molecular orbitary theory. *Journal of Physical Chemistry B* **103**, 3434-3441.

LAZARO, M.J., IBARRA, J.V., MOLINER, R., DE ANDRES, A.G. AND THOMAS, K.M. (1996) The release of nitrogen during the combustion of coal chars: the role of volatile matter and surface area. *Fuel* **75** (8), 1014-1024.

LI, Y.H., LU, G.Q. AND RUDOLPH, V. (1998) The kinetics of NO and N_2O reduction over coal chars influidised-bed combustion. *Chemical Engineering Science* **53**, 1-26.

LI, Y.H., RADOVIC, L.R., LU, G.Q. AND RUDOLPH, V. (1999) A new kinetic model for NO-carbon reaction. *Chemical Engineering Science* **54**, 4125-4136.

LISSIANSKI, V.V., ZAMANSKY, V.M. AND MALY, P.M. (2001) Effect of metal-containing additives on NO_x reduction in combustion and reburning. *Combustion and Flame* **125**, 1118-1127.

LIU, D.C., SHEN, B.X., FENG, B, LIN, Z.J. AND LU, J.D. (1999) Influence of coal properties on emissions of nitrous oxides and nitric oxides. *Energy & Fuels* **13** (6), 1111-1113.

LU, G.Q. AND DO, D.D. (1992). A kinetic study of coal reject-derived char activation with CO_2, H_2O and air. *Carbon* **30** (1). 21-29.

LU, G.Q. AND TOH, K.C. (1993) A kinetic study of the NO-carbon reaction for NO_x reduction. *Gas Separation and Purification*. **7**, 225-228.

MANN, M.D., COLLINGS, M.E. AND BOTROS, P.E. (1992) Nitrous oxide emissions in fluidized-bed combustion: Fundumental chemistry and combustion testing. *Progress in Energy Combustion Science* **18**, 447-461.

MATOS, M.A.A., PEREIRA, F.J.M.A. AND VENTURA, J.M.P. (1990) Kinetics of NO reduction by anthracite char in a fluidized bed reactor. *Fuel* **69**, 1435-1439.

MENDEZ, L.B., BORREGO, A.G., MARTINEZ-TARAZONA, M.R. AND MENENDEZ, R. (2003) Influence of petrographic and mineral matter composition of coal particles on their combustion reactivity. *Fuel* **82**, 1875-1882.

MIREK, P., SEKRET, R. AND NOWAK, W. (2007) The influence of air nozzles' shape on the NO_x emissions in the large-scale 670 MWT CFB boiler. *The 12th International Conference on Fluidization - New Horizons in Fluidization Engineering*. **Fluidization XII**, Paper 119.

MOCHIDA, I. AND SAKANISHI, K. (2000) Catalysts for coal conversions of the next generation. *Fuel* **79**, 221.

MOHR, S.H. AND EVANS G.M. (2009) Forecasting coal production until 2100. *Fuel* **88**, 2059.

NORMANN, F., ANDERSSON, K., LECKNER, B. AND JOHNSSON, F. (2008) High-temperature reduction of nitrogen oxides in oxy-fuel combustion. *Fuel* **87**, 3579-3585.

OLLERO, P., SERRERA, A., ARJONA, R. AND ALCANTARILLA, S. (2002) Diffusional effects in TGA gasification experiments for kinetic determination. *Fuel* **81**, 1989-2000.

PEVIDA, C., ARENILLAS, A., RUBEIRA, F. AND PIS, J.J. (2005) Heterogeneous reduction of nitric oxide on synthetic coal chars. *Fuel* **84**, 2275-2279.

REN, Q., ZHAO, C., WU, X., LIANG, C., CHEN, X., SHEN, J. AND WANG, Z. (2010) Formation of NO_x precursors during wheat straw pyrolysis and gasification with O_2 and CO_2. *Fuel* **89**, 1064-1069.

SHEN, B.X., MI, T., LIU, D.C., FENG, B., YAO, Q.AND WINTER, F. (2003) N_2O emission under fluidized bed combustion condition. *Fuel Processing Technology* **84**, 13-21.

STANLEY-WOOD, N.G. AND LINES, R.W. (1992) Particle size analysis. Royal Society of Chemistry. University of Technology. Loughborough, UK.

SU, S. POHL, J.H., HOLCOMBE, D. AND HART J.A. (2001) A proposed maceral index to predict combustion behaviour of coal. *Fuel* **80**, 699-706.

SUN, S., ZHANG, J., HU, X., WU, S., YANG, J., WANG, Y. AND QIN, Y. (2009) Studies of NO-char reaction kinetics obtained from drop-tube furnace and thermogravimetric experiments. *Energy Fuels* **23**, 74-80.

TAKARADA, T., TAMAI, Y. AND TOMITA, A. (1985) Reactivities of 34 coals under steam gasification. *Fuel* **64**, 1438-1442.

TENG, H., SUUBERG, E.M. AND CALO, J.M. (1992) Studies on the reduction of nitric oxide by carbon: The NO-carbon gasification reaction. *Energy & Fuels* **6**, 398-406.

TENG, H., LIN, H.C. AND HSIEH, Y.S. (1997) Thermogravimetric studies on the global kinetics of carbon gasification in nitrous oxide. *Industrial & Engineering Chemistry Research* **36**, 523-529.

THOMAS, C.G., HOLCOMBE, D., SHIBAOKA, M., YOUNG, B.C., BRUNCKHORST, L.F. AND GAWRONSKI, E. (1989) Determination of Effect of coal Rank and Maceral compositions on pf combustion reactivity. *Proceedings of the 1989 International Conference on Coal Science* NEDO, Tokyo. p257.

THOMAS, K.M. (1997) The release of nitrogen oxides during char combustion. *Fuel* **76**, 457-473.

TOMITA, A. (2001) Suppression of nitrogen oxides emission by carbonaceous reductants. *Fuel Processing Technology* **71**, 53-70.

TSAI, S.C. (1982) Fundamentals of coal beneficiation and utilization, New York, Elsevier Scientific Publishing Company.

UNITED STATES ENVIRONMENTAL PROTECTION AGENCY (EPA). (1998) NO_x How nitrogen oxides affect the way we live and breathe. http://www.epa.gov/oar/urbanair/nox/noxfldr.pdf [Date of access: 24 February 2008].

WALKER JR, P.L., VERNA, S.K., RIVERA-ULTRILLA, J. AND KHAN, M.R. (1988) A direct measurement of expansion in coals and macerals induced by carbon dioxide and methanol. *Fuel* **67** (5), 719.

WANG, S., SLOVAK, V. AND HAYNES, B.S. (2005) Kinetic studies of graphon and coal-char reaction with NO and O_2: direct and non-linear regression from TG curves. *Fuel Processing Technology* **86**, 651-660.

WOJTOWICZ, M.A., PELS, J.R. AND MOULIN, J.A. (1993) Combustion of coal as a source of N_2O emission. *Fuel Processing Technology*. **34** (1), 1-71.

WOJTOWICZ, M.A., PELS, J.R. AND MOULIN, J.A. (1994) N_2O emission control in coal combustion. *Fuel* **73** (9), 1416-1422.

WCI. (2005) Coal: Secure Energy. http://www.worldcoal.org/ [Date of access: 14 January 2008].

WCI. (2007) Coal meeting the climate challenge: Technology to reduce greenhouse gas emissions. http://www.worldcoal.org/ [Date of access: 04 September 2008].

WCI. (2010) Coal statistics. http://www.worldcoal.org/ [Date of access: 05 May 2010].

YAMASHITA, H. AND TOMITA, A. (1993) Influence of char surface chemistry on the reduction of nitric oxide with chars. *Energy & Fuels* **7**, 85-89.

YANG, R.T. (1987) Gas separation by adsorption processes. Butterworth: Boston.

ZHAO, Z., LI, W., QIU, J. AND LI, B. (2002) Catalytic effect of Na-Fe on NO-char reaction and NO emission during coal char combustion. *Fuel* **81**, 2343-2348.

ZHAO, Z., QIU, J., LI, W., CHEN, H. AND LI, B. (2003) Influence of mineral matter in coal decomposition of NO over coal chars and emission of NO during char combustion. *Fuel* **82**, 949-957.

Appendices

Appendix A: Abbreviations, Acronyms and terms used in petrographic analysis

A1. Maceral Analysis

Meanings of the abbreviations used are as follows:

VIT	Vitrinite
PV	Pseudovitrinite
TV	Total vitrinite
S/R/C	Sporinite/resinite/cutinite
ALG	Alginite
TOT L	Total liptinite (formerly called exinite)
RSF	Reactive semifusinite
ISF	Inert semifusinite
F/SEC	Fusinite/secritinite
MIC	Micrinite
R INT	Reactive inertodetrinite
I INT	Inert inertodetrinite
TOT I	Total inertinite

Total Reactives = Vitrinite + Reactive Semifusinite + Reactive Inertodetrinite

A2. Reflectance Measurements

Definations of abbreviations used are as follows:

Rr %	Random reflectance of vitrinite
Rsc %	Reflectance of total maceral scan
σ	Standard deviation

A3. Microlithotype analysis

Explanation of terms used in microlythotype and carbominerite analysis are as follows:

Vitrite	Vitrinite > 95%
Liptite	Liptinite > 95%
Inertite	Inertinite > 95%
Clarite	Vitrinite + Liptinite > 95%
Durite	Inertinite + Liptinite > 95%
Vitrinertite	Vitrinite + Inertinite > 95%
Trimacerite	Vitrinite + Inertinite + Liptinite > 5%
Carbominerite	Total inorganic/organic microlythotypes
Minerite	> 60% (vol) minerals

Appendix B: Outline of classification system for char carbon forms.

Adapted from Du Cann (2008) and Everson *et al.* 2008b.

Group		**Char carbon form**	**Photomicrograph** (Figure)
A	1.	Dense char with frequent tiny pores	3.6(a)
		Dense char with frequent tiny pores	3.6(b)
	2.	Char networks: fine walled more open networks	3.6(c) (above)
	3.	Char networks: thicker walled more open networks	3.6(c) (below)
B	7.	Isotropic thick walled “coke”	3.6(d); 3.6(e)
C	8.	Oxidised features resulting mostly from vitrinite	
	9.	Oxidised features emanating mainly from inertinite	
	10.	Oxidised features derived from low reflecting network	
D	11.	Unaffected original coal	
	12.	Partially reacted macerals (from coal)	3.6(f);3.7(a); 3.7(b) & 3.7(c)
E	13.	Inorganic matter apparently derived from minerals in the parent coal	
	14.	Inorganic matter apparently additive to the parent coal	
F	15.	Process derived depositional carbons including pyrolytic and spherulitic carbons	